Diffusion in Flexible Pipes

Susanne Brogaard Kristensen

Danish Polymer Centre
Department of Chemical Engineering
Technical University of Denmark

30th June, 2000

Contents

Chapter 1

Introduction

The research project is part of a NKT project to improve flexible pipes used in crude oil transport. This report evaluates the progress made during the first year of the modelling project. This part of the project concerns modelling of the flux of gasses through the pipe walls of the flexible pipe. The permeated gasses cause an increase in pressure in the annulus. If this pressure is large it may cause the outer sheath to burst. Also if large amounts of carbon dioxide, hydrogen sulfide and water permeate from the inner of the pipe to the annulus, corrosion of the pressure reinforcements causes a reduced lifetime of the pipe. It is therefore important to be able to predict the gas flux through the pipe walls.

In order to model the permeation of gas a large foundation of experimental data is required. The needed data is supplied by NKT-Research and IVC-SEP, DTU.

The modelling work has been divided in two; a model for the measuring cells used to obtain the required experimental data on permation properties and a model for a flexible pipe consisting of several layers of polymers and steel.

Chapter 2

Literature Study

A literature study has been performed to obtain knowledge on the transport of small molecules through a membrane. In the following pressure-induced permeation is considered. It is believed that the permeation process can be divided in three; the dissolution of gas in the membrane on the high-pressure side, a diffusion through the membrane and a release of gas at the low-pressure side. Therefore, the literature study has focus on the understanding of sorption of gasses in polymer membranes and of the process of diffusion of gasses through polymer membranes.

2.1 Sorption of gasses in polymer membranes

The sorption of gasses in polymer membranes depends strongly on the nature of the polymer, the pressure and temperature. At moderate temperatures and pressures (below the critical values) only small amounts of gas is assumed to be dissolved in the polymer and hence Henry's law apply for the amorphous part of the polymer:

$$C = SP \tag{2.1}$$

where C is the concentration of dissolved gas per volume unit polymer, S is the solubility coefficient or the inverse Henry's law coefficient (volume gas per volume unit polymer and pressure unit) and P is the pressure of the gas. Apparently, very little work has been done on sorption outside the range of Henry's law. According to Stern et al [101] Rogers, Stannett and Szwarc have determined the following empirical expression for the solubility:

$$S = \frac{c}{p} = S_0 \exp \frac{\sigma S_0 p}{(1 - \sigma S_0 p)}$$

where S_0 is the solubility coefficient at zero concentration or pressure and σ is "a temperature-dependent constant that characterizes the concentration

dependence of S". In Stern et al [105] the solubility of a large number of gasses in polyethylene is compared. The following empirical relation is found between the solubility and critical temperature of the gas

$$\log S_0 = -5.64 + 1.14 \left(\frac{T_c}{T}\right)^2$$

where S_0 is Henry's law solubility, $T_c\,(K)$ is the critical temperature of the gas and $T\,(K)$ is the temperature. For temperatures below the glass transition temperature the solubility is given by a combination of Henry's law (amorphous part) and Langmuir sorption (glassy part) [5], called the *Dual Sorption mode.* However, this is not discussed in this survey because the polymers considered are above the glass transition.

2.2 Diffusion of gasses through polymer membranes

Once the gas is dissolved on the high pressure side of the membrane it diffuses towards the low pressure side because of the difference in chemical potential. The amount of gas transported by diffusion is controlled by the applied pressure and temperature, and the nature of the gas and the polymer. In addition, the nature of the gas and the polymer depends strongly on the applied pressure and temperature which must be taken into account in any modelling of solubility as well as diffusion. The temperature dependence is typically given by an Arrhenius expression:

$$D = D_0 \exp \frac{-E_d}{RT}$$

where D_0 is a reference value of the diffusion coefficient. Often this is extrapolated to a value at zero temperature. E_d is the activation energy for the diffusion. Both D_0 and E_d are determined from experimental values of the diffusion coefficient at given temperatures. According to Stern et al [101] Rogers, Stannett and Szwarc have expressed the average diffusion coefficient dependence on temperature and pressure by an empirical expression:

$$\bar{\mathcal{D}} = \mathcal{D}_0 \exp(\tau a) \sim \mathcal{D}_0 \exp\left(\tau \frac{p_h}{p^*}\right)$$

where $\mathcal{D}_0$ is the diffusion coefficient at zero pressure, $a \sim \frac{p_h}{p^*}$ is the penetrant activity, p_h is the applied penetrant pressure, p^* is the vapor pressure of the penetrant and τ is a temperature-dependent constant.

Stern et al has done an extensive work on the applications of the Fujita *free volume model.* The modelling of diffusion is in most cases acceptable, however, the free volume model requires a lot of experimental data to determine all of the needed parameters.

In Appendix A seven articles/books are chosen from the literature list of 127 articles and books and are referred in greater detail. Appendix A also includes a collection of permeability data found in the literature.

As a short conclusion to the literature study it is noted that, eventhough a lot of work is put into relating permeability to temperature and pressure all relations are empirical or semi-empirical and requires a large experimental foundation to use. Also, the focus is on the permeability not the individual diffusion and solubility coefficients.

Chapter 3

Solubility and diffusion from experimental data

The experimental foundation is supplied by NKT Research and IVC-SEP, DTU. At these departments experiments to determination of D, S and Pe are performed at a number of gasses and polymers at a range of temperatures and pressures. Two different measuring techniques are used and described in the following. The techniques are solubility measurements on a high-pressure balance and the *time lag* method.

3.1 Solubility Measurements

The principle for the solubility measurements is that a polymer sample of known geometry is placed on a balance in a closed vessel. Gas is applied at a given temperature and pressure and the weight increase due to absorption of gas is measured as a function of time. The concentration of absorbed gas is determined as the mass of gas, $m(t)$, divided by the mass of the polymer sample at atmospheric pressure. The maximum concentration of gas that can be dissolved in the polymer is easily determined as the plateau of a plot of concentration vs time (illustrated in figure 3.1). If Henry's law applies a plot of C_{max} versus P gives a straight line with the slope S (the solubility coefficient).

Furthermore, the diffusion coefficient is calculated from the transient. From Fick's second law

$$\frac{\partial c}{\partial t} = D\frac{\partial^2 c}{\partial y^2} \tag{3.1}$$

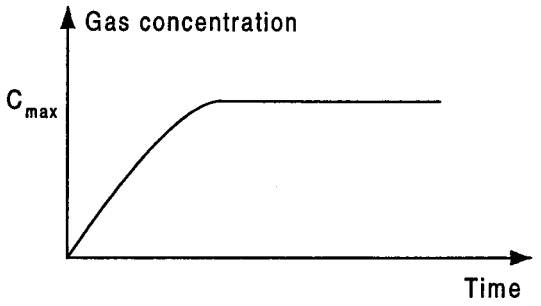

Figure 3.1: Determination of maximum concentration

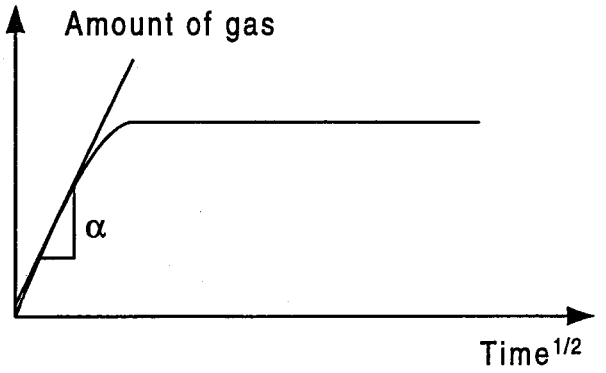

Figure 3.2: Determination of diffusion coefficient

the total amount, $m(t)$, of absorbed gas is given by:

$$m(t) = 4 \cdot 10^3 A\rho C \left(\frac{\mathcal{D}}{\pi}\right)^{0.5} \sqrt{t}$$

where A is the surface area of one side of the sample, ρ is the polymer density, C is the maximum concentration of gas in the polymer, $\mathcal{D}$ is the diffusion coefficient and t is the time. The equation only applies until the polymer is "saturated" with gas. The relation is derived in Appendix D.

A plot of the absorbed amount as a function of the squareroot of time is illustrated in figure 3.2. The diffusion coefficient can now be determined from the slope, α, of the initial straight line of the absorption versus $\sqrt{t}$ curve:

$$D = \pi \left(\frac{0.001\alpha}{4A\rho C}\right)^2 \tag{3.2}$$

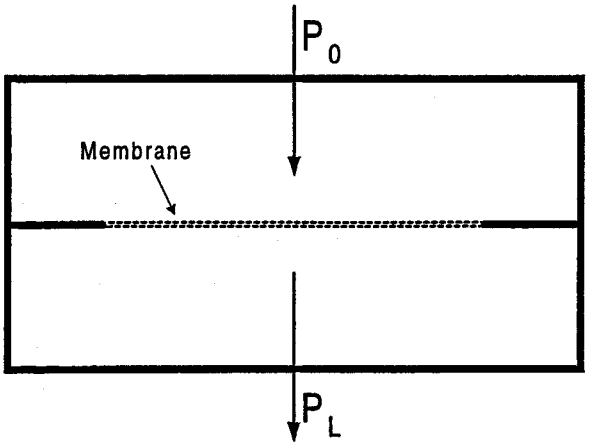

Figure 3.3: Pressure induced flux

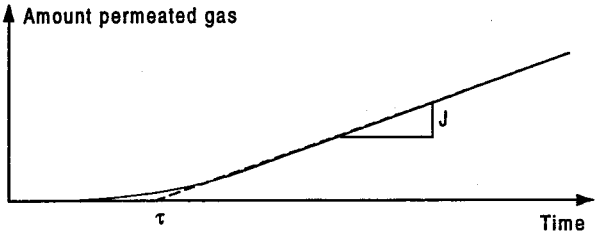

Figure 3.4: A theoretical timelag curve

3.2 Time Lag

The principle for the experimental setup is illustrated in figure 3.3. A high pressure, P_0 is applied to the membrane forcing the molecules to diffuse through the membrane to the low pressure, P_L, side. The amount of gas permeated through the membrane is measured as a function of time and plotted. Figure 3.4 illustrates a typical plot of the flux versus time. The concentration profile in the membrane is given by an analytical solution to Fick's second law (equation 3.1) assuming that the concentration on the low pressure side is zero and the diffusion coefficient is a constant [85]:

$$C = C_0\left(1 - \frac{x}{L}\right) - \frac{2C_0}{\pi}\sum_{n=1}^{\infty}\frac{(1+\alpha)\cos(n\pi) - \alpha}{n}\sin\left(\frac{n\pi x}{L}\right)\exp\left(-\frac{\mathcal{D}n^2\pi^2 t}{L^2}\right)$$

C is the concentration at position x and time t, C_0 is the concentration on the high pressure side, L is the membrane thickness, $\mathcal{D}$ is the binary mass diffusivity, $\alpha = \frac{C_i - C_0}{C_0}$ and $C_i \sim 0$ is the initial gas concentration in the

membrane. Integration with respect to time gives an expression for the total amount of gas leaving the membrane as a function of time:

$$Q = \frac{A\mathcal{D}C_0}{L}\left[t - \frac{L^2}{6\mathcal{D}} - \frac{2L^2}{\pi^2\mathcal{D}}\sum_{n=1}^{\infty}\frac{1}{n^2}\exp\left(-\frac{\mathcal{D}n^2\pi^2 t}{L^2}\right)\right]$$

The timelag is obtained from the linear part of the curve obtained as $t \to \infty$:

$$Q = \frac{A\mathcal{D}C_0}{L}\left[t - \frac{L^2}{6\mathcal{D}}\right] \Rightarrow \tau = \frac{L^2}{6\mathcal{D}}$$

From the intersection (Q=0) of the steady state straight line with the x-axis the timelag, τ, is determined and the diffusion coefficient, $\mathcal{D}$, can be calculated. From the slope, J, of the straight line the permeability coefficient, Pe, is calculated knowing the applied pressure difference across the membrane, Δp:

$$Pe = \frac{J}{\Delta p}$$

Finally, the solubility, S, is obtained from

$$S = \frac{Pe}{\mathcal{D}}$$

Chapter 4

One Dimensional Models

Two models are developed; one for evaluation of experimental data and one for the flexible pipe. The geometries of the two models differ. The membrane used in the measuring cell is flat - this situation is best described in rectangular coordinates. The geometry of the flexible pipe requires cylindrical coordinates.

4.1 Rectangular Coordinates

The principle of the experimental setup is illustrated in figure 3.3. The transport of molecules through the polymer is assumed to be in one direction only and no reaction is occuring. The concentration distribution of component A in the membrane at any time is given by the equation of continuity [4]:

$$\frac{\partial c_A}{\partial t} = -\frac{\partial N_{Ax}}{\partial x}$$

where c_A is the concentration of A in moles per volume unit polymer at time t and position x. N_{Ax} is the molar flux relative to stationary coordinates (mole of A pr surface area polymer and time). The flux independent of position is given by

$$N_A = x_A \left(N_A + N_B\right) - c\mathcal{D}\nabla x_A \tag{4.1}$$

where N_A and N_B are the fluxes, A is the diffusing component, B is the polymer, c is the total concentration in moles/volume, $\mathcal{D}$ is the mass diffusivity in the binary system and x_A is the mole fraction of component A. The first term on the right-hand side is the molar flux of A resulting from the bulk motion and the second term is the molar flux resulting from diffusion. Since only small amounts of A is assumed present in the polymer the bulk flux is

neglected and the one dimensional flux is given by:

$$N_{Ax} = -\mathcal{D}\frac{\partial c_A}{\partial x}$$

The diffusivity is expected to vary with temperature and pressure and therefore also with position. Insertion in the equation of continuity yields:

$$\frac{\partial c_A}{\partial t} = -\frac{\partial}{\partial x}\left(-\mathcal{D}\frac{\partial c_A}{\partial x}\right) \tag{4.2}$$

The needed set of boundary and initial conditions are given by:

$$\begin{aligned} c_A(x,0) &= C_{ini} \\ c_A(0,t) &= C_0 \\ c_A(L,t) &= C_L \end{aligned}$$

where C_{ini} is the initial gas concentration in the membrane, C_0 is a known concentration at the high pressure side of the membrane and C_L is a known concentration on the low pressure side of the membrane, typically this value is set to zero. L is the thickness of the membrane. The initial condition $C_{ini} \sim 0$ expresses that the membrane is initially clean and contains no traces of gas.

The diffusivity is expected to vary with position and equation 4.2 must be solved numerically. As numerical approximation the finite difference method is used. The mesh used in the finite difference approximation is illustrated in figure 4.1. The partial derivatives are approximated by [109]:

$$\begin{aligned} \frac{\partial c_A}{\partial t} &= \frac{c^t_{A,i} - c^{t-\Delta t}_{A,i}}{\Delta t} \\ \frac{\partial c_A}{\partial x} &= \frac{c^t_{A,i+1} - c^t_{A,i-1}}{2\Delta x} \\ \frac{\partial}{\partial x}\left(\mathcal{D}\frac{\partial c_A}{\partial x}\right) &= \frac{\mathcal{D}_{i+1}\left(c^t_{A,i+1} - c^t_{A,i}\right) - \mathcal{D}_i\left(c^t_{A,i} - c^t_{A,i-1}\right)}{\Delta x^2} \end{aligned}$$

where the subscript i refers to the internal nodes of the finite difference mesh. The approximations are inserted into equation 4.2. In short form the rearranged equation is written:

$$a_i c^t_{A,i-1} + b_i c^t_{A,i} + c_i c^t_{A,i+1} = d_i$$

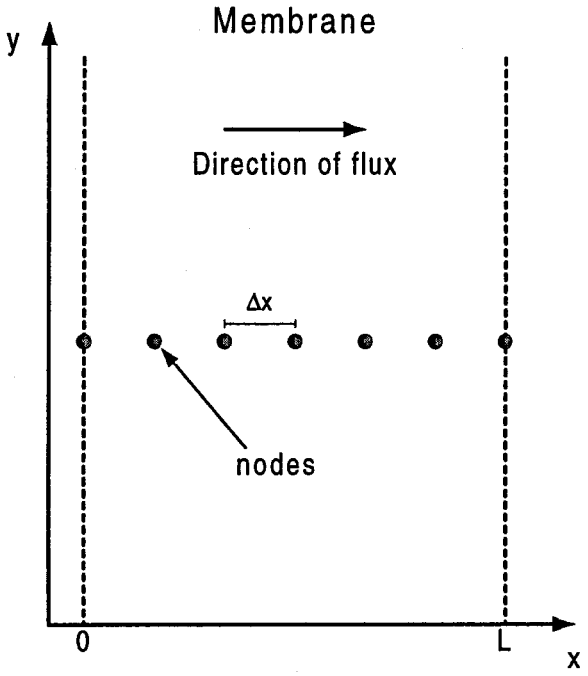

Figure 4.1: The spatial finite difference discretization, N=7 nodes

where the coefficients are given by

$$\begin{aligned} a_i &= -\frac{\Delta t}{\Delta x^2}\mathcal{D}_i \\ b_i &= 1+\frac{\Delta t}{\Delta x^2}\left(\mathcal{D}_{i+1}+\mathcal{D}_i\right) \\ c_i &= -\frac{\Delta t}{\Delta x^2}\mathcal{D}_{i+1} \\ d_i &= c_{A,i}^{t-\Delta t} \end{aligned}$$

The boundary conditions are incorporated to the system of equations by rearranging. At the high pressure side:

$$\begin{aligned} a_2C_0+b_2c_{A,2}^t+c_2c_{A,3}^t &= d_2 \Leftrightarrow \\ b_2c_{A,2}^t+c_2c_{A,3}^t &= d_2-a_2C_0 \end{aligned}$$

and at the low pressure side:

$$\begin{aligned} a_{N-1}c_{A,N-2}^t+b_{N-1}c_{A,N-1}^t+c_{N-1}C_L &= d_{N-1} \Leftrightarrow \\ a_{N-1}c_{A,N-2}^t+b_{N-1}c_{A,N-1}^t &= d_{N-1}-c_{N-1}C_L \end{aligned}$$

In total $N-2$ equations are to be solved for $N-2$ variable concentrations. In matrix form the system of equations is written as:

$$\mathrm{K}\omega = \mathrm{f}$$

where $\mathbf{K}$ is the tridiagonal coefficient matrix, ω is the variable concentration vector ($\omega = (c_{A,2}, ..., c_{A,N-1})$) and $\mathbf{f}$ is the function value vector. The system of equations is solved using a fortran77 subroutine (TRI) programmed by Peter Szabo.

4.2 Cylindrical Coordinates

The modelling of a flexible pipe requires a model for the mass transport considering several layers of diffusion barriers and pressure reinforcements. In this section the modelling is simplified so that the annulus between the two polymeric layers is considered as an empty equilibrium chamber. In section 4.2.1 a model for a single polymeric layer in cylindrical coordinates is derived. This model is extended to a triple layer model consisting of an inner polymeric layer, an equilibrium chamber and an outer polymeric layer in section 4.2.2.

4.2.1 A single polymer layer

The derivation of the governing equations in cylindrical is similar to the rectangular case and will not be treated in detail. The equation of continuity in cylindrical coordinates in radial direction (again reaction is neglected) [4]:

$$\frac{\partial c_A}{\partial t} = -\frac{1}{r}\frac{\partial}{\partial r}(rN_{Ar}) \tag{4.3}$$

The flux is given by equation 4.1 in cylindrical coordinates and neglecting the bulk flux:

$$N_{Ar} = -\mathcal{D}\frac{\partial c_A}{\partial r}$$

For a position dependent diffusivity equation 4.3 is written:

$$\frac{\partial c_A}{\partial t} = -\frac{1}{r}\frac{\partial}{\partial r}\left(r\,(-\mathcal{D})\,\frac{\partial c_A}{\partial r}\right) \tag{4.4}$$

The set of boundary and initial conditions is given by:

$$\begin{aligned} c_A(r,0) &= C_{ini} \\ c_A(R_1,t) &= C_{R_1} \\ c_A(R_2,t) &= C_{R_2} \end{aligned}$$

where R_1 is the inner radius and R_2 is the outer radius of the polymeric layer. The finite difference mesh is analog to figure 4.1 in the radial direction. The finite difference approximation follows accordingly:

$$\begin{aligned}
\frac{\partial c_A}{\partial t} &= \frac{c_{A,i}^t - c_{A,i}^{t-\Delta t}}{\Delta t} \\
\frac{\partial c_A}{\partial r} &= \frac{c_{A,i+1}^t - c_{A,i-1}^t}{2\Delta r} \\
\frac{\partial}{\partial r}\left(r\mathcal{D}\frac{\partial c_A}{\partial r}\right) &= \frac{r_{i+1}\mathcal{D}_{i+1}\left(c_{A,i+1}^t - c_{A,i}^t\right) - r_i\mathcal{D}_i\left(c_{A,i}^t - c_{A,i-1}^t\right)}{\Delta r^2}
\end{aligned}$$

Inserting the approximations in equation 4.4 and rearranging the system of equations is written as:

$$A_i c_{A,i-1}^t + B_i c_{A,i}^t + C_i c_{A,i+1}^t = D_i$$

where

$$\begin{aligned}
A_i &= -\frac{\Delta t}{r_i \Delta r^2} r_i \mathcal{D}_i \\
B_i &= 1 + \frac{\Delta t}{r_i \Delta r^2}\left(r_{i+1}\mathcal{D}_{i+1} + r_i\mathcal{D}_i\right) \\
C_i &= -\frac{\Delta t}{r_i \Delta r^2} r_{i+1}\mathcal{D}_{i+1} \\
D_i &= c_{A,i}^{t-\Delta t}
\end{aligned}$$

The incorporation of the boundary conditions are similar to the rectangular case. Again the equations are written in matrix form and are solved using the tridiagonal matrix solver.

4.2.2 Multiple layers

In figure 4.2 a cross section of the pipe showing the considered situation is illustrated. The figure illustrates two polymeric layers separated by an equilibrium chamber. The equation of continuity in the form given by equation 4.3 must apply to both polymeric layers. The initial and boundary conditions are given by:

$$\begin{aligned}
c_A(r, 0) &= C_{ini} \\
c_A(R_1, t) &= C_{R_1} \\
c_A(R_4, t) &= C_{R_4}
\end{aligned}$$

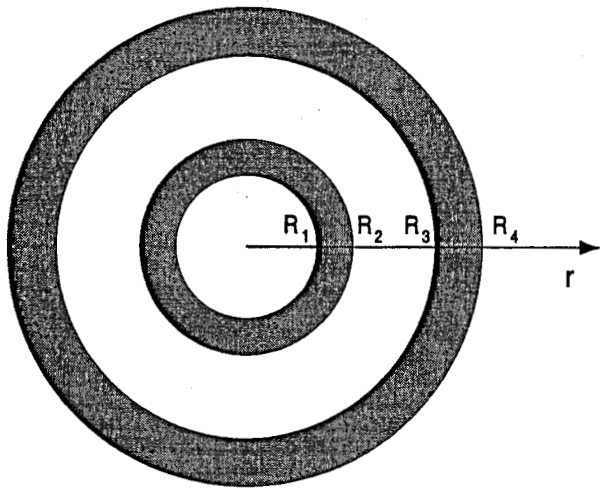

Figure 4.2: Three layers; inner liner, annulus, outer sheath

where R_1 refers to the inner radius of the inner polymeric layer and R_4 refers to the outer radius of the outer polymeric layer. The gas in the annulus is assumed to be in equilibrium with both polymeric layers. A mass balance for the equilibrium layers yields:

$$R_2(-\mathcal{D}_1)\left.\frac{\partial c_A}{\partial r}\right|_{R_2} - R_3(-\mathcal{D}_2)\left.\frac{\partial c_A}{\partial r}\right|_{R_3} = \frac{1}{2}\left(R_3^2 - R_2^2\right)\frac{\partial C_{eq}}{\partial t}$$

where R_3 is the inner radius of the outer polymeric layer and R_2 is the outer radius of the inner polymer layer, $\mathcal{D}_1$ and $\mathcal{D}_2$ are the diffusivities of polymer layer 1 and 2, respectively, and C_{eq} is the accumulated gas in the equilibrium chamber. If ideal gas behavior is assumed and if Henry's law is assumed valid (that is, only small amounts of gas is dissolved in each polymer layer) the finite element approximation to the mass balance is:

$$R_2(-\mathcal{D}_1)\frac{S_1P_{eq} - C_{N-1}}{\Delta R^{[1]}} - R_3(-\mathcal{D}_2)\frac{S_2P_{eq} - C_{N+3}}{\Delta R^{[2]}} = \frac{1}{2RT}\left(R_3^2 - R_2^2\right)\frac{P_{eq}^t - P_{eq}^{t-\Delta t}}{\Delta t}$$

where S_1 and S_2 are the solubilities at the equilibrium boundaries of polymer layer 1 and 2, $\Delta R^{[1]}$ and $\Delta R^{[2]}$ are the node spacing of polymer layer 1 and 2, R is the gas constant and T is the temperature in the equilibrium chamber. R_i refers to the radii given in figure 4.2. The finite difference mesh consists of N number of nodes in layer 1, one node in annulus and M number of nodes in layer 2. Note that the concentration at the node placed on the boundary between polymer layers and the equilibrium is replaced by the equilibrium pressure.

Left are two equations effected by the use of pressure instead of concentration at the intermediate boundaries: 'last' equation for polymer layer 1 and 'first' equation for polymer layer 2. The affected equations are rewritten in terms of equilibrium pressure using Henry's law:

$$\begin{aligned} A_{N-1}c^t_{A,N-2} + B_{N-1}C^t_{A,N-1} + C_{N-1}c^t_{A,N} = D_{N-1} \Leftrightarrow \\ A_{N-1}c^t_{A,N-2} + B_{N-1}C^t_{A,N-1} = D_{N-1} - C_{N-1}S_1P^t_{eq} \\ A_{N+3}c^t_{A,N+2} + B_{N+3}C^t_{A,N+3} + C_{N+3}c^t_{A,N+4} = D_{N+3} \Leftrightarrow \\ B_{N+3}C^t_{A,N+3} + C_{N+3}c^t_{A,N+4} = D_{N+3} - A_{N+3}S_2P^t_{eq} \end{aligned}$$

The boundary conditions are used as in the single layer case. In matrix form the system of equations to be solved is written:

$$\mathbf{K}\omega = \mathbf{f}$$

where $\mathbf{K}$ is the tridiagonal coefficients matrix, $\omega = (c_{A,2}, ..., c_{A,N-1}, P_{eq}, c_{A,N+3}, ..., c_{A,N+M-3})$ where $N + M - 3$ is the total number of variables and the vector $\mathbf{f}$ consists of the function values. The solution to the system of equations is a concentration profile for the two polymeric layers and the pressure in the annulus and is obtained using the TRI solver.

4.3 Heat Transport

For the multilayer case (figure 4.2) the heat transport is modelled. The basis is the equation of energy in one dimension in cylindrical coordinates [4]:

$$\rho C_p \frac{\partial T}{\partial t} = k \frac{1}{r} \frac{\partial}{\partial r} \left(r \frac{\partial T}{\partial r} \right) \tag{4.5}$$

It is assumed that the density and the thermal conductivity are constants, that only solid non-moving materials are considered and that no viscous dissipation occurs. The initial and boundary conditions are given by:

$$\begin{aligned} T(r, 0) &= T_{ini} \\ T(R_1, t) &= T_0 \\ T(R_4, t) &= T_{R_4} \end{aligned}$$

The energy leaving one layer must enter the next, thus for the boundaries between the layers:

$$q^I = q^{II}$$

where the superscripts indicate different layers. From Fourier's law of heat conduction:

$$\begin{aligned} q &= -k\nabla T \Rightarrow \\ k^I \frac{\partial T^I}{\partial r} &= k^{II} \frac{\partial T^{II}}{\partial r} \Leftrightarrow \\ k^I \frac{\partial T^I}{\partial r} - k^{II} \frac{\partial T^{II}}{\partial r} &= 0 \end{aligned} \tag{4.6}$$

The finite difference approximations are given by:

$$\begin{aligned} \frac{\partial T}{\partial t} &= \frac{T_i^t - T_i^{t-\Delta t}}{\Delta t} \\ \frac{\partial}{\partial r}\left(r\frac{\partial T}{\partial r}\right) &= \frac{r_{i+1}\left(T_{i+1}^t - T_i^t\right) - r_i\left(T_i^t - T_{i-1}^t\right)}{\Delta r^2} \end{aligned}$$

Gathering the coefficients the discretized system of equations is written:

$$\alpha_i T_{i-1}^t + \beta_i T_i^t + \gamma_i T_{i+1}^t = \delta_i \tag{4.7}$$

where the coefficients are given by

$$\begin{aligned} \alpha_i &= \frac{k}{\Delta r^2} \\ \beta_i &= -\frac{\rho C_p}{\Delta t} - \frac{k}{r_i \Delta r^2}\left(r_{i+1} + r_i\right) \\ \gamma_i &= \frac{k}{r_i \Delta r^2} r_{i+1} \\ \delta_i &= -\frac{\rho C_p}{\Delta t} T_i^{t-\Delta t} \end{aligned}$$

At the boundaries between the layers equation 4.6 replaces equation 4.5. Discretisation of this yields:

$$\mathcal{A}_i T_{i-1}^t + \mathcal{B}_i T_i^t + \mathcal{C}_i T_{i+1}^t = 0$$

where the coefficients are given by

$$\begin{aligned} \mathcal{A}_i &= -\frac{k^I}{\Delta r^I} \\ \mathcal{B}_i &= \frac{k^I}{\Delta r^I} + \frac{k^{II}}{\Delta r^{II}} \\ \mathcal{C}_i &= -\frac{k^{II}}{\Delta r^{II}} \end{aligned}$$

The boundary conditions are implemented as described for the mass transport. In matrix form the system of equations to be solved is written as above described:

$$\mathbf{K}\omega = \mathbf{f}$$

where $\mathbf{K}$ is the tridiagonal coefficients matrix, $\omega = (T_2...T_{N-1})$ where N is the number of radial nodes and temperature variables and the vector $\mathbf{f}$ consists of the right hand sides to the governing equations. The solution to the system of equations is a temperature profile for the two polymeric layers and the annulus and is obtained using the TRI solver.

Chapter 5

Two Dimensional Models

The one dimensional model for two polymeric diffusion barriers separated by an equilibrium chamber is valid when diffusion is possible from the entire surfaces of the polymers. However, due to the pressure reinforcements in the annulus the major part of the outer surface of the inner liner may be blocked by metal resulting in the concentration variation with axial position important. To simulate the altered diffusion pattern in the inner liner, a 2D model is required.

5.1 Gas diffusion through polymers

The considered pipe configuration is illustrated in figure 5.1. Diffusion from the inner liner to the equilibrium chamber is only possible in the slits between the C-profiles. The concentration profiles are given by the equation of continuity in two dimensions in cylindrical coordinates:

$$\frac{\partial c_A}{\partial t} = \frac{1}{r}\frac{\partial}{\partial r}\left(r\mathcal{D}\frac{\partial c_A}{\partial r}\right) + \frac{\partial}{\partial z}\left(\mathcal{D}\frac{\partial c_A}{\partial z}\right) \tag{5.1}$$

The pipe considered is highly symmetrical; the C-profiles and the slits are repeated throughout the pipe. Therefore, the temperature and concentration profiles obtained for one-half of a C-profile and one-half of a slit are repeated

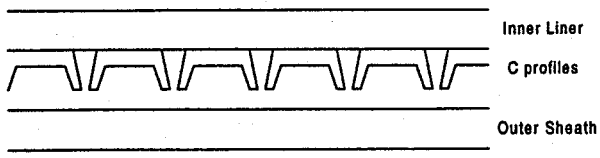

Figure 5.1: The inner liner is partially blocked by metal wires

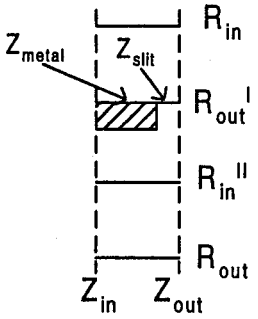

Figure 5.2: Symmetry section - one-half C-profile, one-half slit

throughout the pipe as well. The symmetry section considered is illustrated in figure 5.2. The initial and inner and outer boundary conditions for the pipe section:

$$\begin{aligned} c_A(r,z,0) &= C_{ini} \\ c_A(R_{in},z,t) &= C_{in} \\ c_A(R_{out},z,t) &= C_{out} \end{aligned} \tag{5.2}$$

At the symmetry planes and the boundary between the inner liner and the metal blocking the following constraints have to be fulfilled:

$$\begin{aligned} \tfrac{\partial c_A}{\partial z}(r,Z_{in},t) &= 0 \\ \tfrac{\partial c_A}{\partial z}(r,Z_{out},t) &= 0 \\ \tfrac{\partial c_A}{\partial r}(R^I_{out},Z_{metal},t) &= 0 \end{aligned} \tag{5.3}$$

The nomenclature is given in figure 5.2. Concentrations on the boundaries to the annulus are bounded by an equilibrium equation. The equilibrium equation is derived from a simple mass balance: Accumulated = In - Out, where

$$\begin{aligned} \text{In} &= 2\pi R^I_{out}\Delta t \int_0^{L^I} N_r dz \\ \text{Out} &= 2\pi R^{II}_{in}\Delta t \int_0^{L^{II}} N_r dz \\ \text{Acc} &= V(c^t_{ann} - c^{t-\Delta t}_{ann}) \end{aligned}$$

where superscript I refers to the inner liner and superscript II refers to the outer sheath. Δt is the time interval, N_r is the gas flux across annulus-polymer boundaries, L^I is the length of the slit, L^{II} is the inner surface of

the outer sheath, V is the free volume in the annulus (i.e. the voids between metal wires), c_{ann} is the concentration of gas in annulus at the indicated time. The mass balance yields

$$2\pi \left(R^I_{out} \int_0^{L^I} N_r dz - R^{II}_{in} \int_0^{L^{II}} N_r dz \right) = V \frac{c^t_{ann} - c^{t-\Delta t}_{ann}}{\Delta t} \tag{5.4}$$

The integrals are solved numerically by the trapezoidal formula. For the inner liner:

$$\begin{aligned} \int_0^{L^I} N_r dz &= -\mathcal{D}^I \frac{\Delta z^I}{\Delta r^I} [\frac{1}{2}(c_{N_{rad},1} - c_{N_{rad}-1,1}) + (c_{N_{rad},2} - c_{N_{rad}-1,2}) + \\ &\ldots + (c_{N_{rad},N_{slit}-1} - c_{N_{rad}-1,N_{slit}-1}) + \frac{1}{2}(c_{N_{rad},N_{slit}} - c_{N_{Rad}-1,N_{slit}})] \end{aligned}$$

For the outer sheath

$$\begin{aligned} \int_0^{L^{II}} N_r dz &= -\mathcal{D}^{II} \frac{\Delta z^{II}}{\Delta r^{II}} [\frac{1}{2}(c_{N_{rad}+3,1} - c_{N_{rad}+2,1}) + (c_{N_{rad}+3,2} - c_{N_{rad}+2,2}) + \\ &\ldots + (c_{N_{rad}+3,N_{ax}-1} - c_{N_{rad}+2,N_{ax}-1}) + \frac{1}{2}(c_{N_{rad}+3,N_{ax}} - c_{N_{Rad}+2,N_{ax}})] \end{aligned}$$

The dissolved gas at the polymer boundary is in equilibrium with the gas pressure in the annulus according to Henry's law. This yields:

$$\begin{aligned} Int^I = \int_0^{L^I} N_r dz &= -\mathcal{D}^I \frac{\Delta z^I}{\Delta r^I} [\, (N_{slit} - 1) S^I P_{ann} - \\ &\quad \frac{1}{2} c_{N_{rad}-1,1} - \sum_{i=2}^{N_{slit}-1} c_{N_{rad}-1,i} - \frac{1}{2} c_{N_{Rad}-1,N_{slit}} \,] \\ Int^{II} \int_0^{L^{II}} N_r dz &= -\mathcal{D}^{II} \frac{\Delta z^{II}}{\Delta r^{II}} [\, \frac{1}{2} c_{N_{rad}+3,1} - \\ &\quad \sum_{i=2}^{N_{ax}-1} c_{N_{rad}+3,i} - \frac{1}{2} c_{N_{Rad}+3,N_{ax}} - (N_{ax} - 1) S^{II} P_{ann} \,] \end{aligned}$$

In the above equations N_{rad} is the number of radial nodes in layer 1, N_{slit} is the number of axial nodes on the slit and N_{ax} is the number of axial nodes in layer 2. The annulus gas concentration in equation 5.4 is converted to pressure by the ideal gas law

$$c_{ann} = \frac{p_{ann}}{RT}$$

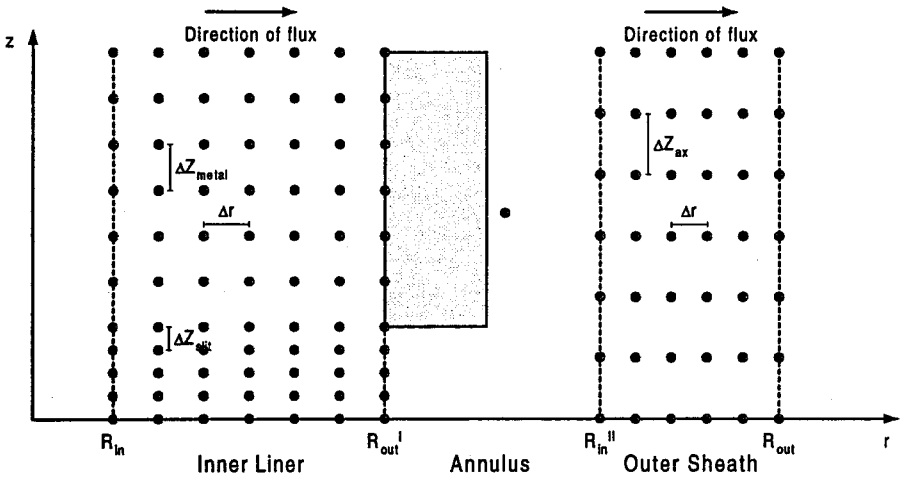

Figure 5.3: Finite difference mesh

where R is the gas constant and T is the temperature. Equation 5.4 is now written

$$2\pi\Delta t\frac{RT}{V}\left(R^I_{out}Int^I - R^{II}_{in}Int^{II}\right) - p^t_{ann} = -p^{t-\Delta t}_{ann} \tag{5.5}$$

Equation 5.5 relates the annulus pressure and the concentrations in the inner liner and the outer sheath given by equation 5.1. The solution to the equations is approximated by finite difference.

5.1.1 Finite Difference Approximation

An example of the finite difference mesh used for the pipe geometry is illustrated in figure 5.3. The second order derivatives in equation 5.1 are approximated according to

$$\frac{\partial}{\partial r}\left(r\mathcal{D}\frac{\partial c}{\partial r}\right) = \frac{(rD)^+_{i+,j}\left(c^t_{i+1,j} - c^t_{i,j}\right) - (rD)^-_{i-,j}\left(c^t_{i,j} - c^t_{i-1,j}\right)}{\Delta r^2}$$

$$\frac{\partial}{\partial z}\left(\mathcal{D}\frac{\partial c}{\partial z}\right) = \frac{D^+_{i,j+}\frac{c^t_{i,j+1}-c^t_{i,j}}{\Delta z^+} - D^-_{i,j-}\frac{c^t_{i,j}-c^t_{i,j-1}}{\Delta z^-}}{\frac{1}{2}\left(\Delta z^+ + \Delta z^-\right)}$$

where i, j is the row, column position of the node. The value of the diffusion coefficient is calculated between two nodes, the minus indicates lower row or column number and the plus indicates higher row or column number. In short form the discretized equation is written

$$U_1 c^t_{i-1,j} + U_2 c^t_{i+1,j} + U_3 c^t_{i,j} + U_4 c^t_{i,j-1} + U_5 c^t_{i,j+1} = U_6$$

where

$$
\begin{aligned}
U_1 &= -\frac{\Delta t}{r_{i,j}\Delta r^2}(r\mathcal{D})^-_{i^-,j} \\
U_2 &= -\frac{\Delta t}{r_{i,j}\Delta r^2}(r\mathcal{D})^+_{i^+,j} \\
U_6 &= c^{t-\Delta t}_{i,j}
\end{aligned}
$$

for the inner liner:

$$
\begin{aligned}
U_3 &= 1+\frac{\Delta t}{r_{i,j}\Delta r^2}\left((r\mathcal{D})^+_{i^+,j}+(r\mathcal{D})^-_{i^-,j}\right)+\frac{2\Delta t}{\Delta z^+ + \Delta z^-}\left(\frac{\mathcal{D}^+_{i,j^+}}{\Delta z^+}+\frac{\mathcal{D}^-_{i,j^-}}{\Delta z^-}\right) \\
U_4 &= -\frac{2\Delta t}{\Delta z^+ + \Delta z^-}\frac{\mathcal{D}^-_{i,j^-}}{\Delta z^-} \\
U_5 &= -\frac{2\Delta t}{\Delta z^+ + \Delta z^-}\frac{\mathcal{D}^+_{i,j^+}}{\Delta z^+}
\end{aligned}
$$

for the outer sheath:

$$
\begin{aligned}
U_3 &= 1+\frac{\Delta t}{r_{i,j}\Delta r^2}\left((r\mathcal{D})^+_{i^+,j}+(r\mathcal{D})^-_{i^-,j}\right)+\frac{\Delta t}{\Delta z^2}\left(\mathcal{D}^+_{i,j^+}+\mathcal{D}^-_{i,j^-}\right) \\
U_4 &= -\frac{\Delta t}{\Delta z^2}\mathcal{D}^-_{i,j^-} \\
U_5 &= -\frac{\Delta t}{\Delta z^2}\mathcal{D}^+_{i,j^+}
\end{aligned}
$$

Note that this formulation of the axial discretization allows for different axial node spacing in blocked and un-blocked part of the inner liner. At the boundaries to the annulus equation 5.5 is used. At the inner and outer boundaries the boundary concentrations given in equation 5.3 replace the concentration variables. At the symmetry planes the concentration constraints given in equation 5.4 are implemented. In matrix form the system of equations is written

$$\mathbf{U}\omega = \mathbf{b}$$

where $\mathbf{U}$ is the U_1, U_2, U_3, U_4, U_5 coefficients at each inner node (that is, nodes not positioned at the boundaries), $\omega = (c_1, ..., c_N, P_{ann}, c_{N+2}, ..., c_{N+M+1})$ is the variable vector, N and M is the number of inner nodes on the inner liner and the outer sheath and $\mathbf{b}$ is the function vector. The leading dimension, LDA, of the coefficient matrix is given by LDA=NUCA+NLCA+1 where NUCA=NLCA is the number of upper and lower diagonals equal to the maximum number of axial nodes. The system of equations is solved using the IMSL double precision band matrix solver DLSLRB.

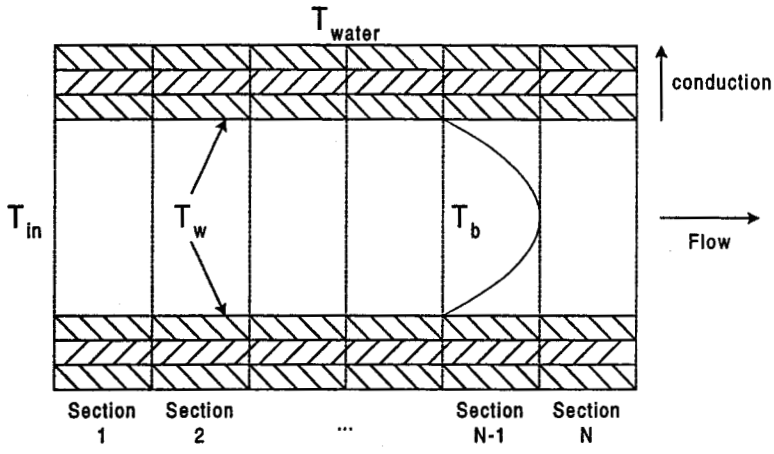

Figure 5.4: The division of a pipe in sections

5.2 2D temperature profiles

Due to the high conductivity of the steel in the annulus a 1D temperature model is sufficient for each symmetry section. However, heat exchange with the surrounding water is inevitable and the temperature of flowing fluid decrease along the pipe. Since it is assumed that the local (a small symmetry section) axial temperature does not vary the "2D" modelling is reduced to determination of the wall temperature, T_w along the pipe and then solve the 1D model across the polymer barriers as described above.

Therefore, the principle of the two dimensional modelling of temperature profiles in the polymeric layers and the annulus is to solve the 1D model at different sections of the pipe (illustrated in figure 5.4). This procedure is possible when the temperature on the inner boundary, T_w, is given.

5.2.1 Estimation of wall temperature

The wall temperature is coupled to the average temperature of the fluid flowing through the pipe. Therefore, an equation for the bulk temperature as a function of axial position is required before the wall temperature can be estimated in each section. The equation of energy in two dimensions relates the axial temperature gradient due to flow to the radial heat transfer due to conduction:

$$v_z \frac{\partial T}{\partial z} = \frac{k}{\rho C_p} \frac{1}{r} \frac{\partial}{\partial r} \left(r \frac{\partial T}{\partial r} \right)$$

Averaging over a cross section of the pipe:

$$2\pi \int_0^{R_1} v_z \frac{\partial T}{\partial z} r dr = 2\pi \int_0^{R_1} \frac{k}{\rho C_p} \frac{1}{r} \frac{\partial}{\partial r} \left(r \frac{\partial T}{\partial r} \right) r dr \tag{5.6}$$

where R_1 is the inner radius of the pipe. The integral on the left side of equation 5.6 is rewritten:

$$\int_0^{R_1} v_z \frac{\partial T}{\partial z} r dr = \frac{\partial}{\partial z} \int_0^{R_1} v_z T r dr$$

The average of the product of velocity and temperature is defined by

$$\begin{aligned} < v_z T > &= \frac{2\pi \int_0^{R_1} v_z T r dr}{2\pi \int_0^{R_1} r dr} \\ &= \frac{2}{R_1^2} \int_0^{R_1} v_z T r dr \end{aligned}$$

Inserting this in the rewritten lefthand side yields:

$$\int_0^{R_1} v_z \frac{\partial T}{\partial z} r dr = \frac{1}{2} R_1^2 \frac{\partial}{\partial z} < v_z T >$$

The right hand side of equation 5.6 is rewritten:

$$\begin{aligned} \int_0^{R_1} \frac{k}{\rho C_p} \frac{1}{r} \frac{\partial}{\partial r} \left(r \frac{\partial T}{\partial r} \right) r dr &= \frac{k}{\rho C_p} \left[r \frac{\partial T}{\partial r} \right]_0^{R_1} \\ &= \frac{k R_1}{\rho C_p} \left. \frac{\partial T}{\partial r} \right|_{R_1} \end{aligned}$$

The transferred energy is given by Fouriers law:

$$q = -k \frac{dT}{dr}$$

The equation of energy is now rewritten as:

$$\frac{\partial}{\partial z} < v_z T > = -\frac{2}{R_1 \rho C_p} q|_{R_1}$$

A bulk temperature, T_b, defined by Bird et al [4] is introduced:

$$\begin{aligned} T_b &= \frac{< v_z T >}{< v_z >} \Rightarrow \\ < v_z > \frac{\partial T_b}{\partial z} &= -\frac{2}{R_1 \rho C_p} q|_{R_1} \end{aligned} \tag{5.7}$$

The overall heat transfer coefficient is defined by [59]

$$q = U\Delta T = U(T_{hot} - T_{cold}) \tag{5.8}$$

In the considered case T_{hot} is the bulk temperature of the flowing fluid in the pipe and T_{cold} is the temperature of the surrounding water cooling the pipe. At steady state the transferred energy, q, must be constant at a given position in the pipe. Inserting 5.8 in 5.7 and assuming the wall temperature to be constant on each section of the pipe yields an expression for evaluation of the bulk temperature in a given section of the pipe:

$$\begin{gathered}
< v_z > \frac{\partial T_b}{\partial z} = -\frac{2U_i}{R_1 \rho C_p} (T_b - T_{water}) \Leftrightarrow \\
\frac{\partial}{\partial z} (T_b - T_{water}) = -\frac{2U_i}{R_1 \rho C_p < v_z >} (T_b - T_{water}) \Leftrightarrow \\
\int_{[T_b - T_{water}]_{inlet}}^{T_b - T_{water}} \frac{1}{T_b - T_{water}} d(T_b - T_{water}) = -\frac{2U_i}{R_1 \rho C_p < v_z >} \int_{z_{inlet}}^{z} dz \Leftrightarrow \\
T_b = T_{water} + [T_b - T_{water}]_{inlet} \exp\left(-\frac{2U_i}{R_1 \rho C_p < v_z >} (z - z_{inlet})\right)
\end{gathered} \tag{5.9}$$

where U_i is the overall heat transfer coefficent based in inner surface area. This is given by [4]

$$U_i = \frac{1}{r_0} \left(\frac{1}{h_i} + \sum_{n=1}^{3} \frac{\ln(r_n / r_{n-1})}{k_n} \right)$$

The outer heat transfer coefficient is neglected. r_0 is the inner radius, h_i is the heat-transfer coefficient for the inner of the pipe, r_n and r_{n-1} are the inner and outer radii, respectively, of the considered layer n and k_n is the conductivity of layer n. The value of the inner heat transfer coefficient is dependent on the type of flow inside the pipe. For laminar flow the coefficient is calculated from [59]:

$$h_i = \frac{2k}{D} N_{Gz}^{\frac{1}{3}} = \frac{2k}{D} \frac{\dot{m} C_p}{kL}$$

N_{Gz} is the Graetz number, $\dot{m}$ is the mass flow rate and L is the section length. For turbulent flow the coefficient is given by [59]:

$$h_i = 0.023 \frac{k}{D} N_{Re}^{0.8} N_{Pr}^{\frac{1}{3}} = 0.023 \frac{k}{D} \left(\frac{D < v_z > \rho}{\mu} \right)^{0.8} \left(\frac{C_p \mu}{k} \right)^{\frac{1}{3}}$$

Once the bulk temperature is known the wall temperature is calculated from [59]

$$\begin{gathered}
T_w = T_b - \Delta T_i = T_b - \frac{\text{inside resistance}}{\text{overall resistance}} \Delta T \Leftrightarrow \\
T_w = T_b - \frac{\frac{D_o}{D_i h_i}}{\frac{1}{U_i}} (T_b - T_{water})
\end{gathered} \tag{5.10}$$

where D_o is the outer pipe diameter and D_i is the inner pipe diameter. From this equation it is possible to determine the wall temperature at each section of the pipe once the bulk temperature is obtained from equation 5.9. It should be noted that an iteration is required if the physical properties of the fluid and the polymers vary with temperature. Knowing the wall temperature distribution it is possible to calculate the temperature profiles in the three layers of the pipe wall using the one dimensional temperature model described in section 4.3.

Chapter 6

Program

The governing equations given in the previous sections are solved by a Fortran90 program made by Susanne Brogaard Kristensen. Three main programmes have been made; a 1D flat, a 1D cylindrical and a 2D cylindrical geometry. The 1D flat geometry programme is for comparison with data measured for application of the time lag method. The 1D cylindrical geometry models the pipe neglecting the effect of the metal boundaries whereas the 2D cylindrical geometry solves for the effects of the metal blocking.

6.1 The 2D Model

In the following subsections the data structure and the subroutines used to solve the 2D diffusion problem are described. The 2D problem is by far the most complicated and the programme to solve this requires more data and subroutines to keep track of where the nodes are placed than what is required to solve 1D problems. Therefore, if the 2D solution procedure is understood it is a relatively simple task to understand the 1D solution procedures (not discussed in this report).

6.1.1 Data Structure

The data structure is similar for the three programmes. Global input and variables are stored in the modules *input* and *variables*. Repeated variables are defined as types and node numbering, coordinates, concentrations and temperatures are related by the use of pointers. Therefore, for a given node number the variables are easily extracted. Also this data structure simplifies the task of making a user interface in Visual C++ if desired.

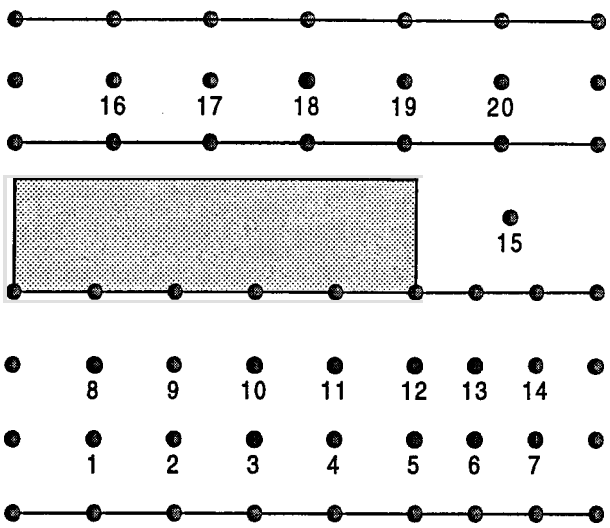

Figure 6.1: The local numbering

6.1.2 Subroutines

Subroutine Data reads the input from a input file and converts to the units used in the calculations. If a User Interface is used the data is stored directly in the modules and the subroutine is not used.
Subroutine InnerNodes assigns global numbers to the inner nodes. The numbering is illustrated in figure 6.1.
Subroutine BoundaryNumbering assigns a "type number" to each nodes. The "type number" indicate the position of the nodes as given in tables 6.1 and 6.2 and illustrated in figure 6.2. These types are used in subroutine CalcCoeff to implement the boundary conditions.
Subroutine GlobalNumbering assigns global numbers to all the nodes. The global numbering is illustrated in figure 6.3.
Subroutine grid calculates the axial and radial coordinates for each node.
Subroutine CalcCoeff calculates the coefficient matrix and function vector from the finite difference discretization. The coefficients and function values are stored in a global matrix and vector, respectively.
Program Cylinder2D is the main programme. The solution procedure is initiated by calling the subroutine Main.
Subroutine Main allocates/deallocates memory and calls the subroutines in the correct sequence in the time and section loops.
Subroutine InitialBoundary stores the initial concentrations in the global concentration vector.
Subroutine ConcReloc relocates the calculated concentrations to the global concentration vector also containing the boundary concentrations. In addi-

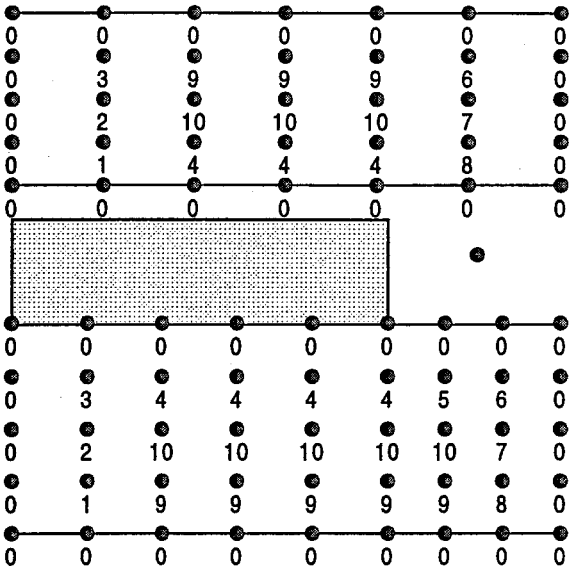

Figure 6.2: The type numbering

Type	Position
0	Boundaries
1	Lower left corner
2	Left column
3	Upper left corner
4	Upper row, metal cover
5	Upper row, no cover
6	Upper right corner
7	Right column
8	Lower right corner
9	Lower row
10	Inner nodes

Table 6.1: Innerliner types

Type	Position
0	Boundaries
1	Lower left corner
2	Left column
3	Upper left corner
4	Lower row
6	Upper right corner
7	Right column
8	Lower right corner
9	Upper row
10	Inner nodes

Table 6.2: Outersheath types

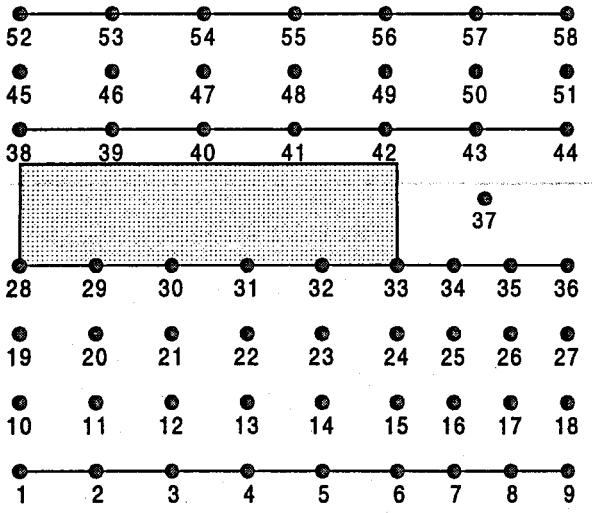

Figure 6.3: The global numbering

tion the calculated equilibrium pressure is relocated to the global equilibrium pressure variable.
Subroutine Flux calculates the gas flux out of and in to the polymeric layers. At steady state the fluxes must be equal for correct solution.
Subroutine ConcOutput writes the output to a file.
Subroutine ConvOutput writes variables necessary for calculation of the convergence order (often this subroutine is commented out).
Subroutine WriteInput writes the used input in a file.
Subroutine Diffusion contains the diffusion equation (e.g. diffusion as a function of pressure and temperature) and calculates the diffusion coefficient at a given position.
Subroutine Solution contains the solubility equation (e.g. solubility as a function of temperature) and calculates the solubility coefficient at a given position.
Subroutine Energy calculates the 1D temperature profiles independent of the concentration calculation.

6.1.3 Input file

Using an input file requires the input to be typed in the following sequence:

1. Number of radial nodes on the inner liner
2. Number of axial nodes on the metal part of the inner liner
3. Number of axial nodes on the slit of the inner liner
4. Inner radius of the inner liner, *cm*
5. Outer radius of the inner liner, *cm*
6. Half-length of metal cover, *cm*
7. "Free-volume" in annulus, %
8. Half-length of slit, *cm*
9. Total pipe length, *cm*
10. Number of radial nodes on the outer sheath
11. Number of axial nodes on the outer sheath
12. Inner radius of the outer sheath, *cm*

13. Outer radius of the outer sheath, cm
14. Number of time steps
15. Size of time steps, s
16. D_0 for inner liner, cm^2/s
17. E_d for inner liner, J/mol
18. 4 constants for pressure modelling, if only temperature modelling the constants 0,0,1,1 are used
19. S_0 for inner liner, $cm^3/cm^3\,bar$
20. E_s for inner liner, J/mol
21. Density of inner liner, kg/cm^3
22. Conductivity of inner liner, $W/cm\,K$
23. Heat capacity of inner liner, $J/kg\,K$
24. D_0 for outer sheath, cm^2/s
25. E_d for outer sheath, J/mol
26. 4 constants for pressure modelling, if only temperature modelling the constants 0,0,1,1 are used
27. S_0 for outer sheath, $cm^3/cm^3\,bar$
28. E_s for outer sheath, J/mol
29. Density of outer sheath, kg/cm^3
30. Conductivity of outer sheath, $W/cm\,K$
31. Heat capacity of outer sheath, $J/kg\,K$
32. Initial concentration in inner liner, mol/cm^3
33. Initial concentration in outer sheath, mol/cm^3
34. Partial gas pressure on the inner of the pipe, bar
35. Partial gas pressure on the outer of the pipe, bar

36. Sea depth, m
37. Inlet temperature, K
38. Water temperature, K
39. Initial temperature, K
40. Density of annulus, kg/cm^3
41. Conductivity of annulus, $W/cm\,K$
42. Heat capacity of annulus, $J/kg\,K$
43. Density of fluid, kg/cm^3
44. Conductivity of fluid, $W/cm\,K$
45. Heat capacity of fluid, $J/kg\,K$
46. Viscosity of fluid, $kg/cm\,s$
47. Fluid inlet pressure, *bar*
48. Fluid outlet pressure, *bar*

Chapter 7

Results

In the following the calculated solubility and diffusion coefficients are reported. From the diffusion and solubility coefficients concentration and temperature profiles are calculated for a horisontal pipe.

7.1 Solubility

The solubility measurements are performed by Abhijit Dandekar at IVC-SEP, DTU as described in section 3.1. So far the polymers polyethylene (PE) and polyamide-11 (PA-11) and the gasses CO_2, CH_4 and He and mixtures of $90mole\%\,CH_4 + 10mole\%\,CO_2$, $90mole\%\,CH_4 + 10mole\%\,He$, $90mole\%\,CO_2 + 10mole\%\,He$, have been examined at $25°C$ and different pressures. In table 7.1 the pressures (in bar) at which the measurements are performed at $25°C$ are listed. The solubility measurements data are reproduced in Appendix B. The maximum concentration of absorbed gas in PE is plotted against pressure in figures 7.1-7.5. The amount of dissolved gas for each gas/gas mixture is compared in figure 7.6.

From the figures it is concluded

gas	PE	PA-11
CO_2	7.02, 20, 30, 40	13.79787, 29.45, 39.05, 49.68
CH_4	5.61, 50, 100, 150	50.68, 100.25, 149.9778
He	50, 100, 150	-
$CO_2 + CH_4$	54.1155, 83.05, 108.787, 150, 149.33	-
$CO_2 + He$	3.09, 15.64, 27.2597	-
$CH_4 + He$	55.356, 100.87, 149.076	-

Table 7.1: Solubility measurements at $25°C$

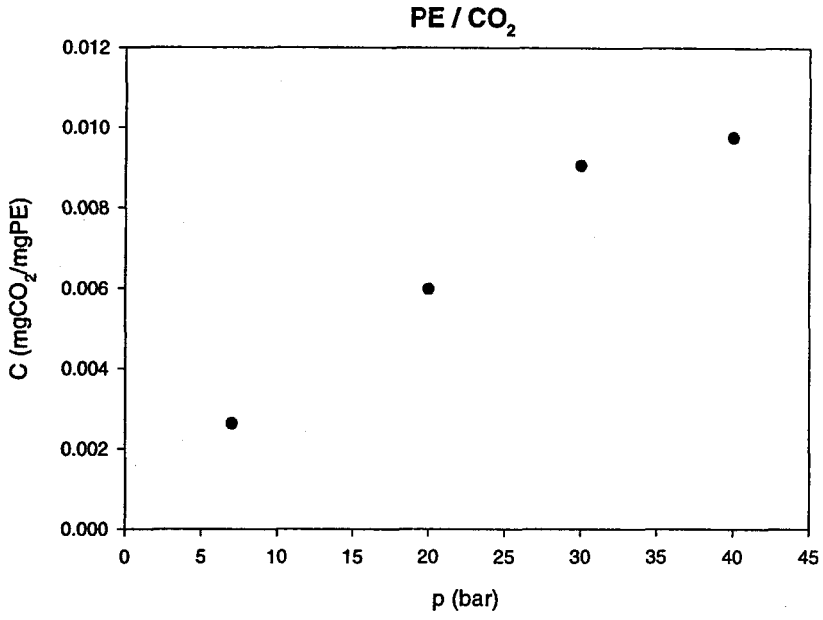

Figure 7.1: Max. gas concentration vs pressure, CO_2 in PE

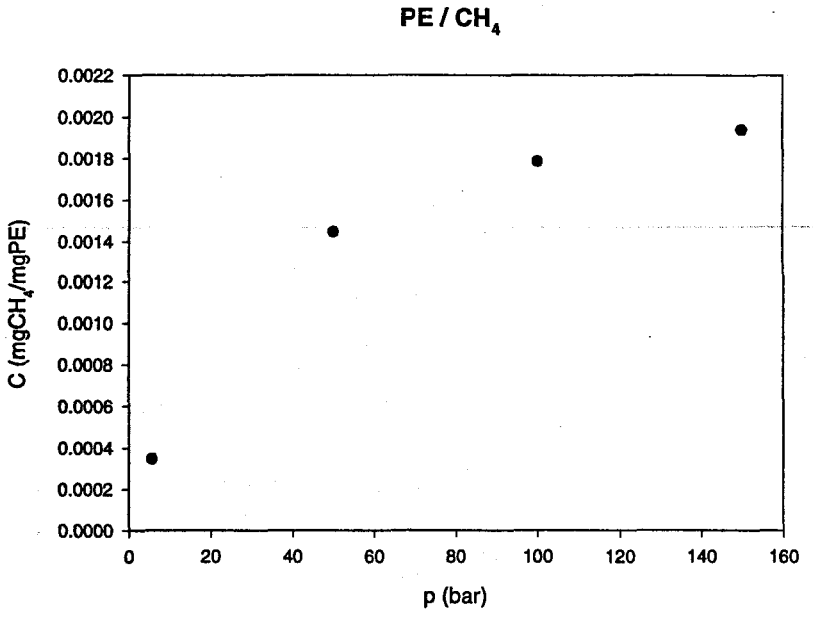

Figure 7.2: Max. gas concentration vs pressure, CH_4 in PE

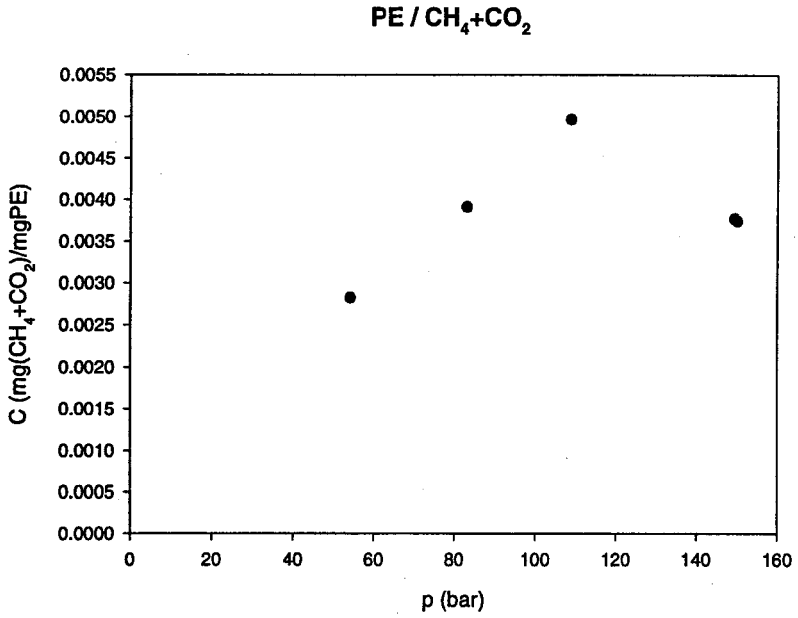

Figure 7.3: Max. gas concentration vs pressure, $CH_4 + CO_2$ in PE

1. CO_2 is more soluble than CH_4 in PE
2. at low pressures the concentration of gas from mixtures of 90mole%CH_4 or 90mole%CO_2 and 10mole% He in PE coincide with the concentrations of pure CH_4 and CO_2, respectively.
3. a mixture of 90mole%CH_4 and 10mole%CO_2 is less soluble than pure CO_2 and more soluble than pure CH_4
4. Henry's law applies only at low pressures

The maximum concentration of absorbed gas in PA-11 is plotted against pressure in figures 7.7-7.8. The amount of gas dissolved in PA-11 is compared in figure 7.9.

From the figures it is concluded

1. CO_2 is more soluble than CH_4 in PA-11
2. Henry's law applies only at low pressures

The effect of the kind of polymer is compared in figures 7.10 and 7.11.

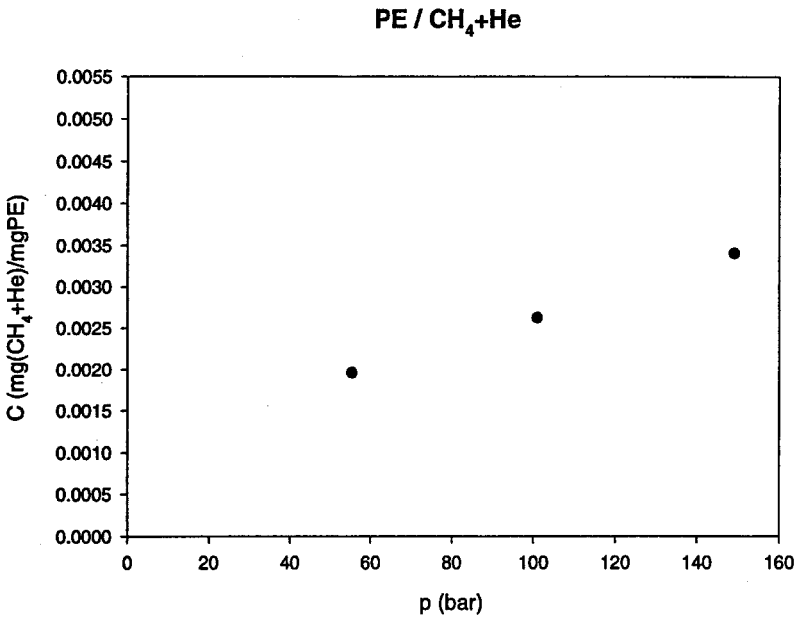

Figure 7.4: Max. gas concentration vs pressure, $CH_4 + He$ in PE

From the two figures it is observed that more gas is dissolved in PA-11 independent of the type of gas. Eventhough the experimental foundation still is limited a few general tendencies seem clear for all combinations of CO_2, CH_4, PA-11 and PE:

- CO_2 is more soluble than CH_4
- more gas is dissolved in PA-11
- Henry's law applies only at low pressures

7.2 Diffusion coefficients

The diffusion coefficients are calculated as described in section 3.1 from the initial slope of the plot of amount of absorbed gas as a function of the square-root of the time. The plots with the fitted linear functions and an example of the calculation procedure are given in Appendix C. The calculated diffusion coefficients are shown in figure 7.12 and 7.13.

For quick comparison all the diffusion coefficients are plotted in the same graph (figure 7.14).

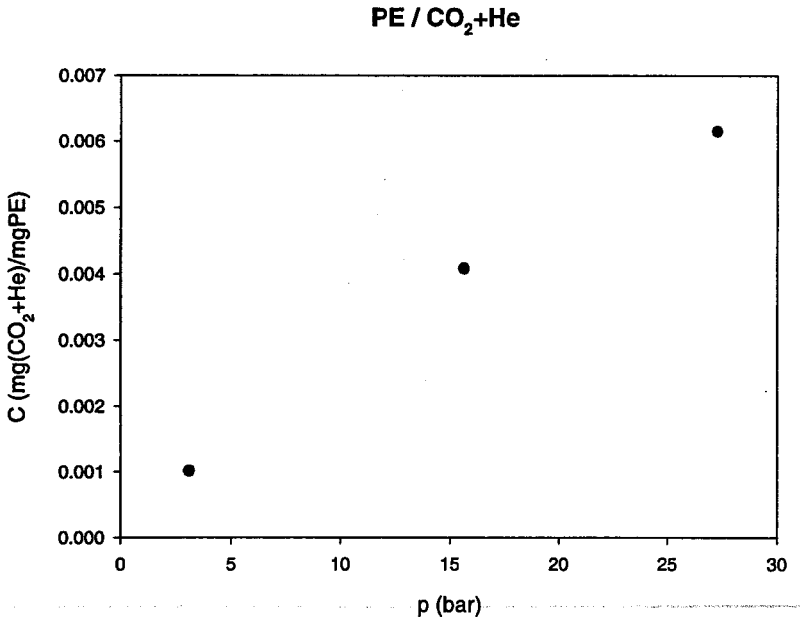

Figure 7.5: Max. gas concentration vs pressure, $CO_2 + He$ in PE

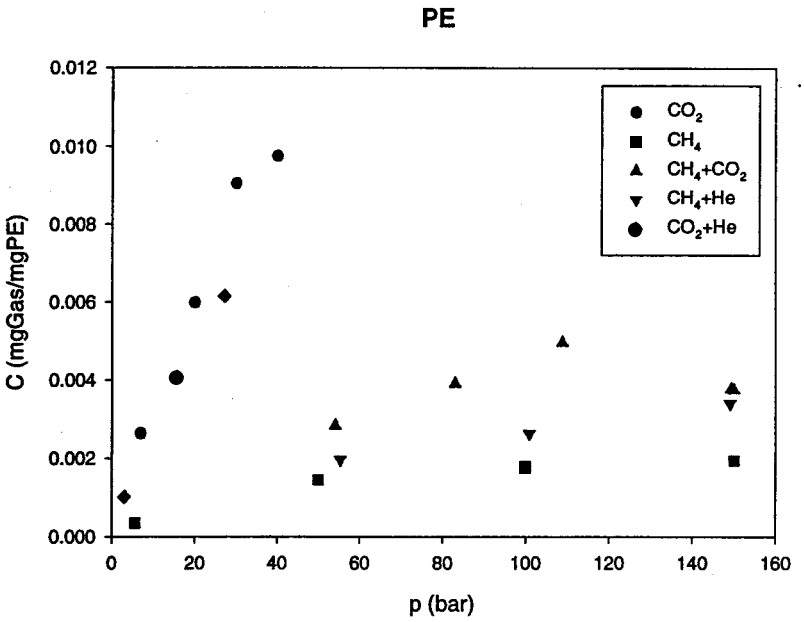

Figure 7.6: Comparison of the measured gas-PE combinations

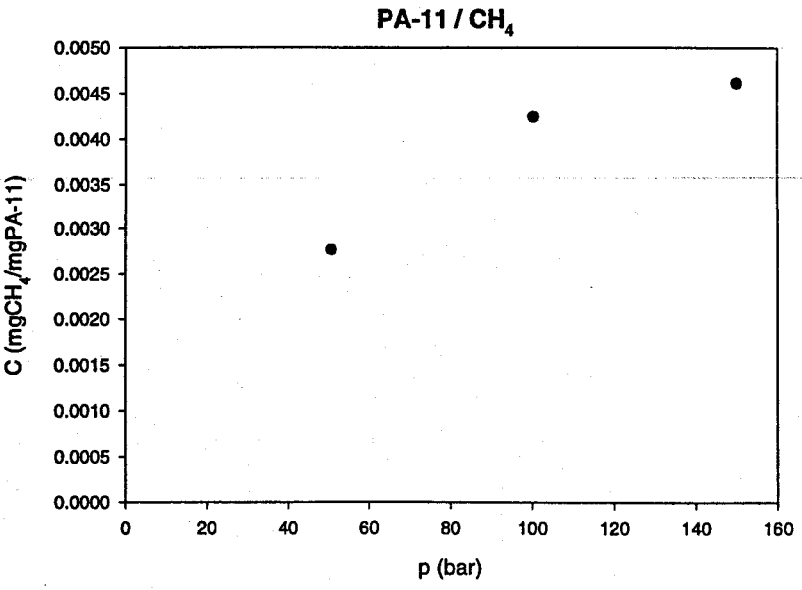

Figure 7.7: Max. gas concentration vs pressure, CH_4 in PA-11

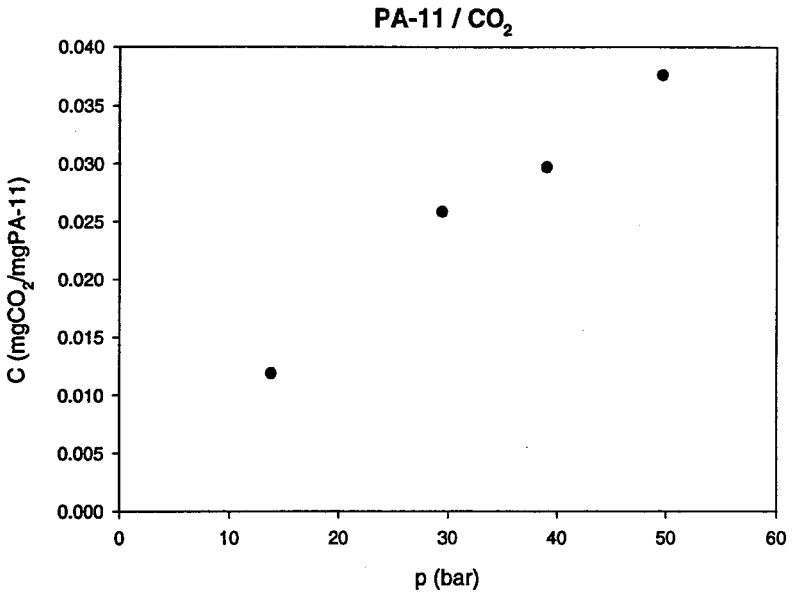

Figure 7.8: Max. gas concentration vs pressure, CO_2 in PA-11

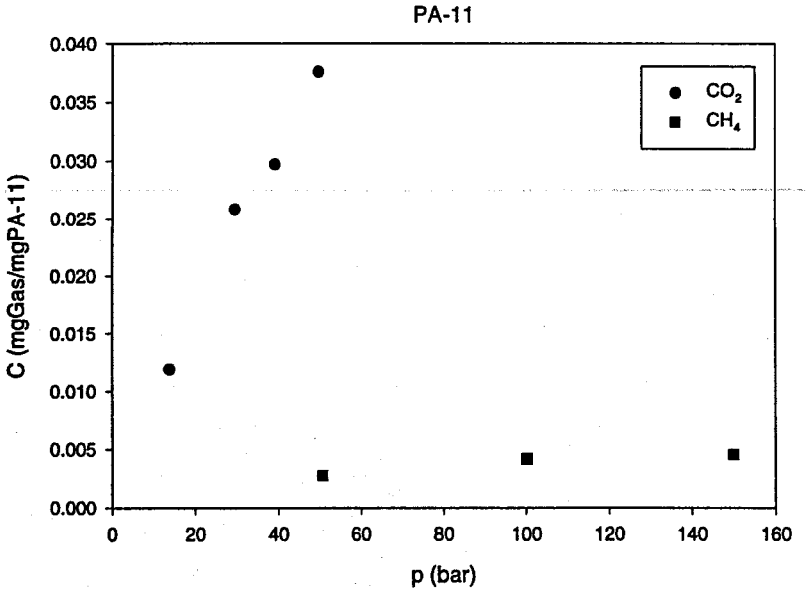

Figure 7.9: Comparison of the measured gas-PA-11 combinations

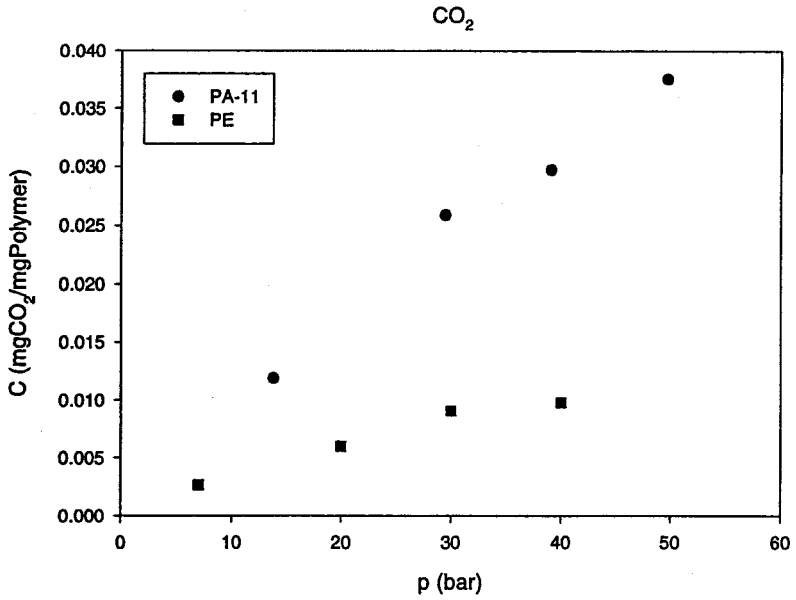

Figure 7.10: Comparison of the solubility of CO_2 in the two polymers

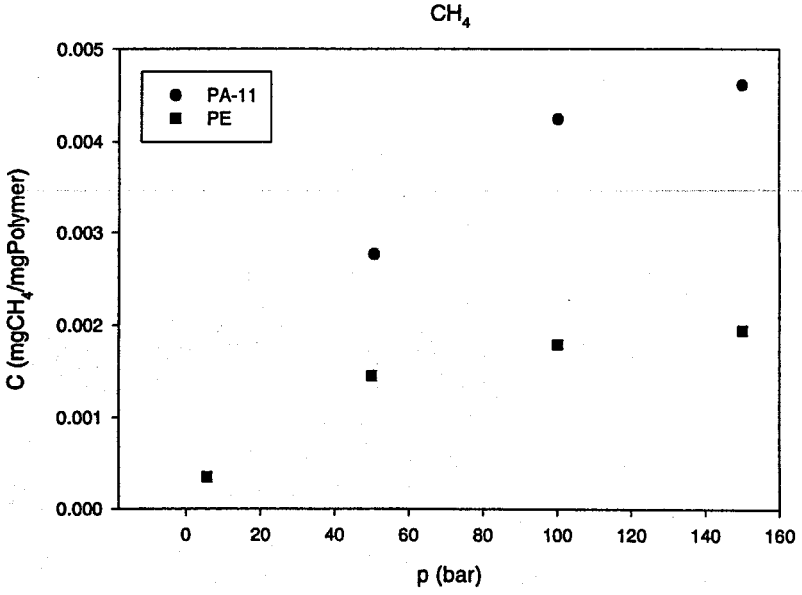

Figure 7.11: Comparison of the solubility of CH_4 in the two polymers

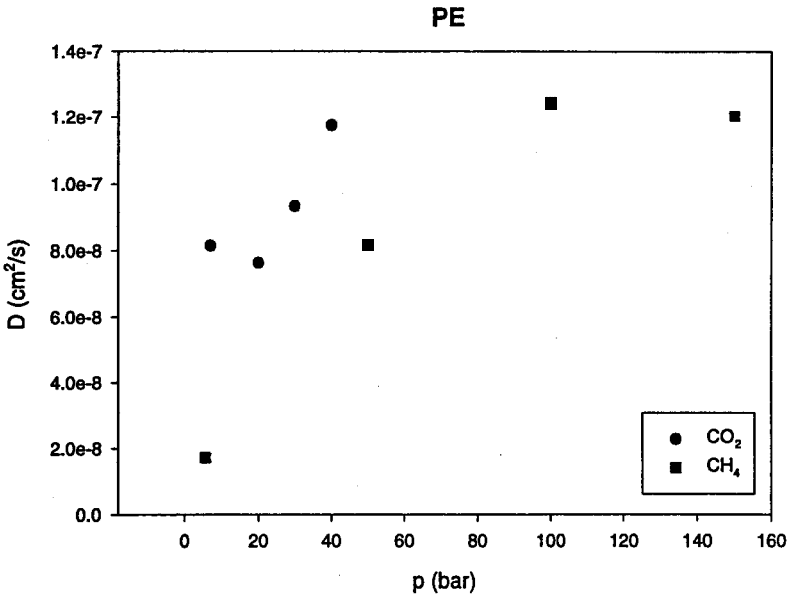

Figure 7.12: Diffusion coefficients in PE at $25°C$

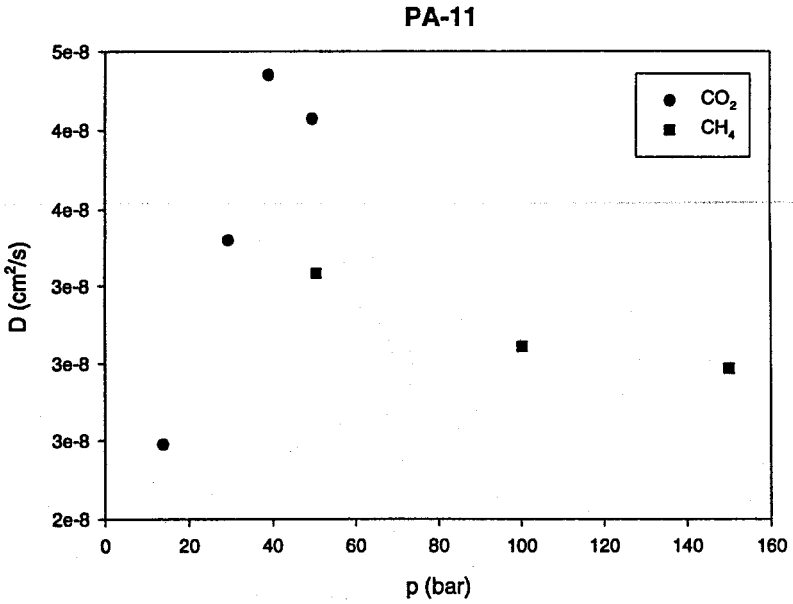

Figure 7.13: Diffusion coefficients in PA-11 at $25°C$

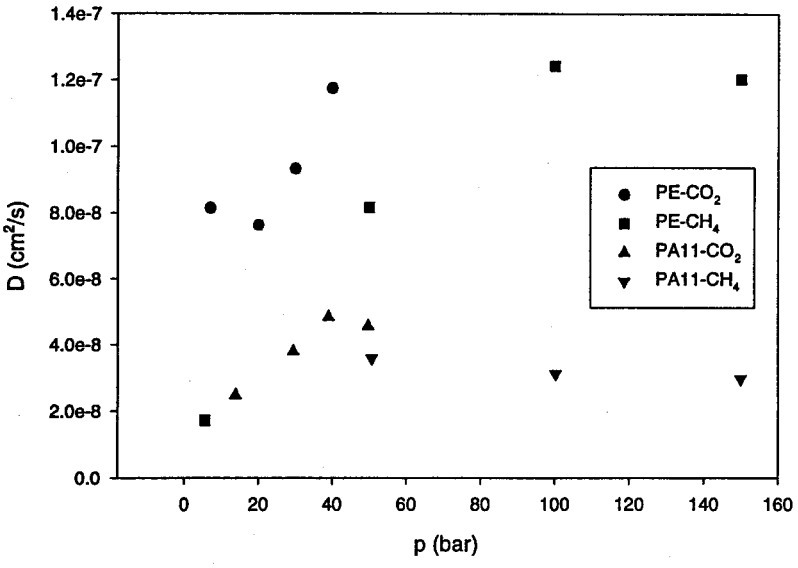

Figure 7.14: Diffusion coefficients in PE and PA-11 at $25°C$

	T_c (K)	P_c (bar)
CO_2	304.2	73.8
CH_4	190.6	46.0
H_2S	373.2	89.4

Table 7.2: Critical gas properties

Please note, that the solubility measurements in PE were not performed on a sample with a well-defined geometry. Therefore, the determination of the surface area is subjected to some uncertainties making the diffusion coefficient of gas in PE qualitative more than quantitative. A few tendencies are observed from figure 7.14:

- the diffusion coefficients is larger in PE than in PA-11
- for a given polymer the diffusion coefficients of CO_2 is larger than CH_4

7.3 Thermodynamic properties

In table 7.2 critical constants [98] for the considered gasses are listed. The glass transition temperature is an important property for understanding the

behaviour of the polymer. The glass transition temperature depends on five factors [83]: the free volume, the attractive forces between the molecules, the internal mobility of the chains, the stiffness and the length of the chains. Therefore, it varies strongly from polymer to polymer. However, since the glass transition temperature is characteristic of the polymer one might expect this temperature as well as the critical gas properties to be of importance for modelling of the solubility/diffusion processes. For the polymers considered in this project following glass transition temperatures are reported by NKT Flexible:

$$\begin{aligned} \text{PA-11: } T_g &= 0 - 10°C \\ \text{MDPE : } T_g &= -80°C \\ \text{PVDF : } T_g &= -28°C \end{aligned}$$

7.4 First approach modelling

For the solubilities the results given above indicate that for experimental conditions close to the critical properties of the gas the solubility increase. The critical properties of CO_2 is not far from the experimental temperature and pressure and it is observed that this gas is the more soluble compared to CH_4. The diffusion may be related to the glass transition temperature of the polymer. The glass transition temperature for PE is the lowest of the three and one can imagine that the movements of the polymeric chains increase with increasing temperature. If this is true the experiments will support the sequence of diffusion coefficients: PE > PVDF > PA-11. The variation of the diffusion coefficients with temperature and pressure is modelled as an Arrhenius temperature relation and a second order polynomial pressure dependence:

$$\begin{aligned} D(T,p) &= K\, f(T)\, g(p) \\ f(T) &= D_0 \exp(-E_d/RT) \\ g(p) &= Ap^2 + Bp + C \end{aligned}$$

where the coefficients A, B, C is fitted to pressure data and D_0, E_d is fitted to temperature data. The coefficient K is fitted to a known diffusion coefficient at a given temperature and pressure.

7.5 Concentration and temperature profiles

The results of the 2D model is illustrated by a case study provided by NKT flexible. A horizontal pipe is considered. Since data for oil flow through the pipe is not yet available the example is based on the flow of water through a pipe with a three layers pipe wall.

The innerliner is made of PA-11 and the outer sheath is made of PE. The experimental foundation does not yet support modelling of the coefficients as function of temperature and pressure, therefore, Arrhenius parameters from Polymer Handbook [75] are used. Note that in the present form the program is prepared to model temperature as Arrhenius and pressure as second order polynomials for the diffusion coefficient. The Henry's law solubility coefficient is assumed to follow an Arrhenius temperature dependence and the effect of pressure is ignored. However, small alterations of the program allow for pressure dependent solubility.

Multicomponent diffusion is not investigated so the permeating gasses, CH_4 and CO_2 is treated separately. If small amounts of gas dissolve in the polymers additive fluxes may be a reasonable approximation. In future experiments will validate or dismiss this hypothesis.

The pipe is $10^5\,cm$ long divided in 10 sections for calculation purposes. Innerliner properties:

$$
\begin{aligned}
D_i &= 20.3cm \\
\Delta D &= 0.6cm \\
\rho &= 1.034 \cdot 10^{-3} kg/cm^3 \\
k &= 0.0021 W/cm\,K \\
C_p &= 2092 J/kg\,K
\end{aligned}
$$

Outer sheath properties:

$$
\begin{aligned}
D_o &= 25.75cm \\
\Delta D &= 0.7cm \\
\rho &= 0.954 \cdot 10^{-3} kg/cm^3 \\
k &= 0.004 W/cm\,K \\
C_p &= 2000 J/kg\,K
\end{aligned}
$$

Annulus properties:

C-profile $= 1.0cm$
slit $= 0.07cm$
free volume $= 15\%$
$\rho = 7.9 \cdot 10^{-3} kg/cm^3$
$k = 0.5W/cm\,K$
$C_p = 460.5J/kg\,K$

Fluid properties:

$\mu = 10^{-5} kg/cm\,s$
$\rho = 1.0 \cdot 10^{-3} kg/cm^3$
$k = 0.006W/cm\,K$
$C_p = 4184J/kg\,K$
$p_{inlet} = 93bar$
$p_{outlet} = 92.99bar$

Finite difference parameters:

No. of time steps $= 20$
Size of time steps $= 5000000s$
No. of radial nodes, inner liner $= 30$
No. of metal nodes $= 30$
No. of slit nodes $= 30$
No. of radial nodes, outer sheath $= 30$
No. of axial nodes, outer sheath $= 30$

Initial and boundary conditions:

$C_{ini} = 0.0mol/cm^3$
$T_{ini} = 281.15K$
$T_{in} = 343.15K$
$T_{out} = 281.15K$

The remaining input parameters depend on the type of gas permeating the

polymers. For CH_4 in PA-11:

$$
\begin{aligned}
D_0 &= 79.2003 cm^2/s \\
E_d &= 59000 J/mol \\
S_0 &= 2.9 \cdot 10^{-3} cm^3/cm^3\, bar \\
E_s &= -16700 J/mol \\
P_{in} &= 93.0 bar
\end{aligned}
$$

For CH_4 in PE:

$$
\begin{aligned}
D_0 &= 19.0020 cm^2/s \\
E_d &= 45600 J/mol \\
S_0 &= 0.2244 cm^3/cm^3\, bar \\
E_s &= 1700 J/mol \\
P_{out} &= 0.0 bar
\end{aligned}
$$

For CO_2 in PE:

$$
\begin{aligned}
D_0 &= 0.2087 cm^2/s \\
E_d &= 35600 J/mol \\
S_0 &= 2.39 \cdot 10^{-3} cm^3/cm^3\, bar \\
E_s &= -5500 J/mol \\
P_{out} &= 0.0 bar
\end{aligned}
$$

For CO_2 in PA-11:

$$
\begin{aligned}
D_0 &= 8.6790 cm^2/s \\
E_d &= 51900 J/mol \\
S_0 &= 3.92 \cdot 10^{-4} cm^3/cm^3\, bar \\
E_s &= -18000 J/mol \\
P_{in} &= 1.0 bar
\end{aligned}
$$

Parameters for diffusion and solubility of CH_4 in PA-11 are not available in Polymer Handbook. These coefficients are therefore approximated by comparison of known data of diffusion of CO_2 through PE and PA-11 and CH_4 through PE:

$$
\frac{\mathcal{D}_{CO_2,PA-11}}{\mathcal{D}_{CH_4,PA-11}} = \frac{\mathcal{D}_{CO_2,PE}}{\mathcal{D}_{CH_4,PE}} \Leftrightarrow
$$

$$
\mathcal{D}_{CH_4,PA-11} = \frac{\mathcal{D}_{CO_2,PA-11}}{\mathcal{D}_{CO_2,PE}} \mathcal{D}_{CH_4,PE}
$$

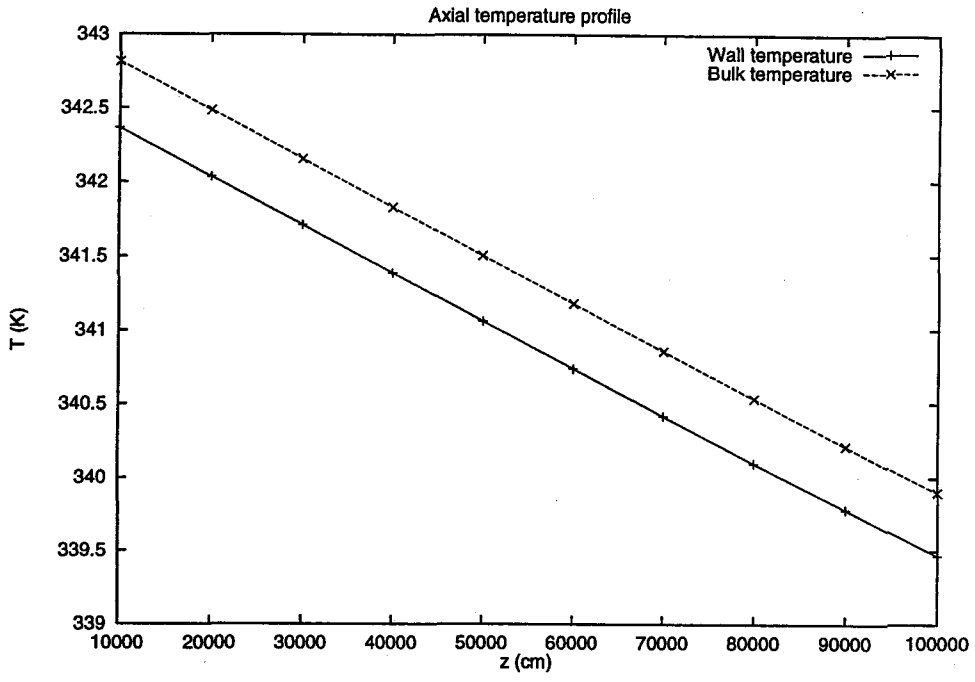

Figure 7.15: Axial temperature profile along the pipe. Each point corresponds to one section

However, eventhough most of the diffusion and solubility data are approximations a qualitatively interpretation of the predicted temperature and concentration profiles serves the purpose of understanding the complex flow pattern, the time constants and the pressure build-up in annulus.

On a Pentium II celeron 400 MHz the duration of calculation is approximately 250 s.

The temperature profiles depend only on the physical constants of the pipe wall and the type of diffusing gas has no influence of the calculated profiles.

The concentration profiles depend strongly of the type of gas diffusing through the polymers.

Therefore, temperature and concentration profiles of the two gasses are discussed separately in the following.

7.5.1 Temperature profiles

The fluid flow in the pipe is turbulent ($N_{Re} = 420000$), therefore, temperature gradients along the pipe is small as illustrated in figure 7.15. The temperature profiles in figure 7.15 is almost perfectly straight lines, that is $\frac{\partial^2 T}{\partial z^2} = 0$. Thus,

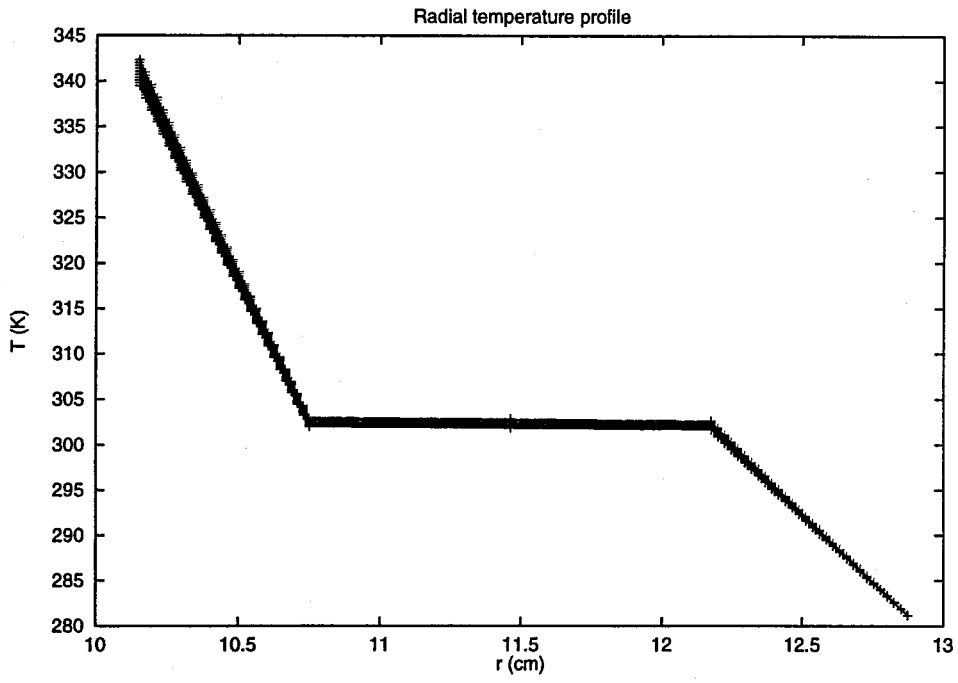

Figure 7.16: Radial temperature profile along the pipe. Each point corresponds to a radial node

the assumption of neglecting the axial conduction is valid. The temperature profiles across the pipe wall is illustrated in figure 7.16 for each section. Only a small variation in the temperature profiles as a function of pipe length can be seen because of the turbulent flow.

7.5.2 Methane diffusion

The concentration profile for diffusion of CH_4 through one symmetry section of one pipe section is illustrated in figure 7.17. The pressure build-up in annulus along the pipe at different time steps is illustrated in figure 7.18. A small axial pressure drop is observed in annulus. The time dependence of the pressure build-up is illustrated in figure 7.19 for the first pipe section (note that in order to obtain acceptable accuracy in the initial pressure-time curve the calculation is performed at $\Delta t = 500000$ and 200 time steps). From the figure it is seen that a steady-state pressure of $\sim$ 1.91 bar is reached after approx. 500 days.

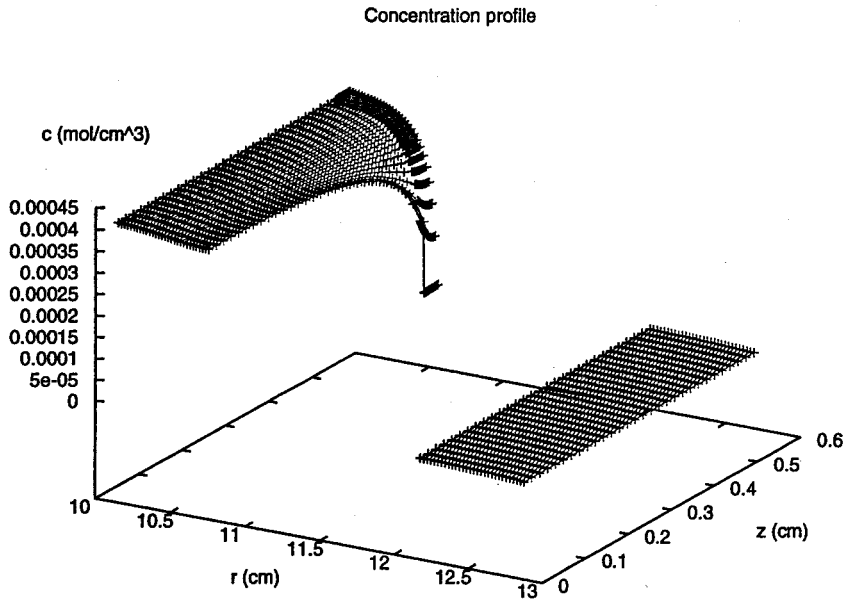

Figure 7.17: Concentration profile for CH_4. Each point corresponds to one node in the finite difference mesh

7.5.3 Carbon dioxide diffusion

The concentration profile for the diffusion of CO_2 through one symmetry section of one pipe section is illustrated in figure 7.20 The axial pressure gradient of CO_2 in the annulus is similar to the pressure gradient of methane and is therefore not illustrated here. The pressure of carbon dioxide in annulus as a function of time is given in figure 7.21. From the figure it is seen that a steady-state pressure of ~ 0.35 bar is reached after approx. 1000 days. This is twice the steady-state time for methane. The partial pressure of CO_2 (1 bar) is much lower than the partial pressure of CH_4 (93 bar) inside the pipe and therefore the driving force for mass transport is much lower causing a longer time to steady state. CO_2 is a more permeable gas than CH_4 in both PA-11 and PE, thus the annulus pressure relative to the partial inner pressure is larger for CO_2

7.5.4 Effect of C-profiles

The effect of the innerliner being pressed against the C-profiles due to the high inner pressure is illustrated by comparing the annulus methane pressure at different coverage degrees of the inner liner. The reduced pressure due

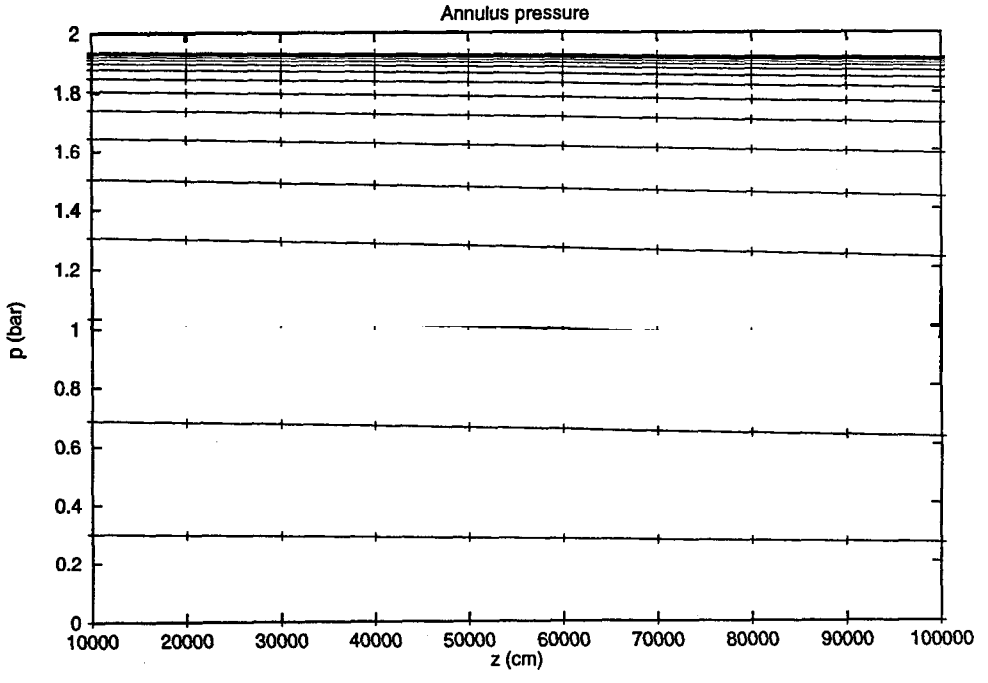

Figure 7.18: Axial CH_4 pressure in annulus along the pipe. Each curve represents a time step, each point on each curve corresponds to one section

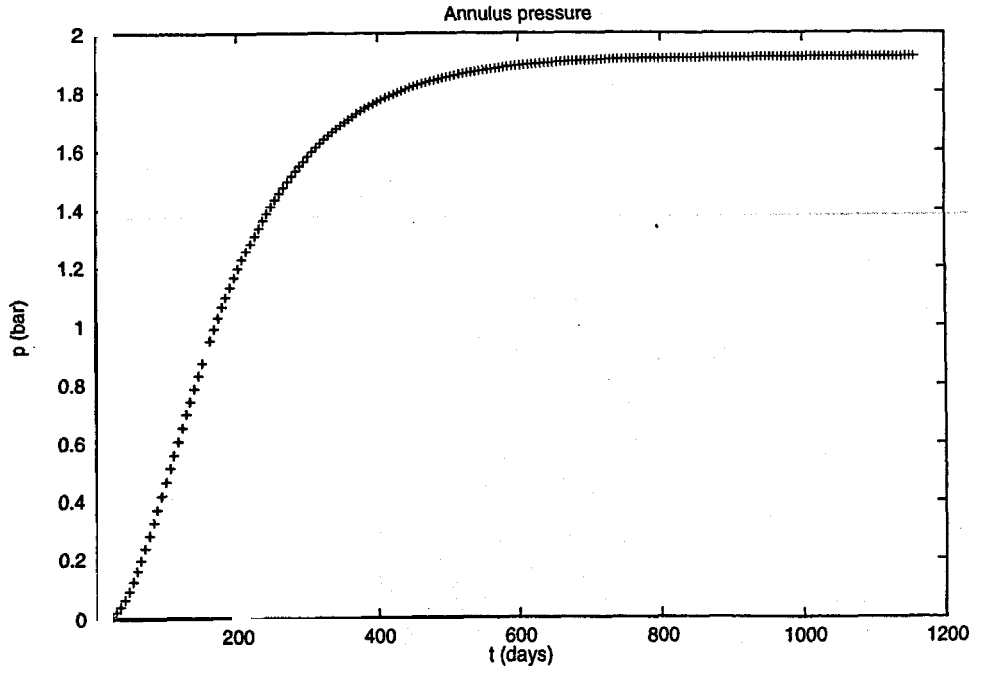

Figure 7.19: Pressure build-up of CH_4 as a function of time for section 1

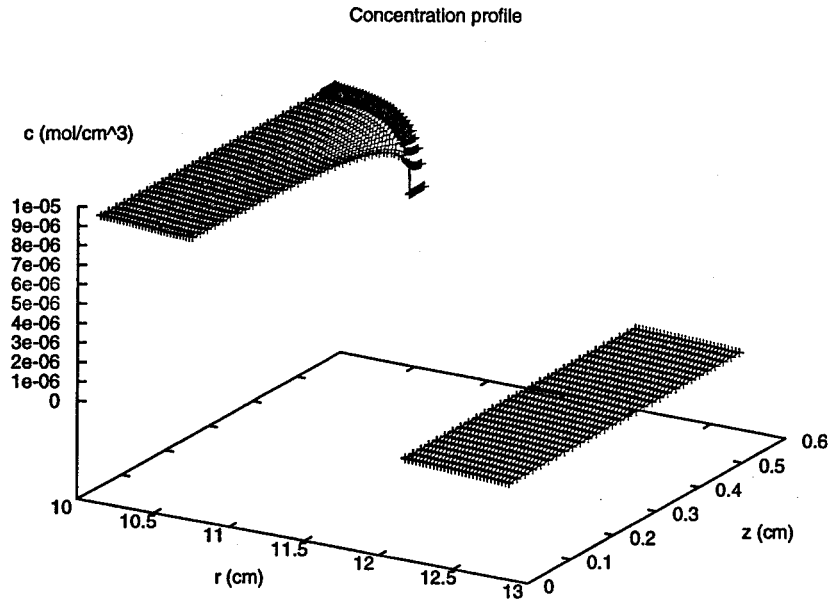

Figure 7.20: Concentration profile for CO_2. Each point corresponds to one node in the finite difference mesh

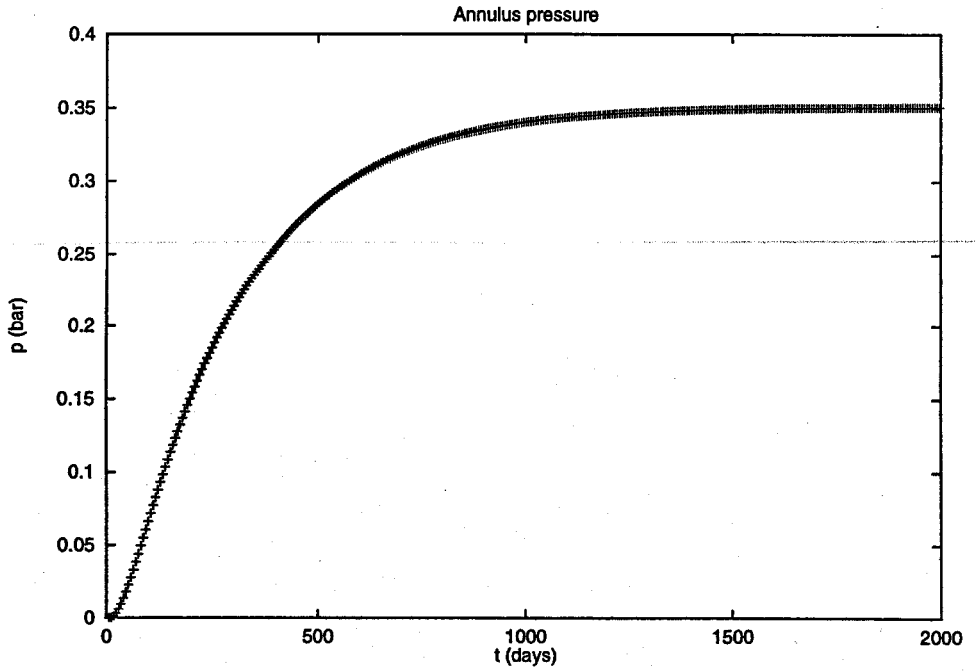

Figure 7.21: Pressure build-up of CO_2 as a function of time for section 1

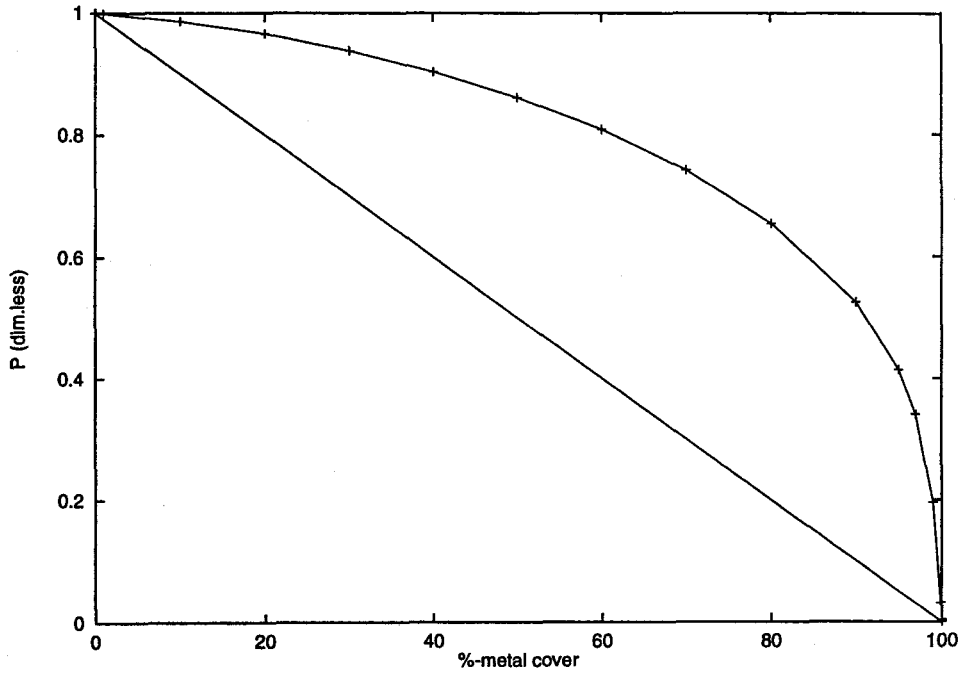

Figure 7.22: The pressure is reduced as a function of C-profile coverage

to the C-profile is compared to the pressure calculated using a C-profile coverage of 1e-3%. The input parameters are as given above for the diffusion of methane. The dimensionless pressure, $P = \frac{P_{partialcover}}{P_{nocover}}$ is plotted against %-coverage in figure 7.22. The diagonal represents the case of diffusion through an unbounded polymer of the width corresponding to the slit width. The determined curve shows pressures higher than the diagonal pressures caused by the 2D flow pattern. The time to reach steady-state is also effected of the C-profiles as illustrated in figure 7.23.

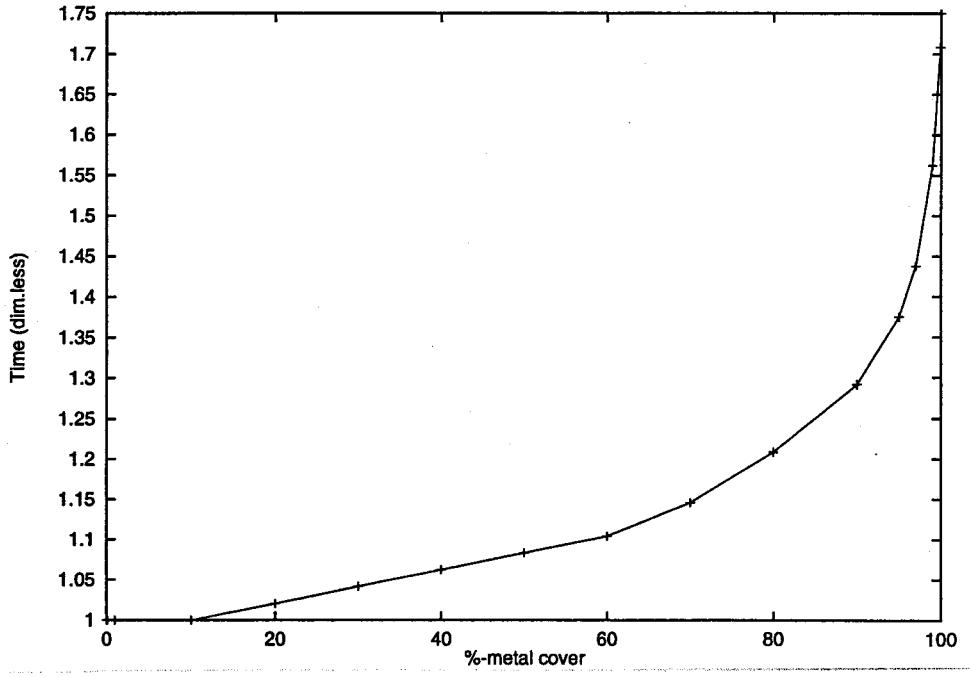

Figure 7.23: The time to steady state is increased as a function of C-profile coverage

Chapter 8

Conclusions and future work

This report describes the work done on modelling and simulation of the complex diffusion of gas through the wall of a flexible pipe. The diffusion and thus the pressure in annulus depends strongly on the diffusion and solubility parameters of the gas-polymer system and on the degree of blocking of the outer surface of the inner liner due to pressure reinforcements. The report evaluates the basis modelling required to describe the complex geometries and flow patterns. Qualitatively results of temperature and concentration profiles are shown in the report. For the program to serve any modelling purpose in 'real life' the results need to be validated and possibly the model needs corrections. Hopefully, a full-scale test of a flexible pipe will provide the required temperatures and pressures in annulus to validate the models.

8.1 Future work

Left is to model diffusion as a function of pressure, hydrogen sulfide diffusion, gas flow in annulus, effect on pressure of venting of annulus, the corrosion of steel in annulus, and a major subject - the multicomponent diffusion. Work on the flow and venting of annulus as well as the corrosion aspects have already been initiated. Thoughts on corrosion is given below whereas the flow in annulus and venting is left for a later report.

Corrosion

In the presence of water the flux of carbon dioxide through the inner liner may cause corrosion of the steel in the annulus. The corrosion process is

given by

$$\begin{aligned} CO_2 + H_2O &\rightarrow H_2CO_3 \\ Fe + H_2CO_3 &\rightarrow FeCO_3 + H_2 \end{aligned}$$

If the amount of CO_2 in annulus is large the corrosion will reduce the lifetime of the pipe drastically and a full pipe model must include corrosion aspects. Before any extensive work on corrosion is initiated it is investigated whether or not the problem really is significant. A worst case estimate of the amount of steel subjected to corrosion is based on the assumptions:

- all diffused CO_2 reacts with Fe
- 1 mol CO_2 reacts with 1 mol Fe
- the 1D one cylindrical polymeric layer model estimates the CO_2 flux (largest flux)

For polyethylene as inner material the following flux is calculated:

$$\sim 16 years : J = 0.478g$$

The metal volume in annulus is obtained by:

$$\begin{aligned} V(cm^3) &= \pi L \left((R_{in}^{II})^2 - R_{out}^{I})^2 \right) \cdot (1 - 0.01 \cdot \%\text{free-volume}) \\ m(g) &= V \cdot \rho_{steel} \end{aligned}$$

Inserting the values

$$\begin{aligned} V(cm^3) &= \pi \cdot 0.535 \cdot (10.75^2 - 10.15^2) \cdot (1 - 0.01 \cdot 15) = 17.92 cm^3 \\ m(g) &= 17.92 \cdot 7.9 = 141.53 g\, Fe \end{aligned}$$

That is, after 16 years $\frac{0.478}{141.53} * 100\% = 0.34\%$ of the metal is corroded. This is an insignificant amount considering the time frame and the high permeability of CO_2 through polyethylene.

However, for oil fields with a higher content of CO_2 corrosion might not be neglected this easily. Therefore, a study of corrosion aspects in annulus of a flexible pipe is initiated.

The aspects of hydrogen embrittlement and corrosion due to hydrogen sulfide in annulus still needs to be examined.

Bibliography

[1]

[2] S.B. Ainbinder and É.L. Tyunina. Effect of hydrostatic pressure on certain thermodynamic properties of polymeric materials. (UDC 678.01:539.32):714–717, 1970.

[3] Moh'd J. Al-Maslamani. Experience with flexible pipe in sour service environment: A case study (the arabian gulf). *Offshore Technology Conference*, 3(OTC8138):213–223, 1996.

[4] R. Byron Bird, Warren E. Stewart, and Edwin N. Lightfoot. *Transport Phenomena.* Wiley International Edition, 1960.

[5] V.I. Bondar, Y. Kamiya, and Yu. P. Yampol'skii. On the pressure dependence of the parameters of the dual-mode sorption model. *Journal of Polymer Science: Part B: Polymer Physics*, 34:369–378, 1996.

[6] Donald J. Buckley, Martin Berger, and Dennis Poller. The swelling of polymer systems in solvents i. method for obtaining complete swelling-time curves. *Journal of Polymer Science*, 56:163–174, 1962.

[7] R.P. Campion. High pressure permeation and diffusion of gases in elastomers and thermoplastics. *Corrosion91, the NACE Annual Conference and Corrosion Show*, (456):1–17, 1991.

[8] R.P. Campion and G.J. Morgan. High pressure permeation and diffusion of gases in polymers of different structures. *Plastic Rubber and Composites Processing and Applications*, 17:51–58, 1992.

[9] M.S. Cayard and R.D. Kane. Large-scale wet hydrogen sulfide cracking performance: Evaluation of metallurgical, mechanical, and welding variables. *Corrosion*, 53(3):227–233, 1997.

[10] Rong-Yeu Chang, Yung-Cheng Hsien, and Feng-Hsien Lin. Modifying the Tait equation with cooling rate effect to predict the pressure-volume-temperature behaviour of semi-crystalline polymers: Model and Experiments. *ANTEC*, pages 2081–2085, 1997.

[11] R.Y. Chang, C.H. Chen, and K.S. Su. Modifying the Tait Equation With Cooling-Rate Effects to Predict the Pressure-Volume-Temperature Behaviours of Amorphous Polymers Modeling and Experiments. *Polymer Engineering and science*, 36:1789–1795, 1996.

[12] R. Chaperon, H.P. Boccacio, and M.J. Bouvard. A new generation of flexible pipe. *Offshore Technology Conference, OTC6584*, pages 207–214, 1991.

[13] C.C. Chau and O.C. Raspor. Gas transport and diffusive resistance in highly oriented high-density polyethylene. *Journal of Polymer Science: Part B: Polymer Physics*, 28:631–645, 1990.

[14] T.S. Chow. Free volume distributions in amorphous polymers. *Macromol. theory simul.*, 4:397–404, 1995.

[15] Morrel H. Cohen and David Turnbull. Molecular transport in liquids and glasses. *The Journal of Chemical Physics*, 31(5):1164–1169, 1959.

[16] J. Crank. *The Mathematics of Diffusion.* Oxford University Press, 1956.

[17] J. Crank, editor. *Diffusion in Polymers.* Academic Press - London & New York, 1968.

[18] F. Dawans, J. Jarrin, and J. Hardy. Improved thermoplastic materials for offshore flexible pipes. *SPE production Engineering.*

[19] F. Dawans, J. Jarrin, T.O. Lefevre, and M. Pelisson. Improved thermoplastic materials for offshore flexible pipes. *Offshore Technology Conference, OTC5231*, pages 91–99, 1986.

[20] H.A. Destefanis, E. Erdmann, D.A. Tarzia, and L.T. Villa. A free boundary model applied to the estimation of the diffusion coefficient in a gas-solid system. *Int. comm. heat mass transfer*, 20:103–110, 1993.

[21] Sukhtej S. Dhingra and Eva Marand. Mixed gas transport study through polymeric membranes. *Journal of Membrane Science*, 141:45–63, 1998.

[22] K. Ehrhardt, K. Klusacek, and P. Schneider. Finite-difference scheme for solving dynamic multicomponent diffusion problems. *Comput. chem. Eng.*, 12(11):1151–1155, 1988.

[23] D.H. Ender. Elastomeric seals. *ChemTech*, January:52–56, 1986.

[24] S.M. Fang, S.A. Stern, and H.L. Frisch. A "free-volume" model of permeation of gas and liquid mixtures through polymeric membranes. *Chemical Engineering Science*, 30:773–780, 1975.

[25] R.M. Felder. Estimation of gas transport coefficients from differential permeation, integral permeation, and sorption rate data. *Journal of Membrane Science*, 3:15–27, 1978.

[26] Hiroshi Fujita. Diffusion in polymer-diluent systems. *Fortschr. Hochpolym.-Forsch.*, 3:1–47, 1961.

[27] F.W. Grealish, A. Bliault, and K.P. Caveny. New standards in flexible pipe technology including api spec 17j. *Offshore Technology Conference*, 4(OTC8181):293–298, 1996.

[28] Esam Z. Hamad. Volume-explicit equation of state for hard chains, their mixtures, and copolymers. *AIChE*, 44(12):2766–2774, 1998.

[29] Georg Härtel and Frank Rompf. Trennung eines kohlendioxid/wasserstoff-gasgemisches unter hohen drücken mit polymeren membranmaterialien. *Chemie Ingenieur Technik*, 69:506–510, 1997.

[30] Bruce Hartmann and Mustafa A. Haque. Equation of state for polymer solids. *J. Appl. Phys.*, 58(8):2831–2836, 1985.

[31] M. Hedenqvist, A. Angelstok, L. Edsberg, P.T. Larsson, and U.W. Gedde. Diffusion of small-molecule penetrants in polyethylene: free volume and morphology. *Polymer*, 37(14):2887–2902, 1996.

[32] William Heilman, Viljo Tammela, Meyer J.A., Vivian Stannett, and Szwarc Michael. Permeability of polymer fils to hydrogen sulfide gas. *Industrial and Engineering Chemistry*, 48(4), 1955.

[33] E.R. Hensema, M.H.V. Mulder, and C.A. Smolders. On the mechanism of gas transport in rigid polymer membranes. *Journal of Applied Polymer Science*, 49:2081–2090, 1993.

[34] Jan Izydorczyk, Józef Podkówka, and Janusz Salwiński. Application of mcinnes's electrode for the determination of carbon dioxide diffusion coefficients through polymer membranes. *Journal of Membrane Science*, 2:235–243, 1977.

[35] Simha Robert Jain, R.K. Equation of state of semicrystalline and crystalline polymers. *Journal of Polymer Science: Polymer Physics Edition*, 17:1929–1946, 1979.

[36] Anne Jonquiéres, Laurent Perrin, Stéphanie Arnold, and Pierre Lochon. Comparison of UNIQUAC with related models for modelling vapour sorption in polar materials. *Journal of Membrane Science*, 150:125–141, 1998.

[37] Mark Kalman, John Belcher, Bin Chen, Dana Fraser, and Andrew Ethridge. Development and testing of non-bonded flexible pipe for high temperature/high pressure/deep water/dynamic sour service applications. *Offshore Technology Conference*, 3(OTC8263):355–373, 1996.

[38] H. Denny Kamaruddin and William J. Koros. Some observations about the application of fick's first law for membrane separation of multicomponents mixtures. *Journal of Membrane Science*, 135:147–159, 1997.

[39] Yoshinori Kamiya, Takuji Hirose, Keishin Mizoguchi, and Yasutoshi Naito. Gravimetric study of high-pressure sorption of gases in polymers. *Journal of Polymer Science: Part B: Polymer Physics*, 24:1525–1539, 1986.

[40] V.-H. Karl, F. Asmussen, and K. Ueberreiter. Eine einfache formel zur darstellung des druckeinflusses auf das spezifische-volumen von teilkristallinen polymeren. *Progr. colloid & polymer sci.*, 64:97–102, 1978.

[41] T.H. Kim, W.J. Koros, G.R. Husk, and K.C. O'Brien. Relationship between gas separation properties and chemical structure in a series of aromatic polyimides. *Elsevier*, 1988.

[42] R. Kirchheim. Permeation von wasser und anderen kleinen molekülen durch polymere. *Materials and corrosion*, 49:175–179, 1998.

[43] A. Kishimoto and Y. Enda. Diffusion of benzene in polyacrylates. *Journal of Polymer Science: Part A*, 1:1799–1811, 1964.

[44] A. Kreituss and H.L. Frisch. Free-volume estimates in heterogeneous polymer systems. I. diffusion in crystalline ethylene-propylene copolymers. *Journal of Polymer Science: Polymer Physics Edition*, 19:889–905, 1981.

[45] P.S. Ku. Equations of state of organic high polymers.

[46] S.S. Kulkarni and S.A. Stern. The diffusion of CO_2, CH_4, C_2H_4, and C_3H_8 in polyethylene at elevated pressures. *Journal of Polymer Science: Polymer Physics Edition*, 21:441–465, 1983.

[47] Karl H. Lange and Rolf K. Popperling. Control of co_2 corrosion by special production tubulars in offshore operation. *Offshore Technology Conference*, 4(OTC3890):355–360, 1980.

[48] W.M. Lee. Selection of barrier materials from molecular structure. *Polymer Engineering and Science*, 20(1):65–69, 1980.

[49] N.N. Li and E.J. Henley. Permeation of gases through polyethylene films at elevated pressures. *AIChE*, pages 666–670.

[50] Morton Litt. Free volume concepts connecting pvt behaviuor and gaseous diffusion through polymers. *The Society of Rheology*, 30(4):853–868, 1986.

[51] Kyriakos Loufakis and Bernhard Wunderlich. Heat capacities of polyethylene and linear fluoropolymers. *Polymer*, 26:1875–1884, 1985.

[52] J.L. Lundberg and E.J. Mooney. Diffusion and solubility of methane in polyisobutylene. *Journal of Polymer Science: Part A-2*, 7:947–962, 1969.

[53] J.L. Lundberg, M.B. Wilk, and Marilyn J. Huyett. Estimation of diffusivities and solubilities from sorption studies. *Journal of Polymer Science*, 57:275–299, 1962.

[54] Y. Makino, K. Ishii, T. Yamaguchi, and Y. Goto. Design of flexible pipe and high-temperature fluid. *Offshore Technology Conference*, (OTC6727):281–288, 1991.

[55] Y. Makino, T. Kagoura, K. Ishii, E.H. Kawakama, and T. Yamaguchi. Development and verification of flexible pipes for deepwater applications. *Society of Petroleum Engineers*, pages 569–576, 1995.

[56] Y. Makino, T. Okamoto, Goto T., and M. Araki. The problem of gas permeation in flexible pipe. *Offshore Technology Conference, OTC5745*, pages 537–542, 1988.

[57] E.A. Mason, L.F del Castillo, and R.F. Rodríguez. Coupling-constant description of coupled flow and diffusion. *Journal of Membrane Science*, 74:253–261, 1992.

[58] E.A Mason and L.A. Viehland. Statistical-mechanical theory of membrane transport for multicomponent systems: Passive transport through open membranes. *J. Chem. Phys.*, 68(8), 1978.

[59] Smith Julian C. Harriott Peter McCabe, Warren L. *Unit Operations of Chemical Engineering*. McGraw-Hill, 1993.

[60] C.T. Meyer and Chamel A. Water and ion absorption by polyethylene in relation to water treeing. *IEEE Transactions on Electrical Insulation*, EI-15(5):389–393, 1980.

[61] Alan S. Michaels and Harris J. Bixler. Flow of gases through polyethylene. *Journal of Polymer Science*, L:413–439, 1961.

[62] Hitoshi Miyake, Masao Matsuyama, Kan Ashida, and Kuniaki Watanabe. Permeation, diffusion, and solution of hydrogen isotopes, methane, and inert gases in/through tetrafluoroethylene and polyethylene. *J. Vac. Sci. Technol. A 1*, 3:1447–1451, 1983.

[63] Florian Müller-Plathe. Diffusion of penetrants in amorphous polymers: A molecular dynamics study. *J. Chem. Phys.*, 94(4):3192–3199, 1991.

[64] Florian Müller-Plathe. Towards a computational approach to penetrant diffusion in semicrystalline polymers. *Chemical physics letters*, 177(6):527–535, 1991.

[65] Yasutoshi Naito, Yoshinori Kamiya, Katsuhiko Terada, Keishin Mizoguchi, and Jin-Sheng Wang. Pressure dependence of gas permeability in a rubbery polymer. *Journal of Applied Polymer Science*, 61:945–950, 1996.

[66] Yasutoshi Naito, Keishin Mizoguchi, Katsuhiko Terada, and Yoshinori Kamiya. The effect of pressure on gas permeation through semicrystalline polymers above the glass transition temperature. *Journal of Polymer Science: Part B: Polymer Physics*, 29:457–462, 1991.

[67] Chitoshi Nakafuku. Unit cell variations of polyethylene crystal with temperature and pressure. *Polymer*, 19:149–154, 1978.

[68] Satu Niemelä, Jukka Leppänen, and Franciska Sundholm. Structural effects on free volume distribution in glassy polysulfones:molecular modelling of gas permeability. *Polymer*, 37(18):4155–4165, 1996.

[69] M. Novák, K. Ehrhardt K., Klusáček, and P. Schneider. Dynamics of non-isobaric diffusion in porous catalysts. *Chemical Engineering Science*, 43(2):185–193, 1988.

[70] H. Omidian, S.A. Hashemi, P.G. Sammes, and I. Meldrum. A model for the swelling of superabsorbent polymers. *Polymer*, 39(26):6697–6704, 1998.

[71] R.J. Pace and A. Datyner. Model of sorption of simple molecules in polymers. *Journal of Polymer Science: Polymer Physics Edition*, 18:1103–1124, 1980.

[72] Jiho Park and Kim Hwayong. A new equation of state based on hole theory: application to low molecular weight materials. *Fluid Phase Equilibria*, 150-151:173–180, 1998.

[73] J.Y Park and Paul D.R. Correlation and prediction of gas permeability in glassy polymer membrane materials via a modified free volume based group contribution method. *Journal of Membrane Science*, 125:23–29, 1997.

[74] W. Parks and R.B. Richards. The effect of pressure on the volume, thermodynamic properties and crystallinity of polythene. pages 203–211, 1948.

[75] S. Pauly. *Permeability and Diffusion Data.* Polymer Handbook.

[76] D.S. Pope, I.C. Sanchez, W.J. Koros, and G.K. Fleming. Statistical thermodynamic interpretation of sorption/dilation behaviour of gases in silicine rubber. *Macromolecules*, 24:1779–1783, 1991.

[77] John D. Ramshaw. Hydrodynamics theory of multicomponent diffusion and thermal diffusion in multitemperature gas mixtures. *J. Non-Equilib. Thermodyn.*, 18:121–134, 1993.

[78] K. Kameswara Rao, K.A. Sarma, V. Srinivas, and A.A. Khan. A generalized model for permeation of multicomponent gas mixtures through

polymeric membranes. *Indian Journal of Chemical Technology*, 1:146–152, 1994.

[79] L. Rodier-Renaud, S.L. Randzio, J.-P. E. Grolier, J.R. Quint, and J. Jarrin. Isobaric Thermal Expansivities of Polyethylenes with Various Crystallinities Over the Pressure Range from 0.1 to 300 MPa and Over the Temperature Range from 303 to 393 K. *Journal of Polymer Science: Part B: Polymer Physics*, 34:1229–1242, 1996.

[80] C. Rogers, Meyer J.A, V. Stannett, and Szwarc M. Studies in the gas and vapor permeability of plastic films and coated papers, part I. determination of the permeability constant. *TAPPI*, 39(11):737–741, 1956.

[81] C. Rogers, J.A. Meyer, V. Stannett, and M. Szwarc. Studies in the gas and vapor permeability of plastic films and coated papers. *TAPPI*, 39(11):741–747, 1956.

[82] C.E. Rogers, V. Stannett, and M. Szwarc. The sorption, diffusion and permeation of organic vapors in polyethylene. *Journal of Polymer Science*, XLV:61–82, 1960.

[83] Stephen L. Rosen, editor. *Fundamental principles of polymeric materials.* John Wiley & sons, inc. 2. ed., 1993.

[84] Bernd Rudolf, Toshiaki Ougizawa, and Takashi Inoue. Influence of the lattice site size in cell model theories on the prediction of thermodynamic properties of polymers and their mixtures. *Polymer*, 39(4):873–882, 1998.

[85] S.W. Rutherford and D.D. Do. Review of time lag permeation technique as a method for characterisation of porous media and membranes. *Adsorption*, 3:283–312, 1997.

[86] S. Saeki, S. Takei, Y. Ookubo, M. Tsubokawa, T. Yamaguchi, and T. Kikegawa. Pressure dependence of melting temperatures in branched polyethylene up to 2 gpa. *Polymer*, 39(18):4267–4271, 1998.

[87] S. Saeki, M. Tsubokawa, and T. Yamaguchi. Semiempirical equation of state for polymers and simple liquids under high pressure. *Polymer*, 30(April):672–676, 1989.

[88] S. Saeki, M. Tsubokawa, and T. Yamaguchi. Semiempirical equation of state for polymers and simple liquids: 2. temperature and volume

dependence of thermal pressure coefficient. *Polymer*, 32(7):1244–1251, 1991.

[89] Isaac C. Sanchez and Junhan Cho. A universal equation of state for polymer liquids. *Polymer*, 36(15):2929–2939, 1995.

[90] Y. Sato, M. Yurugi, K. Fujiwara, S. Takishima, and H. Masuoka. Solubilities of carbon dioxide and nitrogen in polystyrene under high temperature and pressure. *Fluid Phase Equilibria*, 125:129–138, 1996.

[91] Hongjian Sha and Ian R. Harrison. CO_2 permeability and amorphous fractional free-volume in uniaxially drawn HDPE. *Journal of Polymer Science: Part B: Polymer Physics*, 30:915–922, 1992.

[92] M.M. Shahin, R.H. Olley, D.C. Bassett, A.S. Maxwell, A.P. Unwin, and I.M. Ward. Morphological changes in pressure annealed polyethylene. *Journal of Materials Science*, 31:5541–5549, 1996.

[93] James E. Shelby. *Handbook of Gas Diffusion in Solids and Melts.* ASM International, 1996.

[94] Robert Simha and R.K. Jain. Statistical thermodynamics of polymer crystal and melt. *Journal of Polymer Science: Polymer Physics Edition*, 16:1471–1489, 1978.

[95] Robert Simha and Hankun Xie. Applying lattice-hole theory to gas solubility in polymers. *Polymer Bulletin*, 40:329–335, 1998.

[96] Aleksander M. Simon, Paul Doran, and Russell Paterson. Assessment of diffusion coupling effects in membrane separation. Part I. Network thermodynamics modelling. *Journal of Membrane Science*, 109:231–246, 1996.

[97] Klemen Skaarup and Charles M. Hansen. Concentration dependence, boundary layer resistance and the "time-lag" diffusion coefficient. *Polymer Engineering and Science*, 20(4):259–263, 1980.

[98] J.M. Smith and H.C. Van Ness. *Introduction to chemical engineering thermodynamics.* McGraw-Hill, 4.ed, 1987.

[99] R.M. Sok, H.J.C. Berendsen, and W.F. van Gunsteren. Molecular dynamics simulation of the transport of small molecules across a polymer membrane. *J. Chem. Phys.*, 96(6):4699–4704, 1992.

[100] Ferdinand C. Stehling and Leo Mandelkern. The glass temperature of linear polyethylene. *Macromolecules*, 3(2):242–252, 1970.

[101] S.A. Stern, S.M. Fang, and H.L. Frisch. Effect of pressure on gas permeability coefficients. a new application of "free volume" theory. *Journal of Polymer Science: Part A-2*, 10:201–219, 1972.

[102] S.A. Stern, P.J. Gareis, T.F. Sinclair, and P.H. Mohr. Performance of a versatile variable-volume permeability cell. comparison of gas permeability measurements by the variable-volume and variable-pressure methods. *Journal of Applied Polymer Science*, 7:2035–2051, 1983.

[103] S.A. Stern, S.S. Kulkarni, and H.L. Frisch. Tests of a "free-volume" model of gas permeation through polymer membranes. I. pure CO_2, CH_4, C_2H_4, and C_3H_8 in polyethylene. *Journal of Polymer Science: Polymer Physics Edition*, 21:467–481, 1983.

[104] S.A Stern, G.R. Mauze, and Frisch H.L. Tests of a free-volume model for the permeation of gas mixtures through polymer membranes. CO_2-C_2H_4, CO2-C_3H_8, and C_2H_8 Mixtures in Polyethylene. *Journal of Polymer Science: Polymer Physics Edition*, 21:1275–1298, 1983.

[105] S.A. Stern, J.T. Mullhaupt, and P.J. Gareis. The effect of pressure on the permeation of gases and vapors through polyethylene. usefulness of the corresponding states principle. *AIChE*, pages 64–73, 1969.

[106] S.A. Stern, S.R. Sampat, and S.S. Kulkarni. Tests of a "free-volume" model of gas permeation through polymer membranes. II. pure Ar, SF_6, CF_4 and $C_2H_2F_2$ in polyethylene. *Journal of Polymer Science: Part B: Polymer Physics*, 24:2149–2166, 1986.

[107] H. Stöger, R. Stubbe, and M. Ulrich. Stresses and behaviour of polyethylene sheaths. *8th International Conference on Electricity Distribution (IEE Conf. Publ. No. 250)*, pages 225–230, 1985.

[108] Suresh Sunderrajan, Carol K. Hall, and Benny D. Freeman. Chemical potential gradient driven permeation of small molecules through polymeric media. *J. Chem. Phys.*, 107(24):10714–10722, 1997.

[109] Peter Szabo. Modelling of heat and mass transport. *not published*, pages 2–5.

[110] Peter Szabo, Ole Hassager, and Esben Stroebech. Modelling of pressure effects in hvdc cables. *IEEE Transactions on Dielectrics and Electrical Insulation*, 6(6):845–851, 1999.

[111] K. Tamai, H. Tanaka, and K. Nakanishi. Molecular design of polymer membranes using molecular simulation technique. *Fluid Phase Equilibria*, 104:363–374, 1995.

[112] A. Tanioka, A. Oobayashi, Y. Kageyama, K. Miyasaka, and K. Ishikawa. Effects of carbon filler on sorption and diffusion of gases through rubbery materials. *Journal of Polymer Science: Polymer Physics Edition*, 20:2197–2208, 1982.

[113] Z. K. Telli. General theory of multi-component gas diffusion in continous systems. *Chemische Technik*, 31(4), 1979.

[114] John S. Tokarski, A.J. Hopfinger, J. David Hobbs, Davis M. Ford, and Jean-Loup M. Faulon. Molecular modelling of polymers 17. simulation and QSPR analyses of transport behaviour in amorphous polymeric materials. *Computational and Theoretical Polymer Science*, 7(3/4):199–214, 1997.

[115] G.J. van Amerongen. The permeability of different rubbers to gases and its relation to diffusivity and solubility. *Journal of Applied Physics*, pages 972–985, 1946.

[116] G.J. van Amerongen. Influence of structure of elastomers on their permeability to gases. *Journal of Polymer Science*, V(3):307–332, 1949.

[117] G.J. van Amerongen. Diffusion in elastomers. *Rubber Chemistry and Technology*, 37(2):1065–1152, 1964.

[118] Nico F.A. van der Vegt, Wim J. Briels, Matthias Wessling, and Heiner Strathmann. Free energy calculations of small molecules in dense amorphous polymers. effect of the initial guess configuration in molecular dynamics studies. *J. Chem. Phys.*, 105(19):8849–8857, 1996.

[119] K. Videm and J. Kvarekvål. Corrosion of carbon steel in carbon dioxide-saturated solutions containing small amounts of hydrogen sulfide. *Corrosion science*, 51(4):260–269, 1995.

[120] F. Wang, S. Saeki, and T. Yamaguchi. Temperature and pressure dependence of thermal expansion coefficient and thermal pressure coefficient for amorphous polymers. *Polymer*, 38(1):3485–3492, 1997.

[121] F. Wang, S. Saeki, and T. Yamaguchi. Investigation of melting phenomenon and thermodynamic behaviour in crystalline polymers. *Polymer*, 39(11):2235–2239, 1998.

[122] R.G. Wissinger and M.E. Paulaitis. Swelling and sorption in polymer-CO_2 mixtures at elevated pressures. *Journal of Polymer Science: Part B: Polymer Physics*, 25:2497–2510, 1987.

[123] Wolfe, W.F. Hines, J.J. Papay, and R.U. Pagilagan. Realistic evaluation techniques for flexible pipe polymers proposed to wellbore fluids. *Offshore Technology Conference*, 4(OTC6725):263–272, 1991.

[124] Donald H. Wolfe and John J. Baron. Flexible pipe combats corrosion threat at sour brine injection site. *Oil & Gas Journal*, pages 48–51, 1997.

[125] Hankun Xie and Robert Simha. Theory of solubility of gases in polymers. *Polymer International*, 44:348–355, 1997.

[126] Matsui Shigetomo Itoga Koyu Yoshida, Toshio. Corrosion problems of pipeline and a solution. *Offshore Technology Conference*, 4(OTC3891):361–370, 1980.

[127] John M. Zielinski. An alternative interpretation of polymer/solvent jump size units for free-volume diffusion models. *Macromolecules*, 29:6044–6047, 1996.

[128] P. Zoller and P. French. The thermal analysis of polymers at high pressures. *Journal of Thermal Analysis*, 47:993–1012, 1996.

Appendix A

Literature Study

In this appendix seven articles are referred in details. it should be noted that the text represents an initially thorough literature study that is not complete. The seven articles are chosen arbitrarily and do not discuss all aspects of solubility and diffusion. In 1960 Rogers et al [82] reported a number of measurements of solubility and diffusion coefficients of methyl bromide, isobutylene, n-pentane - n-octane, cyclohexane, benzene, toluene, ethyl benzene, p-xylene, chloroform, carbon tetrachloride and ethyl bromide in PE at temperatures from $-8°C$ to $30°C$. The effects of crystallinity of the polymer on the solubility are discussed. An empirical linear relationship between the solubility coefficient and the molar volume of the penetrant is presented:

$$S_0 = S_0^\circ \exp\left(G\bar{V}\right)$$

where S_0 is the solubility coefficient, S_0° is the solubility coefficient at zero concentration for a penetrant of zero molar volume (probably dependent of the shape of the penetrant molecule), G is a constant probably dependent on the nature of the polymer and $\bar{V}$ is the molar volume of the penetrant. The dependence of the solubility coefficient on the concentration of the absorbed penetrant is shown empirically to be exponential:

$$S = S_0 \exp\left(\sigma c\right)$$

where S_0 is the solubility coefficient from the intercept at $c = 0$ of (S, c) plots amd σ is a constant characterizing the concentration dependence of the solubility coefficient. Three method for determination of the diffusion coefficient are compared - rate of sorption-desorption, transmission time-lag and $\bar{D} = \frac{P}{S}$. It is concluded that for some penetrants the coefficients are the same independent of the choice of measuring technique/used equation and

for some penetrants the diffusion coefficients depends on the method used for determination. The experimental data suggest that the integral diffusion coefficient

$$\bar{D} = \frac{1}{c_1 - c_2} \int_{c_2}^{c_1} D dc$$

depends exponentially on the activity of the penetrant

$$\bar{D} = D_0 \exp(\alpha a_1)$$

where D_0 is the diffusion coefficient at zero activity, pressure and concentration, α is a constant for a penetrant-polymer system at a given temperature and $a_1 = \frac{p}{p^0}$ is the approximation to the vapor activity when p^0 is the saturated vapor pressure at a given temperature. After mathematical manipulations the permeability coefficent is now given by

$$P = P_0 \exp(\alpha a_1 + \sigma c)$$

where $P_0 = D_0 S_0$.

In Fujitas 'personal note' from 1961 [26] the general theory of diffusion and sorption is discussed for the cases where the penetrant is a solvent or a plasticizer. In the case of Fickian sorption (usually above the glass transition temperature) detailed description of how to determine $D(c)$ from sorption/desorption measurements - based on Crank - is given. In addition the variation of $D(c)$ to temperature is illustrated in two graphs. It is concluded that the dependence of the diffusion coefficient of the concentration of the penetrant is determined by the nature of the polymer-penetrant system. If the penetrant is a solvent the dependence is pronounced where as a non-solvent does not give a strong concentration dependence of the coefficient. Variable surface concentration is explained by slow establishment of the equilibrium concentration in the glassy polymer and an equation to relate surface concentration to time is given - however, it is a fact that equilibrium is attained instantaneously in rubbery polymers. Two-stage sorption curves are discussed in details. An equation for timelag:

$$t_L(c_1^\infty) = L^2 \frac{\int_0^{c_1^\infty} wD(w) \left[\int_w^\infty D(u)du\right] dw}{\left[\int_0^{c_1^\infty} D(u)du\right]^3}$$

where t_L is the timelag, c_1^∞ is the constant surface concentration, L is the thickness of the membrane, w and u are concentration vectors and D is a function of the concentration. The concentration dependence of the diffusion

coefficient is discussed by derivation of the free volume method based on Cohen and Turnbull. Analogies to the theory for viscosity (WLF) are drawn.

Stern et al have done extensive work on the effect of pressure on the permeability and the applications of the free volume theory. In [101] permeability coefficients have been measured for $C_2H_2F_2$ and CHF_3 in polyethylene at penetrant pressures up to 35 atm and temperatures $-18-70°C$. It is concluded that $log(\bar{P})$ versus $log(\Delta p)$ is linear expect for the lowest temperature. The data is representaed by an empirical relation

$$\bar{P} = P(0) \exp m\Delta p$$

where $\bar{P}$ is the permeability, $P(0)$ and m are constants depend on the temperature and Δp is the pressure across the membrane. The Arrhenius plots of the same data different behaviour of the two gasses in the polymer. Following empirical equation is given for the permeability:

$$\bar{P} = \bar{D}\bar{S} = P_0 \exp \frac{\left[\frac{\tau}{p^*} + S_0\sigma\right] p_h - \frac{\tau S_0 \sigma}{p^*} p_h^2}{1 - S_0\sigma p_h}$$

where Henry's law does not have to apply. τ and σ are temperature dependent constants, p^* is the vapor pressure of the penetrant and S_0 is the reciprocal of the Henry' law constant. The free volume theory is derived. In [103] permeability coefficients for Ar, SF_6, CF_4 and $C_2H_2F_2$ in polyethylene are given at temperatures $5 - 50°C$ and at applied gas pressures up to 15 atm. Free volume parameters are calculated using steady-state permeability measurements and unsteady-state absorption measurements. The parameters agree acceptably. Free volume parameters are given for comparison for CO_2, CH_4, C_2H_4 and C_3H_8. When using the free volume model expansion and compressibility coefficients for the pure polymer are required. In [105] a number of permeability coefficients of gasses in poly ethylene are listed at a wide range of temperatures and pressures. For carbon dioxide data is given up to 54.4 atm. and up to $61.0°C$. The dominating trend is that log(P) is independent of the applied pressure at a wide temperature range - the lowest temperature being an exception. Pressure dependence is detected when Henry's law does not apply or if the diffusivity is concentration dependent. The solubility and the diffusion coefficients are correlated to critical temperatures by the corresponding states principle - satisfactory agreement.

In 1964 Li and Henley [49] report experimental data of permeation of polar as well as nonpolar gases through polyethylene at pressures up to 11 atm. The density of the membrane is $\rho = 0.922 g/cc$ and the volume fraction amorphous phase is $\alpha = 0.533$. The temperature dependence of the

permeation of CO_2 in the range $15 - 40°C$ obeys an Arrhenius expression:

$$P = P' \exp(-\frac{E_p}{RT}) \Leftrightarrow$$
$$P = 5.625 \cdot 10^{-5} \exp(-\frac{5.98}{RT})$$

Li and Henley comment that P' and E_p are functions of pressure when the permeability varies with pressure. The pressure dependence is expressed as a modified Fick's law:

$$N = \left(P_0 \exp^{Ap}\right) \left(\frac{\Delta p}{Z}\right)$$
$$N = (P_0 + P_1) \left(\frac{\Delta p}{Z}\right)$$

where N is the flux, P_0 is the permeability at a zero downstream pressure, P_1 is *a second permeation constant* that is a pressure correction term, Δp is pressure across the membrane and Z is the membrane thickness. The activation energy is correlated to the Hildebrands solubility parameters. No pressure dependence is observed for the permeation of carbon dioxide whereas the permeability of methane increases with increasing pressure. Li cites a number of researchers - the solubility and diffusion constants can be correlated to exponential equations similar to the permeability. Finally, it is concluded that the thickness of the membrane does not affect the constants.

Naito et al, 1991, discuss the pressure effect on gas permeation for, amongst others, carbon dioxide and methane through polyethylene and polypropylene. Based on Stern et al and Li et al the premeability is assumed to depend exponentially on pressure as a consequence of the diffusion coefficient's exponentially dependence of pressure.

$$\bar{P} = \bar{P}_0 \exp(\beta p_2)$$
$$\bar{D} = \bar{D}_0 \exp(\beta p_2)$$

The expression for the diffusion coefficient introduces a parameter,$\beta = \beta_h + \frac{1}{2}\alpha S$, related to the hydrostatic pressure and the concentration of penetrant. The expression is based on a simplified Free Volume model given by Stern et al. The used PE membrane has a density of $\rho = 0.915 g/cm^3$ and a crystallinity of 0.43. Henry's law is assumed valid in the pressure range and the solubility constant is measured by the timelag method at presures below 1 atm and at $T = 25°C$. The β parameter is related to molecular diameters. Graphs of $\log \bar{P}$ vs p_2 show an increase in permeability with pressure up to 50 atm ($25°C$).

Miyake et al, 1983, reports experimental data of solubility and diffusion coefficents obtained by the time lag method for hydrogen isotopes, methane and inert gases through tetrafluoroethylene and polyethylene. Relations to heat of vaporization and the Lennard-Jones force constants of the gases to the coefficients give no good agreement for methane - good agreement only for the inert gases.

Handbook of Gas Diffusion in Solids and Melts by Shelby [93] discussed many aspects of diffusion of gasses through glasses, ceramics, metals, polymers, nanoporous materials and melts. However, the diffusion of gasses through semi-crystalline polymers above the glass transition temperature is not discussed in greater detail. The behaviour of partially crystalline materials are concluded to correspond to that of inorganic glass-ceramics and ceramics with amorphous grain boundary phases. The permaability and diffusion are - as before - given by

$$D = D_0 e^{-\Delta H_d/RT}$$
$$K = K_0 e^{-E_k/RT}$$

where D and K are diffusion and permeability, ΔH_d and E_k are activations energies and D_0 and K_0 are constants. The diffusion of gasses in crystalline polymers are corrected for the longer path due to the crystals by a *tortuosity* factor:

$$D = D^*/\tau\beta \tag{A.1}$$

where D^* is the diffusitity of the gas in the amorphous phase, τ is the tortuosity factor and β is a *chain immobilization factor* that account for the changes in the amorphous phase near the crystals. Chemical bonding might be important for the solubility of gasses in the polymer. The trend for inert gasses being that the solubility increases with increasing size of dissolved entity. According to Shelby *the correct relationship between gas solubility and gas identity in polymers is not clear.* The solubility is related to atomic diameters of the gas molecules, to the Lennard-Jones force constants, to the critical temperature and boiling point of the gas but none gives a unique relation. The solubility and diffusivity may vary 'opposite' causing the permeability to decrease, increase or even remain constant. A big molecule as carbon dioxide might have a higher permeability than a small molecule as helium eventhough the diffusion of helium is much higher because the solubility of carbondioxide is higher.

Experimental data found in the literature

Only a few data on diffusion and solubility are available in literature. A few more data is found for the permeability. The data found in literature is gathered and converted to the same units. Data presented graphically has been scanned from original work and is reproduced in the following.

In table A.1 and A.2 constants for permeation of polyethylene to carbon dioxide and methane are given.

Polymer	ρ	α	T	p	S	D	Pe	Ref
PE	0.922	0.533	306	1	0.221	$9.24 \cdot 10^{-7}$	$2.04 \cdot 10^{-7}$	[49]
LDPE	0.915	–	298	< 1	0.257	–	see figure A.3	[66]
Alathon 14	0.918	0.552	308	[a]	0.234	–	–	
Alathon 14	0.918	0.552	293	[a]	0.242	–	–	[46]
Alathon 14	0.918	0.552	298	[a]	0.268	–	–	
Grex	0.964	0.23	298	~ 1	–	$1.24 \cdot 10^{-7}$	$2.71 \cdot 10^{-9}$	
Alathon 14	0.9137	0.57	298	~ 1	–	$3.72 \cdot 10^{-7}$	$9.47 \cdot 10^{-8}$	[61]

Table A.1: Permeability to CO_2

[a] reported independent of pressure

Polymer	ρ	α	T	p	S	D	Pe	Ref
PE	0.922	0.533	306	1	0.040	$31 \cdot 10^{-7}$	$1.24 \cdot 10^{-7}$	[49]
LDPE	0.915	–	298	< 1	0.104	–	see figure A.3	[66]
PE	0.92	0.47-0.53	ambient	–	0.17 ± 0.01[b]	$2.12 \pm 0.06 \cdot 10^{-7}$		[62]
Alathon 14	0.918	0.552	308	[a]	0.100	–	–	
Alathon 14	0.918	0.552	293	[a]	0.098	–	–	[46]
Alathon 14	0.918	0.552	298	[a]	0.100	–	–	
Grex	0.964	0.23	298	~ 1	–	$0.57 \cdot 10^{-7}$	$2.92 \cdot 10^{-9}$	
Alathon 14	0.9137	0.57	298	~ 1	–	$1.93 \cdot 10^{-7}$	$2.17 \cdot 10^{-8}$	[61]

Table A.2: Permeability to CH_4

[a] reported independent of pressure

[b] apparently dimensionless

ρ is the density in g/cm^3, α is the volume fraction amorphous phase, T is the temperature in K and p is the pressure in bar. Solubility, S, is given in cm^{3}STP/(cm^3 polymer bar), diffusion, D, in cm^2/s and permeability, Pe, in cm^3 cm/(s cm^2 bar) unless otherwise is noted. Where necessary the units have been converted. In the following original figures are reproduced.

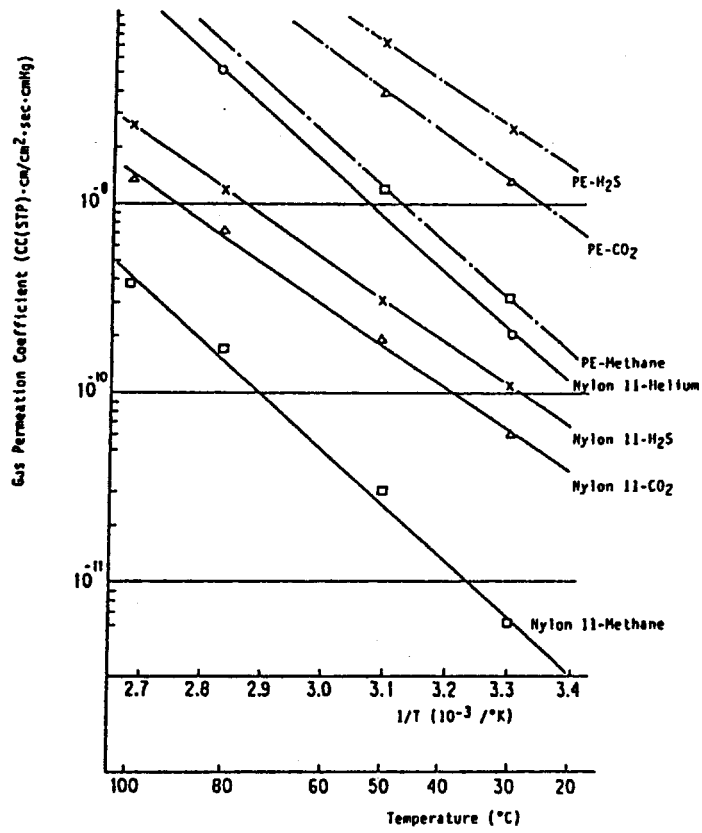

Figure A.1: The temperature dependence of the permeability of PE and PA-11 to H_2S, CO_2 and CH_4, [56]

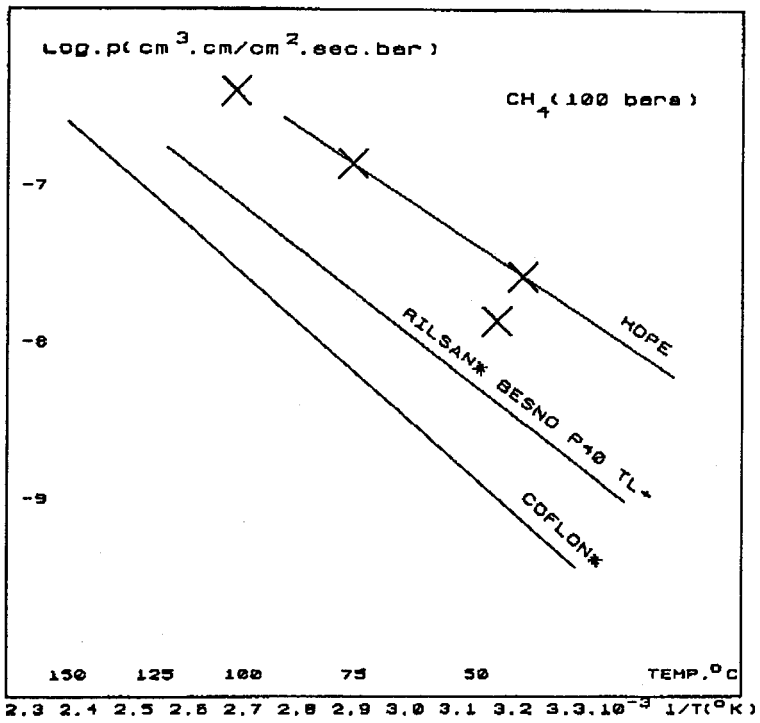

Figure A.2: Permeability curves of polymers, [12]. Rilsan=PA-11, COFLON=PVDF. The crosses is CROSSFLEX=Cross linked PE.

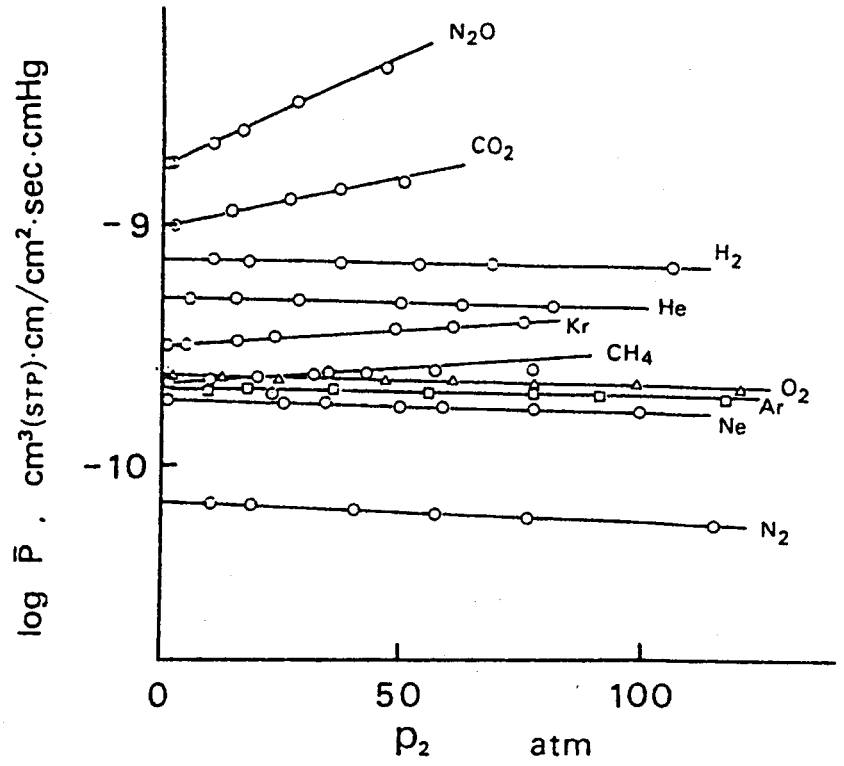

Figure A.3: Pressure dependence of permeability for various gases in LDPE at 25°C, [66]

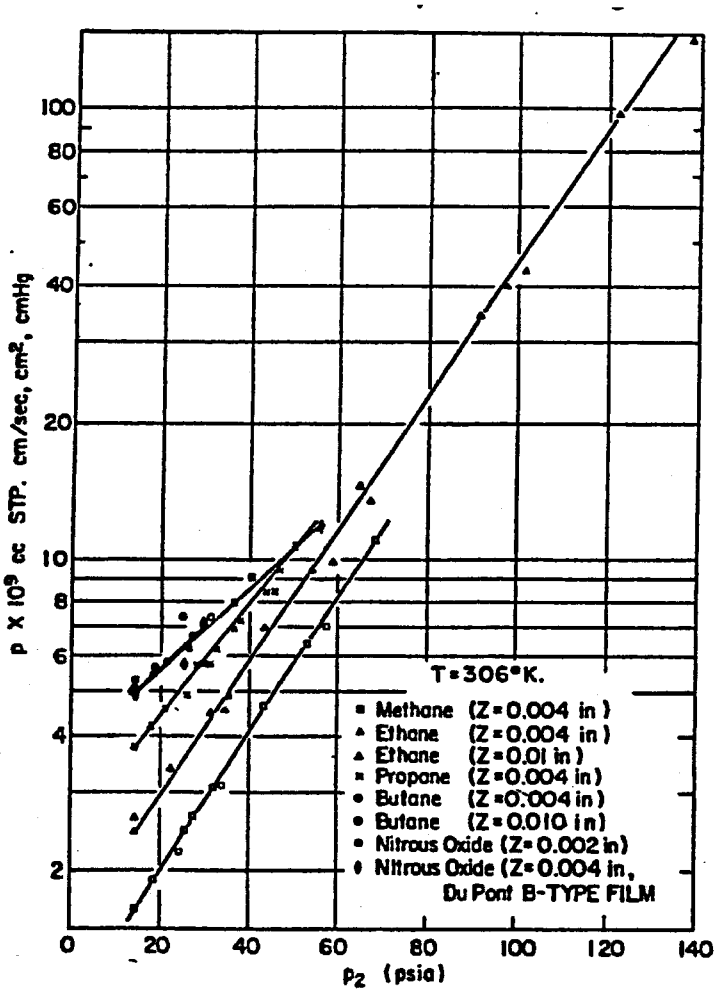

Figure A.4: Permeation constants of methane, ethane, propane, butane, and nitrous oxide through polyethylene, Z is the thickness of the membrane, [49]

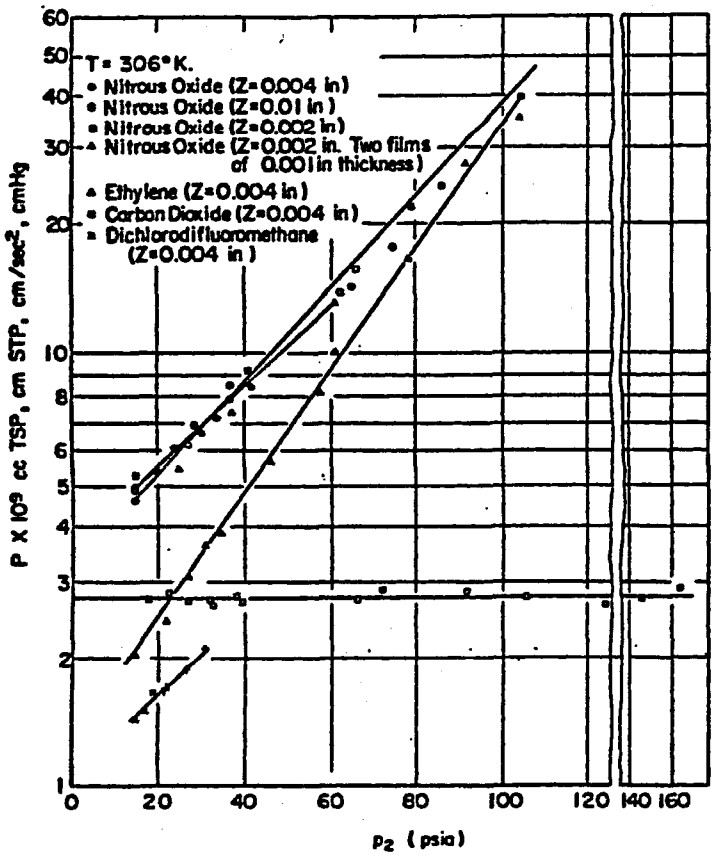

Figure A.5: Permeation constants of ethylene, nitrous oxide, carbon dioxide and dichlorodifluoromethane through polyethylene, Z is the thickness of the membrane, [49]

Li and Henley [49] also report constants for calculation of the permeability from the following equation:

$$P = P' e^{-\frac{-E_p}{RT}}$$

The constants for the permeability of carbon dioxide to polyethylene in the temperature range $15 - 40°C$ are given in table A.3

E_p	P'
$2.50 \cdot 10^4$	0.004
$2.84 \cdot 10^4$	0.135
$2.98 \cdot 10^4$	0.025
$3.01 \cdot 10^4$	–

Table A.3: Permeability constants

Li and Henley state that the constants must be functions of pressure if the permeability is pressure dependent. Pressure dependent permeabilities are illustrated in figures A.4 and A.5.

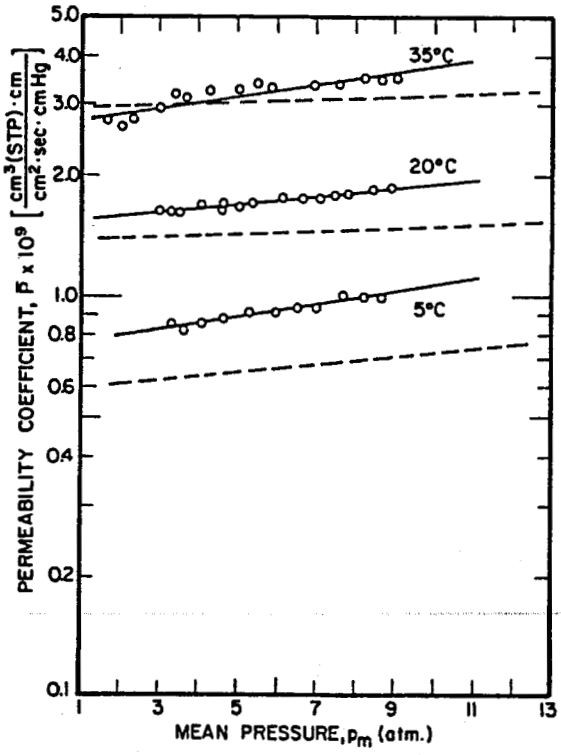

Figure A.6: Dependence of permeability coefficients for carbon dioxide in polyethylene on mean pressure. The experimental permeability coefficients (-o-) are compared with values calculated from a free volume model (- - -) in conjunction with free-volume parameters evaluated from independent solubility and unsteady-state diffusivity measurements, [103]

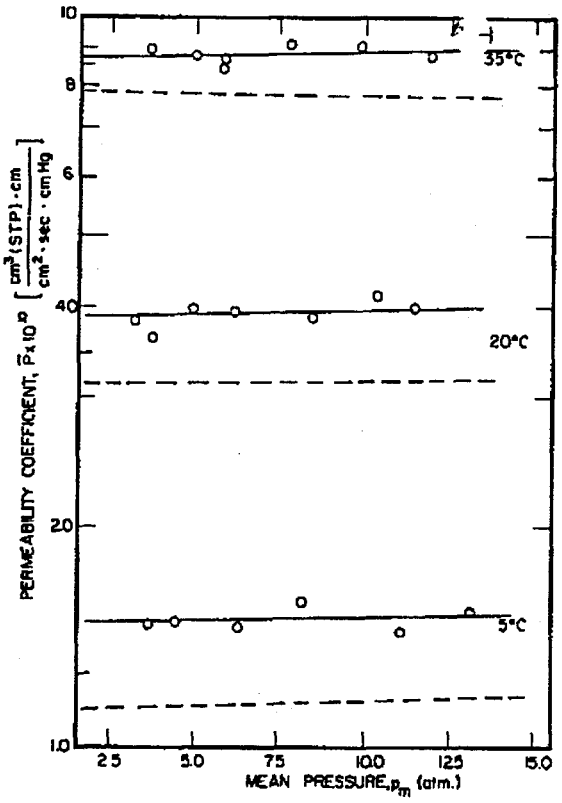

Figure A.7: Dependence of permeability coefficients for methane in polyethylene on mean pressure. The experimental permeability coefficients (-o-) are compared with values calculated from a free volume model (- - -) in conjunction with free-volume parameters evaluated from independent solubility and unsteady-state diffusivity measurements, [103]

Stern et al [103] reports constants for evaluation of permeability coefficients. From the data in table A.4 and A.5 the permeability is calculated from:

$$\ln \bar{P}(p_m) \sim \ln \bar{P}(0) + m p_m$$

where $\bar{P}$ is the mean permeability coefficient for one-dimensional, isothermal transport of a penetrant gas through a planar non-porous membrane, $p_m = \frac{1}{2}(p_h + p_l)$ is the mean pressure on the membrane, $\bar{P}(0)$ is the value of $\bar{P}$ at zero penetrant pressure and m is a measure of the pressure dependence of $\bar{P}$.

Polymer	ρ	T	p_h	P_0	m
PE	0.918	293	–	$1.13 \cdot 10^{-7}$	$2.37 \cdot 10^{-2}$
PE	0.917	293	59.2	$1.35 \cdot 10^{-7}$	$1.97 \cdot 10^{-2}$
PE	0.918	298	–	$1.35 \cdot 10^{-7}$	$2.86 \cdot 10^{-2}$
PE	0.914	298	< 1	$9.75 \cdot 10^{-8}$	–
PE	0.918	306	–	$2.03 \cdot 10^{-7}$	$2.86 \cdot 10^{-2}$
PE	0.922	306	10.9	$2.03 \cdot 10^{-7}$	0

Table A.4: Permeability to CO_2

Polymer	ρ	T	p_h	P_0	m
PE	0.918	293	–	$2.70 \cdot 10^{-8}$	$2.76 \cdot 10^{-3}$
PE	0.917	293	54.3	$2.63 \cdot 10^{-8}$	$4.93 \cdot 10^{-3}$
PE	0.918	298	–	$3.60 \cdot 10^{-8}$	$2.76 \cdot 10^{-3}$
PE	0.922	298	93.8	$1.43 \cdot 10^{-8}$	$4.64 \cdot 10^{-3}$
PE	0.914	298	< 1	$2.18 \cdot 10^{-8}$	–
PE	0.918	306	–	$5.85 \cdot 10^{-8}$	$9.87 \cdot 10^{-4}$
PE	0.922	306	4.9	$6.00 \cdot 10^{-8}$	$2.47 \cdot 10^{-1}$

Table A.5: Permeability to CH_4

ρ is the density in g/cm^3, T is the tem perature in K and p_h is the "highest applied pressure" in bar. The permeability, P(0), is given in cm^3 cm/(s cm^2 bar) and m is in bar.

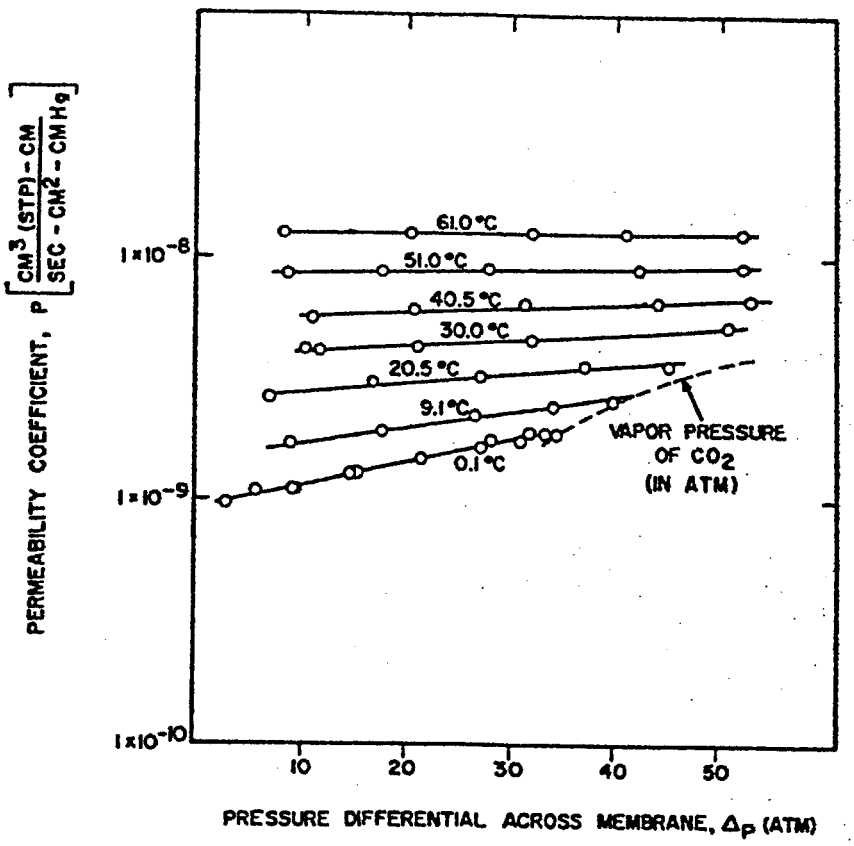

Figure A.8: Permeability coefficient for the system carbon dioxide-Alathon 15 polyethylene as a function of pressure differential up to 54.4 atm, [105]

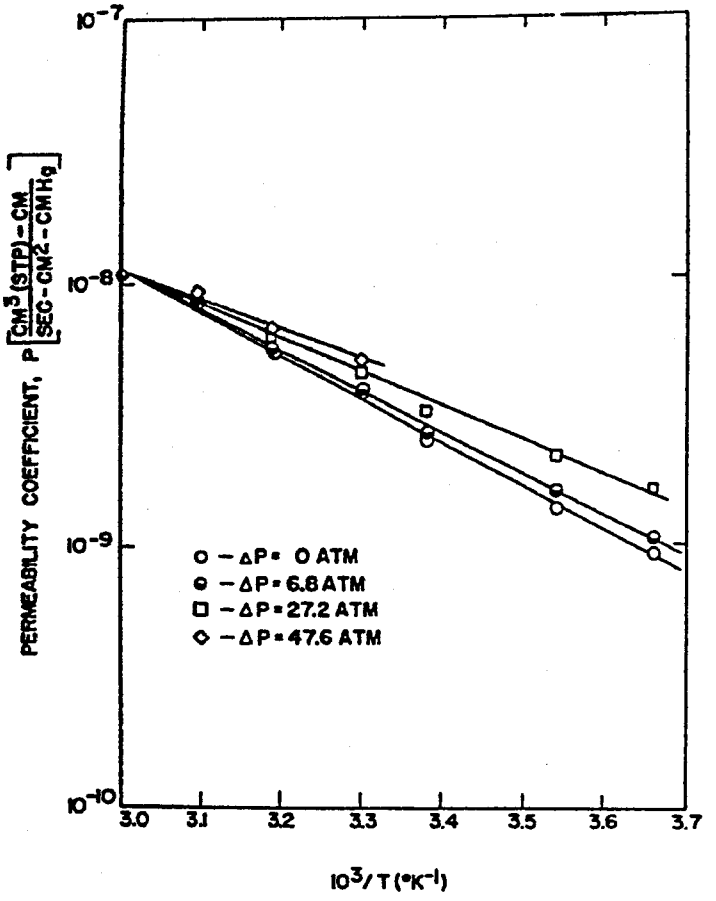

Figure A.9: Effect of temperature on permeability of alathon 15 polyethylene to carbon dioxide as a function of pressure differential, [105]

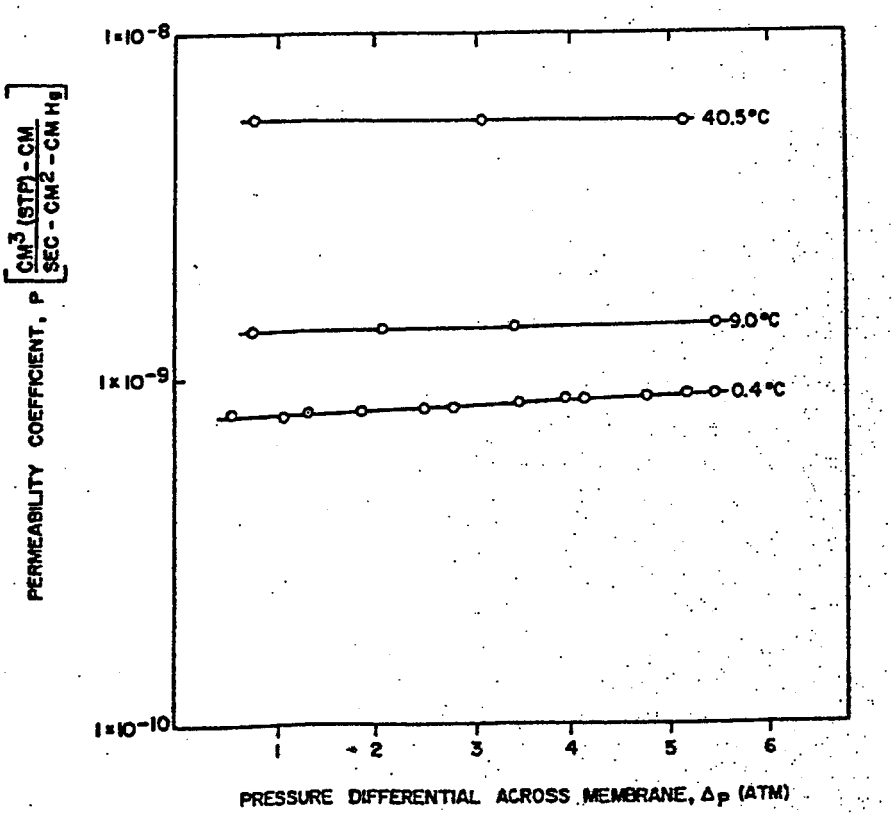

Figure A.10: Permeability coefficient for the system carbon dioxide-Alathon 15 polyethylene as a function of pressure differential up to 6.0 atm, [105]

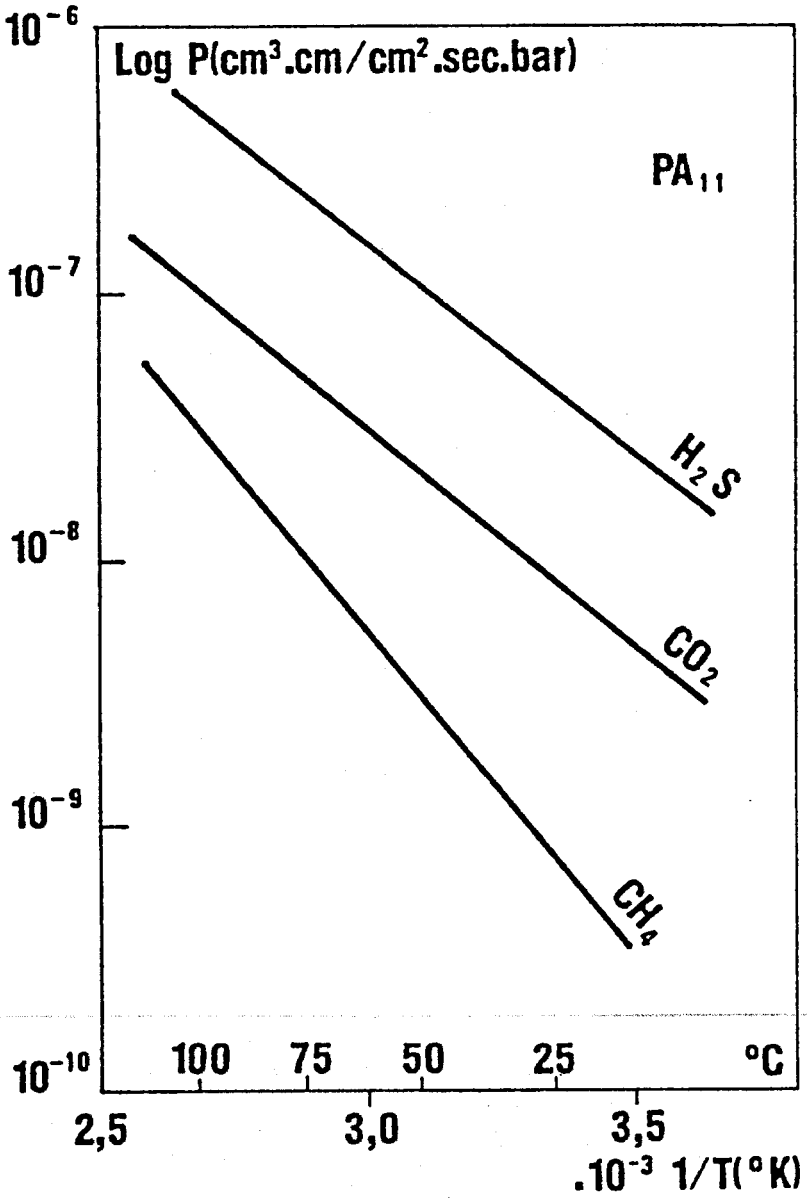

Figure A.11: Permeability of PA11 to H_2S, CO_2 and CH_4 gases, [19]

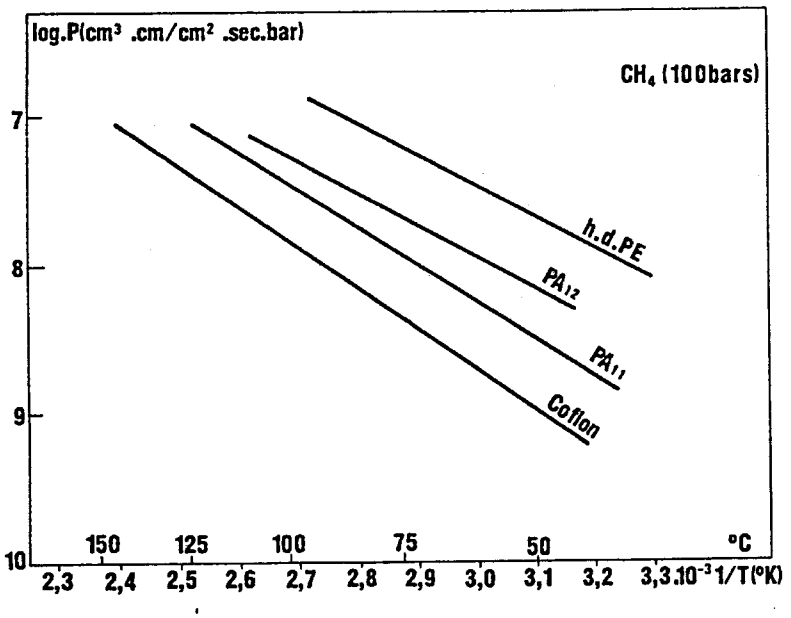

Figure A.12: Permeability of HDPE,PA11 and 12 and COFLON to CH_4 gas, [19]

Summary

Eventhough the amount of data is small some tendencies are observed.

Solubility

It is a general assumption that Henry's law applies for the solubility of gas in polymer, thus the solubility given by $c = S \cdot P$ (where c is concentration, S is the solubility and P is the pressure) must be independent of pressure. An expection to this assumption was reported in 1969 by Stern et al [105]. In this article the solubility coefficient is related to the pressure and the temperature. However, not many references to this relation has been found in the literature.

A comparison of the few data on solubility of carbon dioxide and methane in polyethylene (table A.1 and A.2) indicates that CO_2 is more than twice as soluble as CH_4.

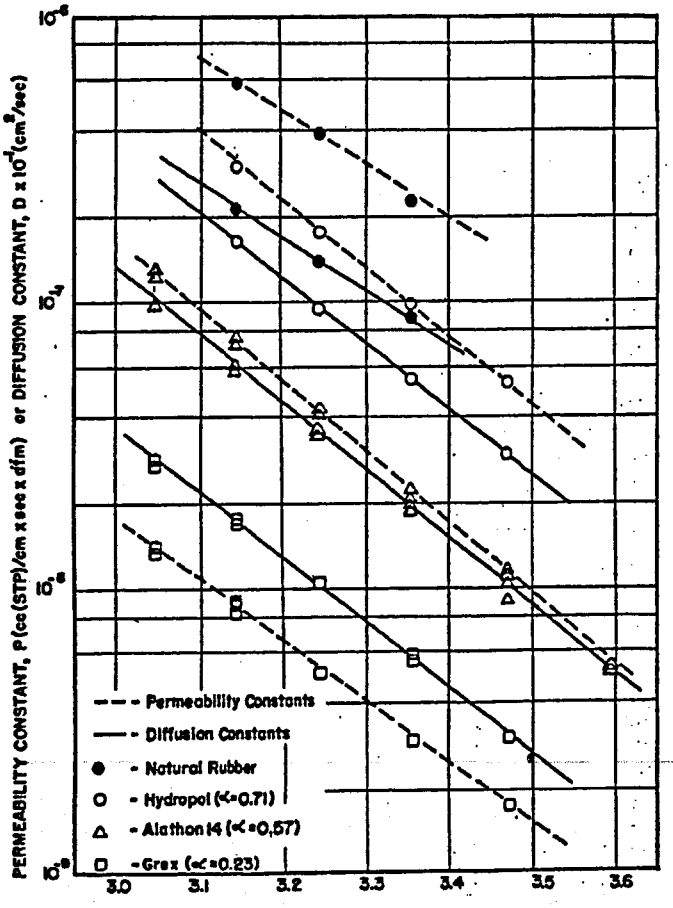

Figure A.13: Methane diffusion and permeability constants, [61]

Diffusion

Not much can be concluded from the diffusion coefficients in table A.1 and A.2. Except for the measurement made by Li and Henley [49] the diffusion of methane tends to be lower than diffusion of carbon dioxide. In figure A.13 the temperature dependence of the diffusion coefficient for permeation of methane through polyethylene is shown.

Permeability

Most of the data reported in this section concerns the permeability. The temperature dependence of the permeability for all the gas-polymer systems under consideration is obvious (figures A.1, A.2, A.9, A.11, A.12 and A.13).

A comparison of the permeability of methane in polyethylene at low pressure (low pressure is assumed in figures A.1 and A.13) and at high pressure (figure A.12) indicates an increase in permeability with pressure at constant temperature. The same tendency is observed in figures A.3, A.4 and A.7. However, in figures A.3 and A.7 the pressure dependence is of a smaller order of magnitude.

For the permeability of carbon dioxide through polyethylene the figures indicate two kinds of behaviour. The permeability is independent of pressure, figures A.5, or the permeability is an increasing function of pressure, A.3 and A.6. Figure A.8 illustrates both types of behaviour depending of the temperature. The isoterms is constant at high temperatures and increase with pressure at low temperature.

However, the figures can only be compared qualitatively because the crystallinity and experimental conditions affect the measured values. In tables A.1 and A.2 the general tendency is a decreasing permeability with increasing crystallinity (low α).

Considering figures A.1, A.2, A.11 and A.12 the sequence of low to high permeable polymers is PVDF $<$ PA $-$ 11 $<$ PA $-$ 12 $<$ PE and the sequence of low to high permeating gasses is $CH_4 < CO_2 < H_2S$. According to Naito et al [66] the molecular diameters of carbon dioxide and methane are:

$$d_{CO_2} = 3.897\text{Å}$$
$$d_{CH_4} = 3.796\text{Å}$$

Note that eventhough CO_2 is the larger molecule it permeates faster. Shelby [93] explains this fact by the higher solubility of carbon dioxide in the given polymers.

Appendix B

Solubility Measurements

In the following the solubility measurements made by Abhijit Dandekar, IVC-SEP, DTU is reproduced.

Solubility

CO_2 in PE

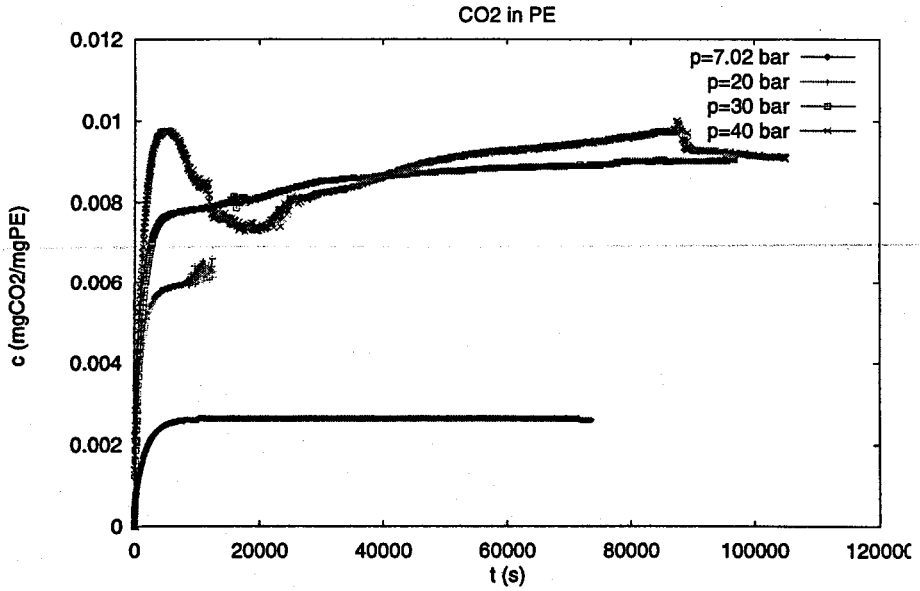

CO_2 in PA-11

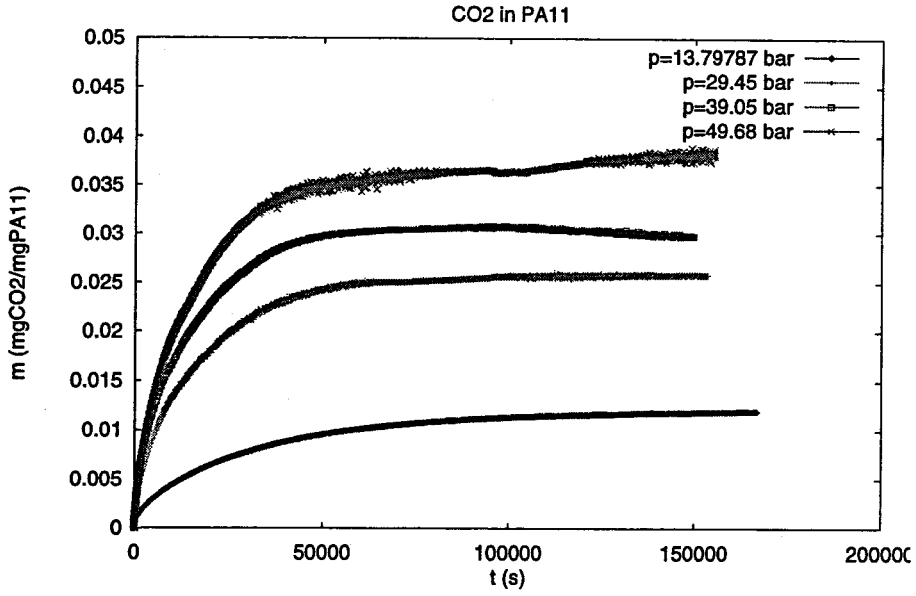

CH_4 in PE

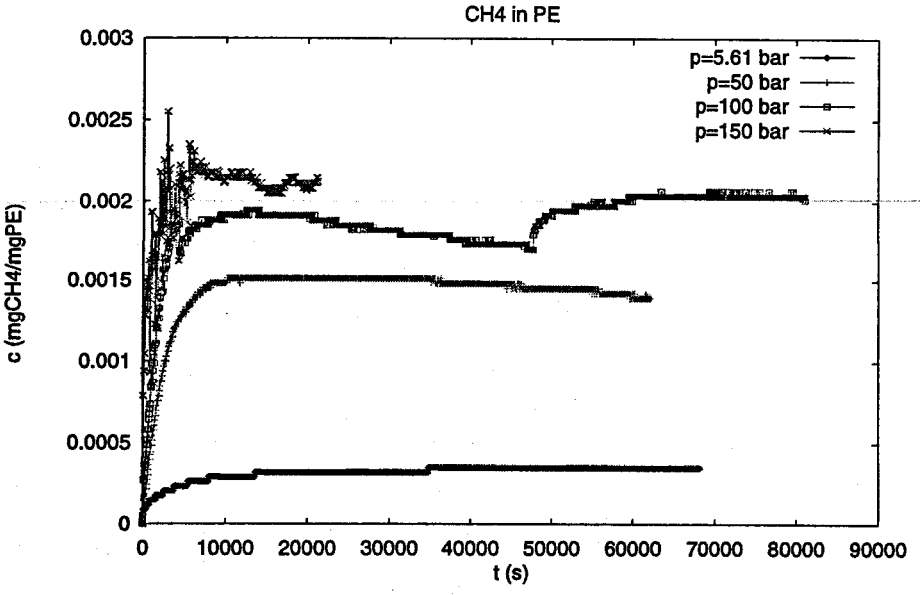

CH_4 in PA-11

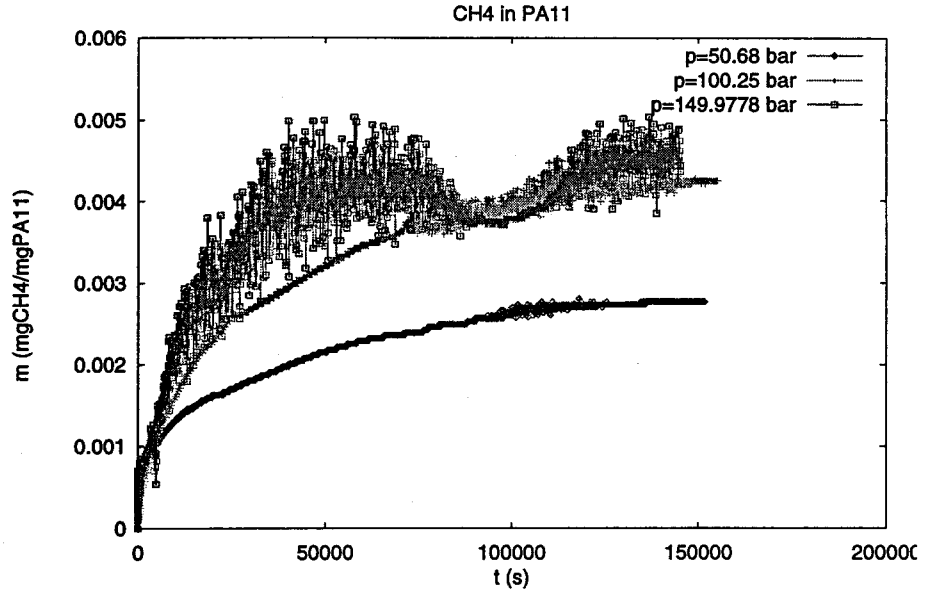

He in PE

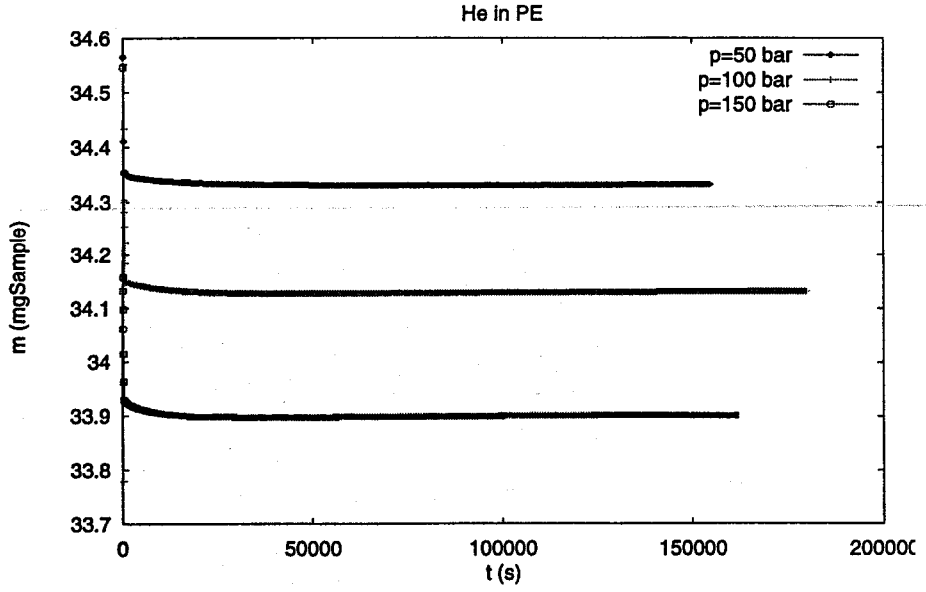

10mol% CO_2 + 90 mol% CH_4 in PE

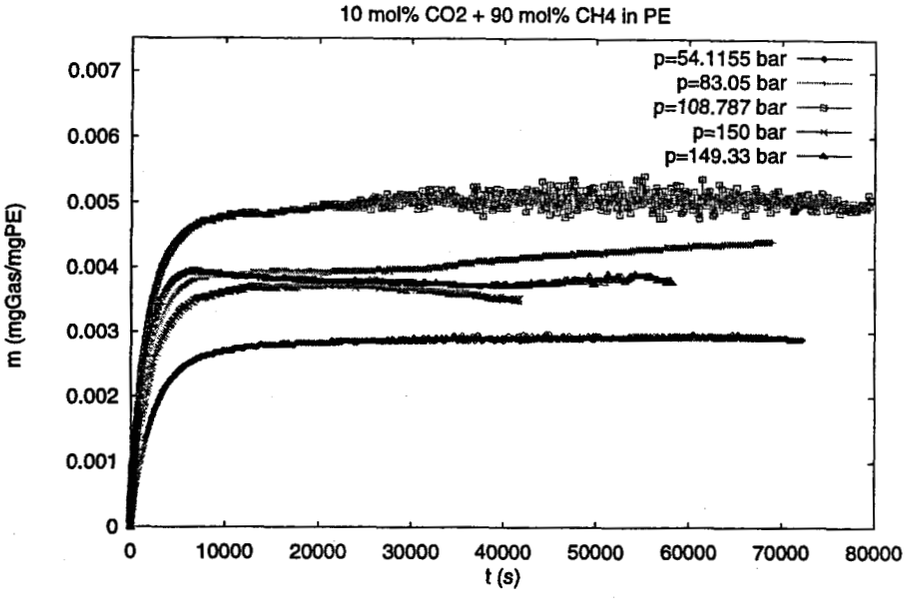

10mol% He + 90 mol% CH_4 in PE

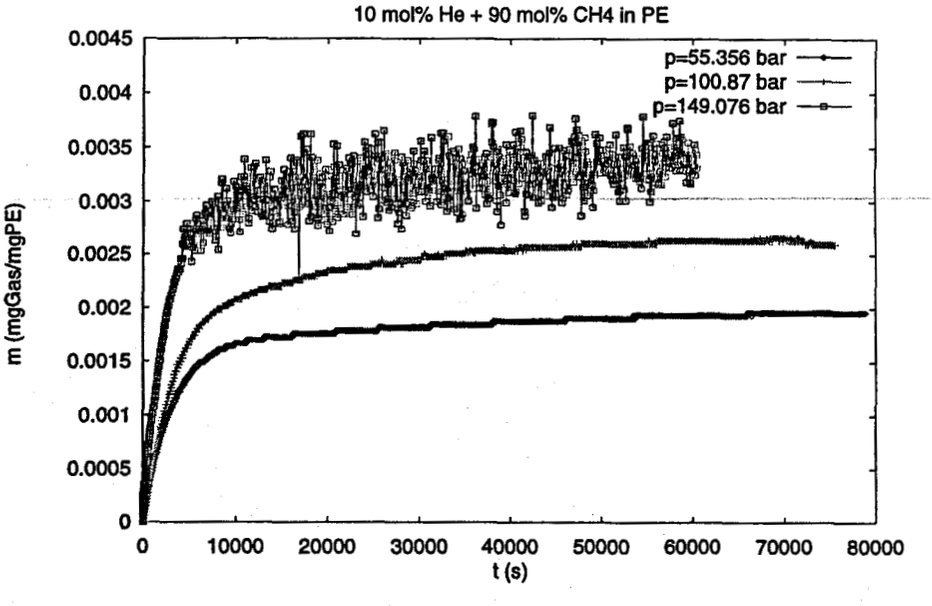

10mol% He + 90 mol% CO_2 in PE

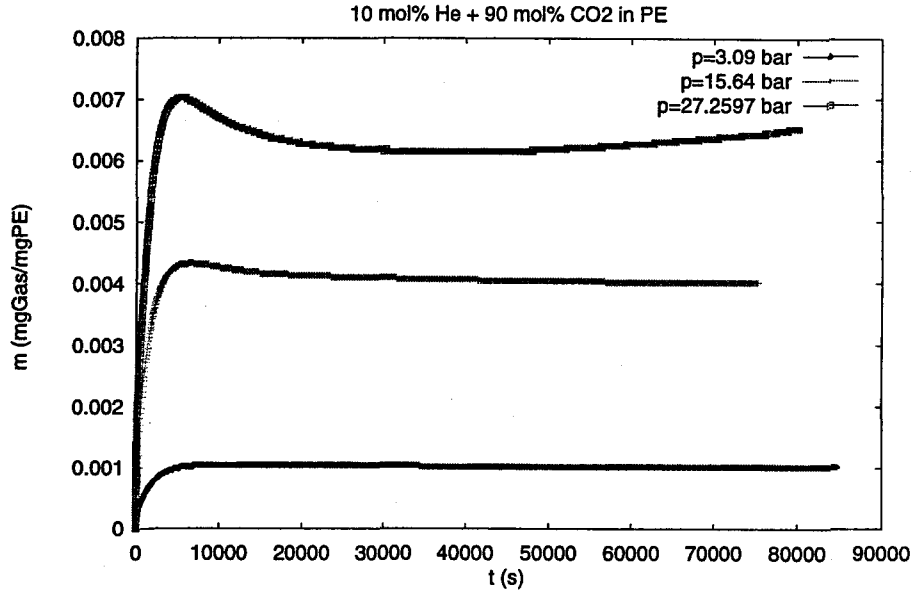

Appendix C

Diffusion Coefficients

In this section the calculation procedure and the linear fits made for determination of diffusion coefficients are described.

Linear fits

CO_2 in PE

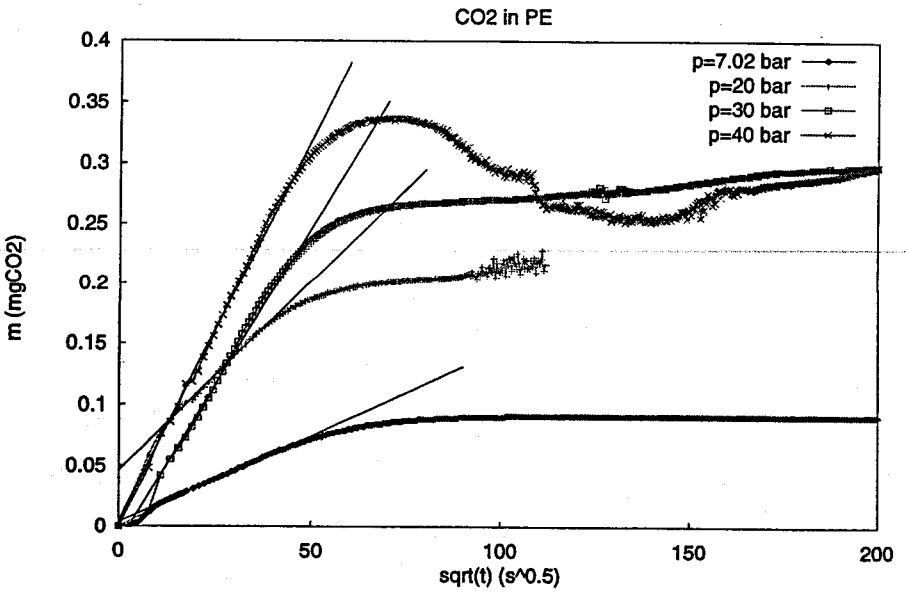

CO_2 in PA-11

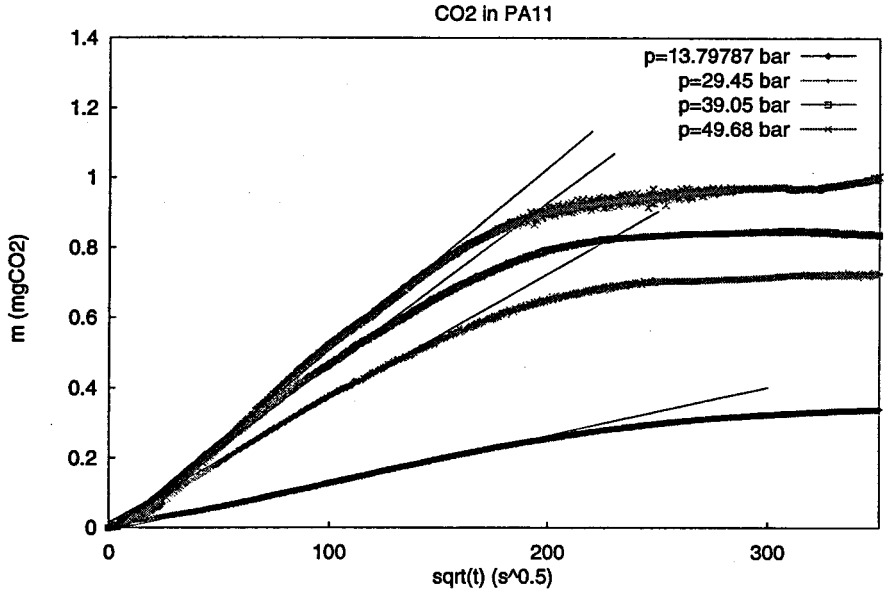

CH_4 in PE

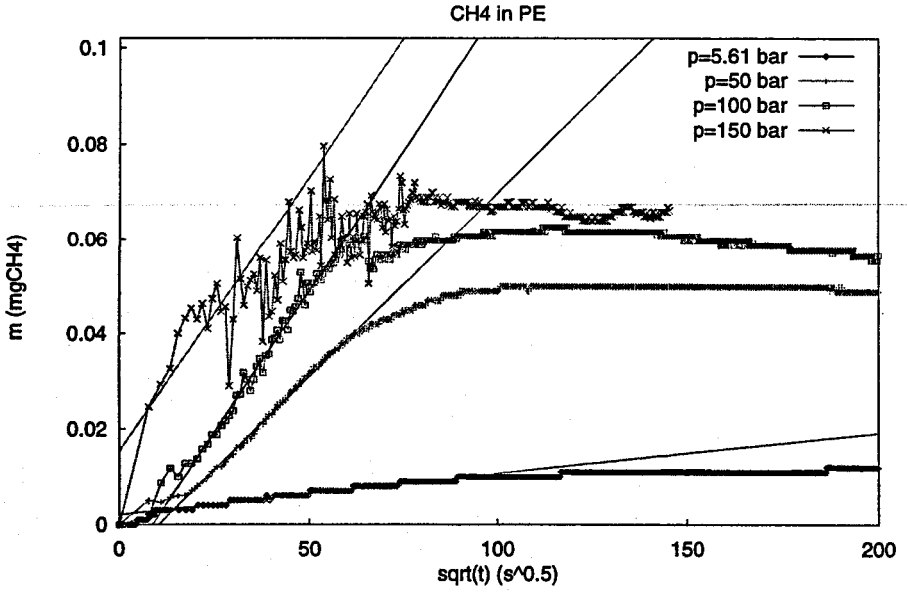

CH_4 in PA-11

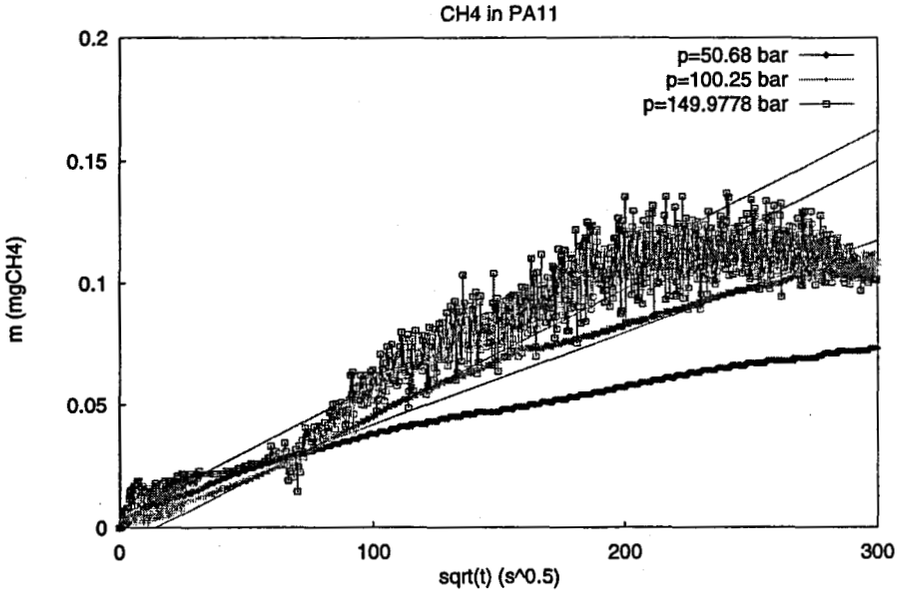

Calculation procedure

The calculation procedure is illustrated using the example of CO_2 diffusion through polyethylene at 7.02 bar. The slope of the linear fit to the initial gas weight increase is read to $\alpha = 1.4182 \cdot 10^{-3} mg/s^{\frac{1}{2}}$. The surface area of one side of the sample is determined to $A = 0.875 cm^2$ and the polymer density is $\rho = 0.954 g/cm^3$ (from NKT data sheets). From the solubility measurements: $C_{max} = 0.0026 \frac{mgCO_2}{mgPE}$. The diffusion coefficient is given by

$$D = \pi \left(\frac{0.001\alpha}{4A\rho C_{max}} \right)^2 = \pi \left(\frac{0.001 \cdot 1.4182 \cdot 10^{-3}}{4 \cdot 0.875 \cdot 0.954 \cdot 0.0026} \right)^2 = 8.146 \cdot 10^{-8} cm^2/s$$

Appendix D

Diffusion Coefficient Equation

In this section an equation to determination of the diffusion coefficient from solubility measurements is derived. The considered situation is illustrated in figure D.1. For constant diffusion coefficient Fick's second law is valid:

$$\frac{\partial c}{\partial t} = \mathcal{D}\frac{\partial^2 c}{\partial y^2}$$

In the illustrated situation the boundary conditions are:

$$\begin{aligned} t \leq 0 &: \; c = C_0 = 0 \\ y = 0 &: \; c = C_1 \\ y \to \infty &: \; c = C_0 = 0 \end{aligned}$$

A dimensionless concentration, $\phi = \frac{C}{C_0}$ is introduced:

$$\begin{aligned} \frac{\partial \phi}{\partial t} &= \mathcal{D}\frac{\partial^2 \phi}{\partial y^2} \\ t \leq 0 &: \phi = 0 \\ y = 0 &: \phi = 1 \\ y \to \infty &: \phi = 0 \end{aligned}$$

This problem is analog to example 4.1-12 and 11.1-8 in Bird et al [4]. Thus the solution is given by

$$\begin{aligned} \phi &= 1 - \tfrac{2}{\sqrt{\pi}} \textstyle\int_0^\eta e^{-\eta^2} d\eta, \; \eta = \tfrac{y}{\sqrt{4\mathcal{D}t}} \\ &= 1 - erf\tfrac{y}{\sqrt{4\mathcal{D}t}} \\ &= 1 - \tfrac{y}{\sqrt{\pi\mathcal{D}t}} \end{aligned}$$

That is

$$c = C_1 - \frac{y}{\sqrt{\pi\mathcal{D}t}} C_1$$

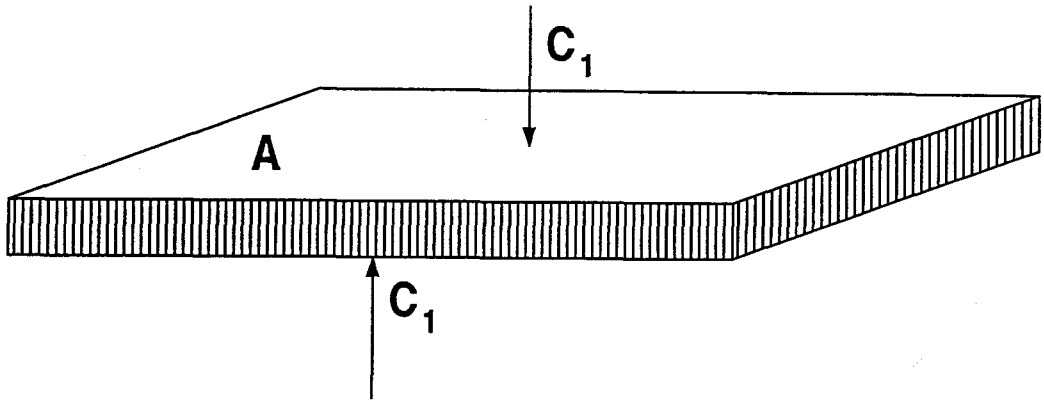

Figure D.1: The sample is enclosed in gas

The flux across boundary of the sample in mol/cm^2s is given by

$$\begin{aligned} q|_{y=0} &= -\mathcal{D}\frac{\partial c}{\partial y}|_{y=0} \\ &= \mathcal{D}\frac{C_1}{\sqrt{\pi \mathcal{D} t}} \\ &= C_1\sqrt{\frac{\mathcal{D}}{\pi t}} \end{aligned}$$

The total amount of gas after a given time interval is obtained by integration in time and mulitiplication of the total surface area (assuming the sample is thin):

$$\begin{aligned} m(t) &= 2AM\int_0^t C_1\sqrt{\frac{\mathcal{D}}{\pi t'}}dt' \\ &= 4AMC_1\sqrt{\frac{\mathcal{D}t}{\pi}} \end{aligned}$$

where $A(cm^2)$ is the surface area of one side of the sample, $M(g/mol)$ is the molar weight of the gas, $\mathcal{D}(cm^2/s)$ is the diffusion coefficient, $t(s)$ is the time and $C_1(mol/cm^3)$ is the concentration in the boundary equal to the maximum concentration of gas in the polymer when steady state is reached. It should be noted that this equation is only valid as long as the assumption of zero gas concentration in the middle of the sample is a fair approximation. From the equation a straight line with the slope $\alpha = 4AMC_1\sqrt{\frac{\mathcal{D}}{\pi}}$ is expected when $m(t)$ is plotted against $\sqrt{t}$. The diffusion coefficient can be calculated from the slope by:

$$\mathcal{D} = \pi\left(\frac{\alpha}{4AMC_1}\right)^2$$

The maximum concentration of gas in the polymer is commonly determined as $mgGas/mgPolymer$. If this is the case the equation

$$\mathcal{D} = \pi \left(\frac{0.001\alpha}{4A\rho C_1'} \right)^2$$

should be used. Here $\rho(g/cm^3)$ is the polymer density and $C_1'(mgGas/mgPolymer)$ is the maximum concentration.